The Formation Reactions of Some Volatile Fluorides(Dissertation_全文)

AUTHOR(S):

Iwasaki, Matae

The Formation Reactions of Some Volatile Fluorides

MATAE IWASAKI

The Formation Reactions of Some Volatile Fluorides

MATAE IWASAKI

August, 1969

Preface

The study presented here has been carried out as a part of the basic research concerning the fluoride volatility process under the direction of laboratory chief S. Tsujimura.

The main purpose of this work was to elucidate the behavior of the fluorination reactions to form volatile inorganic fluorides like metal hexafluorides and interhalogen compounds; the information will be useful for development of the fluoride volatility process. When the work was undertaken, these reactions had not been reported in detail. Since that time, however, a number of reports have been made promoting developments in the field. It is intended for the present paper to contribute the advance in this field.

The author is greatly indebted to Professor Dr. S. Yoshizawa and Professor Dr. N. Watanabe for their kind guidance, valuable suggestions and discussion through the work, and for their review of the manuscript. The author also wishes to thank Dr. K. Motojima, Mr. S. Tsujimura, Professor Dr. T. Mukaibo, and Professor Dr. K. Oshima for their encouragement, support, and comments during the work; further to Mr. K. Mori for his kind aid in writing the report. It is a pleasure to acknowledge with thanks the support from J.A.E.R.I., especially in the Reactor Chemistry Division, Mechanical Workshop Section, and Electronics Workshop Section. Many works and helps were recieved from Mr. T. Sakurai as collaborator, and from Mr. K. Suzuki and Mr. T. Yawata as former collaborators, and helps from Mr. N. Ishikawa, Mr. G. Fujisawa, Mr. A. Takahashi and Miss. Y. Kobayashi in performing the experiments. Thanks are due to all these colleagues.

June, 1969

Matae Iwasaki
Fluorine Chemistry Laboratory
Reactor Chemistry Division
J.A.E.R.I.

CONTENTS

Introduction

Incentive for the present study

Elementary fluorine and some halogen fluorides can fluorinate various metals and their compounds to the fluorides with high valency and volatile nature, such as hexafluoride. Of these fluorides, the uranium hexafluoride is of special importance because it is necessary for separation of the isotopes by gaseous diffusion. The volatile nature of uranium hexafluoride has also been studied for application in the reprocessing of irradiated fuels from a nuclear reactor,[1] in the treatment of the ores of uranium,[2] and in the refining of uranium.[3] In the method of fuel reprocessing, called fluoride volatility process, the uranium is fluorinated to volatile hexafluoride and is separated from most of the fission products left as non-volatile fluorides, and then purified by distillation or adsorption-desorption process from the small amounts of other volatile fluorides. In this connection, many studies have been made on the fluorination of various uranium compounds, but only few for the compounds of other metals.

From the thermodynamical point of view, it is evident that all uranium compounds, when heated with fluorine to a reasonable temperature, will give uranium hexafluoride. Ruff and Heinzelman first synthesized uranium hexafluoride by the action of elementary fluorine on uranium metal or uranium carbide in 1909.[4] Katz and Rabinowitch summarized the temperatures required for the fluorination of various uranium compounds, UO_3, U_3O_8, UO_2, UO_2F_2, and UF_4 with fluorine.[5] Large amounts of uranium hexafluoride are produced at present from UF_4 in the United States.[6,7,8] Sharpe et al. found that the interhalogen compounds such as BrF_3 and ClF_3 are also effective fluorinating reagents for making UF_6 from uranium compounds.[9,10] For the fluoride volatility process, studies have been carried on the fluorination process by the research groups in the United States. In the early stage of their studies, liquid bromine trifluoride was considered as a suitable reagent for the fluorination of uranium metal, a nuclear fuel used at that time,[11,12,13] but this fluorination process was given up shortly thereafter because of the difficulty in controlling the reaction rate.[14] Subsequently, with the development of ceramic fuels such as uranium dioxide, the direct fluorination of uranium oxides by fluorine in the fluid-bed system has been investigated on the kilogram scale by the chemical engineering group in Argonne National Laboratory.[15,16,17]

In the fluoride volatility method, we will have to fluorinate the irradiated fuels having a very complex solid system in which transuranium elements and many fission products would be present in the uranium compound, constituting the major

component of the nuclear fuel. Furthermore, since uranium has four oxidation states (+3, +4, +5, and +6), the reaction behavior of uranium compounds would be complex. In general, these fluorination reactions proceed rapidly, dissipating large reaction heats, which cause troubles such as caking of solid powder in the fluid-bed, as often reported, or destruction of the reactor. Thus accumulation of the basic data on the fluorination reactions seems necessary for the developments in this field.

Purpose of the study

The present study was made to obtain information on the fluorination reactions to form volatile fluorides which are related to the process chemistry described above, that is, the fluorination of uranium and its compounds, and bromine (to synthesize bromine fluorides). Most of the studies hitherto made on the fluorination of uranium compounds was done mainly in engineering scale. Then, the reaction behavior will be influenced by the type and scale of the reactor, so that the results obtained will be complicated. An attempt was made in the present work to know as much as possible the basic and absolute nature of the fluorination reactions; such investigations were rather lacking in this field.

Scope of the study

We studied the flurination reactions on the laboratory scale, using mainly a thermobalance. The solid sample was placed in the stream of the reacting gas at a constant flow rate under atmospheric pressure. The reacting gas was diluted with argon to a constant partial pressure. There are various fluorinating reagents such as F_2, ClF, ClF_3, BrF_3, and BrF_5 which, convert the uranium compounds to UF_6. The physical properties of these reagents are summarized in Appendix IV. Fluorine and ClF are gaseous fluorinating reagents, ClF_3 and BrF_5 can be used as either liquid or gaseous fluorinating reagents, and BrF_3 is generally used as liquid fluorinating reagent. We chose elementary fluorine and BrF_3 as the fluorinating reagents in order to examine the fluorination behavior both in gas and liquid phases. The fluorine gas was produced from a cell by electrolysis, and then using this fluorine, the reaction conditions for the production of BrF_3 were studied.

Experiments of the fluorination was made first with tungsten, because the element occupies a position nearest to uranium, among the non-radioactive elements in the periodic table. Then, the fluorination of uranium metal, uranium oxides, and uranium carbides were studied; these substances are

actually used as nuclear fuels at present, or are being developed for the purpose.

Since the fluorinating reagents are very reactive, the use of constructional materials, resistant to these reagents, and the airtightness become necessary in the construction of the experimental apparatus. At the time of start of the present study, we had neither these fluorinating reagents commercially available nor handling technologies of these reagents. Hence, we started with making a system supplying pure fluorine.

The present paper consists of the following five chapters and appendixes.

Chapter I Fluorination of tungsten and uranium by fluorine
Chapter II Fluorination of uranium oxides by fluorine
Chapter III Fluorination of uranium oxides by BrF_3
Chapter IV Fluorination of uranium carbides by fluorine
Chapter V Fluorination of bromine by fluorine
Appendix I Handling of fluorine cell
Appendixes II ~IV Supplementary data

The first chapter deals with the fluorination of tungsten and uranium metals to their hexafluorides by fluorine; the results and technical experiences obtained in these experiments were partly applied to the subsequent works. In the fluorination of various uranium oxides with fluorine, it was found that the reaction behavior depends largely upon the state of solid sample. In particular, in the case of uranium dioxide, the reaction behavior differed depending on whether the sample was in powder or in pellets. These reactions are described in Chapter II. The fluorinations of uranium oxides with liquid BrF_3 proceeded explosively. It was found, however, that the gaseous BrF_3 fluorinates the uranium oxides mildly but more rapidly than fluorine; these reactions are described in Chapter III. Chapter IV reports the fluorination of uranium carbides, UC and UC_2, with fluorine; both the reaction proceeded with the same mechanism. In Chapter V, the reaction between bromine vapor and fluorine is given. Technical problems in the operation of the fluorine cell are described in Appendix I.

Review of the previous studies

The studies hitherto made on the formation reactions of volatile metallic fluorides are mainly for the hexafluoride of uranium; but few for other volatile fluorides.

When this study was started, very few data were available on the direct fluorinations of uranium compounds. Since that time, considerable reports have been published on this problem, and useful informations were obtained

from these reports. The studies will be reviewed below.

Fluorination of uranium oxides by fluorine

In 1958:

Brater and Simley[18] described the batch process of the fluorination of UO_3, U_3O_8, and UO_3 at about 300°C. The oxide powders were converted rapidly to uranyl fluoride, but the subsequent reaction to form uranium hexafluoride was much slower. No quantitative details are given, however. Steindler and Steidl[19,20] fluorinated UO_2 and UO_3 powder in the following conditions: sample weight, 700 to 1700 mg (in a nickel boat); fluorine, 100% at 1 atm.; temperature range, 200° to 375°C. The UO_2 powder was converted to UF_6 through the intermediate UO_2F_2, while UO_3 appeared to be converted without the formation of UO_2F_2. The activation energies are 19.5 and 14.0 kcal/mole for UO_2 and for UO_3 respectively.

In 1960:

Mecham et al.[15,16,17] fluorinated directly the UO_2 pellets in a fluid-bed in the following conditions: pellet sizes, 1 cm × 1 cm dia. and 1/2 in × 1/2 in dia.; pellet charge, 2 to 5 kg; fluid-bed, 3 in dia. with MgF_2 (60 to 100 meshes) powder as the inert fluidizing material; temperature range, 400° to 500°C; fluorine concentration, 10 to 40 vol %; diluting gas, nitrogen. In the reactor, the MgF_2 particles were fluidized and the dense uranium dioxide pellets were submerged in the MgF_2 fluid-bed. X-ray analysis of the fine particles, produced by disintegration of the pellets, showed UO_2F_2 as the major species and U_3O_8 as the minor species. The following two steps reaction was proposed:

$$UO_2 + F_2 \longrightarrow UO_2F_2$$

$$UO_2F_2 + 2\,F_2 \longrightarrow UF_6 + O_2$$

in which the first step proceeds much faster than the second step. Fisher, Jarry, and Baker[21] studied the kinetics of the fluorination of U_3O_8 powder, using a thermobalance, in the reaction conditions: sample weight, 400 mg; temperature range, 300° to 400°C; fluorine, 100% at 1 atm. They found the apparent activation energy to be 30 or 31 kcal/mole.

Fluorination of uranium metal by fluorine

In 1963:

Jarry, Gunther, and Fisher[22] reviewed the fluorination of metal coupons. The reaction conditions are: size of coupon, 10 × 25 × 1.65 (thickness) mm;

temperature range, 300° to 500°C; fluorine, 100% at 1 atm.; flow rate, 50 ml/min. The formation of UF_4 and unknown white intermediate were observed.

Fluorination of uranium metal and oxides by BrF_3

In 1953:

Hoekstra and Katz[23] reported that the various uranium oxides reacted with BrF_3, liberating their combined oxygen.

In 1957 and 1958:

Vogel and Steunenberg[11,12,13] reported the reaction behaviors of the fluorination of uranium metal with BrF_3.

Fluorination of bromine by fluorine

Bromine trifluoride was first produced by Lebeau[24]; by Ruff et al., it was found that there are three bromine fluorides, BrF, BrF_3, BrF_5.[25,26] Bromine monofluoride is too unstable to be isolated in pure state, and is identified only in gas phase by infrared spectroscopy.[27] BrF_3 and BrF_5 were both formed by the gas phase reaction between fluorine and bromine; at temperatures from 20° to 100°C, BrF_3 was mainly formed, and above 200°C BrF_5 was formed.[25,28,29]

References

1) Symposium on the Reprocessing of Irradiated Fuels held at Brussels, May 20 - 25 (1957), TID-7534, Book 2.
Aqueous Reprocessing Chemistry for Irradiated Fuels, Brussels Symposium 1963, ENEA-OECD.
Proc. 1st, 2nd, and 3rd Int. Conf. Peaceful Uses of Atomic Energy Geneva, Vol.9 (1956), Vol.17 (1958), Vol.10 (1965).

2) Lawroski S., et al.; Progress in Nuclear Energy, Series III, Process Chemistry, Vol. 3, pp. 98 - 125 (1961).

3) Geertsma, J. C., et al., PEL-121, Vol. 2 (1965).

4) Ruff, O., Heinzelmann, A., Ber., 42, 495 (1909).

5) Katz, J. J., Rabinowitch, E., The Chemistry of Uranium, National Nuclear Energy Series, Division VIII, Vol. 5, p. 397, Dover Publications INC., New York (1951).

6) Simley, S. H., Brater, D. C., P/525 (1958).

7) Powell, C. A., P/1840 (1958).

8) Lawroski, S., et al., Progress in Nuclear Energy, Series III, Vol. 3, p. 98 (1961).

9) Sharpe, A. G., Emeléus, H. J., J. Chem. Soc., 2135 (1948).
10) Davis, W., Jarry, R. L., U.S.A.E.C. Report, K-849 (1953).
11) Vogel, R. C., Steunenberg, R. K., TID-7534, Symposium on the Reprocessing of Irradiated Fuels, Book 2, Session IV, p. 498 (1957).
12) Steunenberg, R. K., et al., P/539 (1958).
13) Steunenberg, R. K., Vogel, R. C., P/2388 (1958).
14) Strickland, G., Horn, F. L., Johnson, R., BNL-471 (1957).
15) Mecham, W. J., Jonke, A. A., Gabor, J. D., Wehrle, J., ANL-6145, p.103 (1960).
16) Mecham. W. J., Jonke, A. A., Gabor, J. D., Wehrle, J., Gates, J., Rashinskas, A., ANL-6183, p. 98 (1960).
17) Mecham., W. J., Gabor, J. D., Gates, J., Rashinskas, A., Wehrle, J., ANL-6284, p. 147 (1960).
18) Brater, D. C., Smiley, S. H., Process Chemistry, Progress of Nuclear Energy, Series III, 4-4, p. 136 (1958).
19) Steindler, M. J., Steidl, D. V., ANL-5924, p. 28 (1958).
20) Steindler, M. J., Steidl, D. V., ANL-5959, p. 21 (1958).
21) Fisher, J., Jarry, R. L., Baker, T. D., ANL-6725, p. 125 (1963).
22) Jarry, R. L., Gunther, W. H., Fisher, J., ANL-6145 (1960).
23) Hoekstra, H. R., Katz, J. J., Anal. Chem., 25, 1608 (1953).
24) Lebeau, P., Compt. rend., 141, 1018 (1905).
25) Ruff, O., Menzel, W., Z. Anorg. Chem., 202, 49 (1933).
26) Ruff, O., Braida, A., ibid., 214, 81 (1933).
27) Stein, L., J. Am. Chem. Soc., 81, 1273 (1959).
28) Sheft, I., Hyman, H. H., Katz, J. J., Anal. Chem., 25, 1877 (1953).
29) Simons, J. H., Fluorine Chemistry, Vol. 1, p. 191, Academic Press, New York and London (1950).

Chapter I

Fluorination of tungsten* and uranium by fluorine

When studying the fluorination reactions of metals or their compounds to the hexafluorides, experience in handling the gaseous hexafluoride is necessary, because, in general, the metal hexafluorides themselves are highly reactive; for instance, they reacts rapidly with moisture in the air and are converted into the oxy-fluorides. Moreover, in the case of uranium hexafluoride, the safety for the radioactivity must be considered. Thus, the fluorination of tungsten was studied first because of the easiness in handling due to its non-radioactivity and of the resemblance in the physico-chemical properties of tungsten hexafluoride to those of uranium hexafluoride.

1. Fluorination of tungsten metal

Tungsten metal is readily fluorinated to tungsten hexafluoride with fluorine;[1] however, the relationships among the reaction rate, the reaction temperature, the fluorine concentration, and the sample form have not been reported. The present investigation was made to clarify these relationships.

1.1 Experimental method

The most of the fluorination experiments were made in a monel reactor; Fig. I-1 shows the detailed sectional view of the reactor. The sample metal was placed in a monel vessel, hanged at the tip of the thermocouple sheath through the holes located at the vessel wall. This method of setting the sample was to measure and control the reaction temperature as close as possible.

Two other experimental methods were also tried; in one method, the fluorination was performed in a transparent silica tube in order to observe directly a change in appearance of the sample during the reaction; in another method, the continuous measurement of the sample weight during the fluorination was made by using an automatic thermobalance specially constructed for the study.

In all the fluorination experiments, the following procedure was employed. A sample of 300 ~ 500 mg in weight, was used in each experimental run. After the system was evacuated to less than 10^{-5} mmHg, nitrogen was introduced in it to atmospheric pressure, and then the reactor was kept at a desired temperature. Finally, fluorine gas, diluted with nitrogen, was allowed to flow through the system at a constant rate. In several experimental runs, the reaction product was

---

* Published in Kogyo Kagaku Zassi, 65, 1165 (1962).

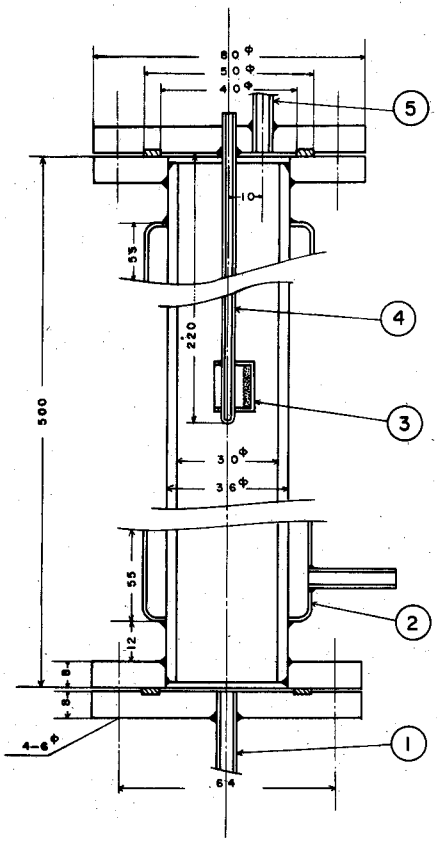

Fig. I-1. Horizontal reactor used for the fluorination of tungsten and uranium metal.
(1) gas inlet, (2) mantle for cooling water, (3) sample vessel, (4) thermocouple sheath, (5) gas outlet.
Materials: all the parts except the cooling water system, monel; packings, daiflon.

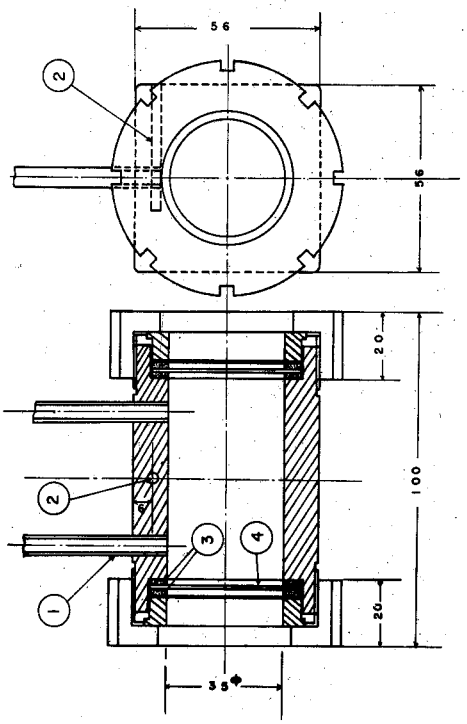

Fig. I-2. Infrared cell for the measurement of gaseous hexafluorides.
(1) inlet and outlet of sample gas, (2) hole for thermocouple, (3) packings (fluorocarbon elastomer), (4) AgCl window (2 mm thick).
Cell body was made of brass and plated with nickel.

collected in a cold trap cooled to -80°C, and then transferred to an infrared gas cell specially made for corrosive gases. Fig. I-2 shows the schematic view of the cell.

Materials

Tungsten metals used are as follows.

Sample	Size	Maker
powder	1.25 microns[a)]	Mitsubishi Kinzoku Kogyo
powder	3.6 microns[a)]	ditto
powder		Kanto Kagaku
rod	2 mm in dia., 5 mm in length	

a) measured by Fisher's sub-sieve sizer.[2)]

Figure I-3 shows the microphotographs of powder samples taken by an electron microscope.

Fluorine gas was used after removal of its hydrogen fluoride contained by the method described in Appendix I.

Nitrogen with purity more than 99.9 mole %, was used after purification by passage through a copper net, heated at about 900°C, and through a bed of phosphor pentoxide to reduce the contents of oxygen and water respectively.

1.22 Results and discussion

An attempt was first made to obtain approximate information on the reaction behavior by observing directly the reaction which proceeds in a transparent silica tube. At temperatures below 300°C, the silica tube could be used as the reactor material under fluorine atmosphere without corrosion. Tungsten powder was spread on an alumina boat to a thin layer, and fluorine gas was passed at a constant flow rate. When the reaction temperature was raised gradually, the reaction began with inflammation at a temperature and a white smoke was generated at the same time. In Table I-1, the inflammation temperatures are listed for the different reaction conditions.

Table I-1. Influence of fluorine concentration on the inflammation temperature of tungsten powder (Kanto Kagaku).

Fluorine flow rate (l/h)	Nitrogen flow rate (l/h)	Total gas flow rate (l/h)	Fluorine conc. (vol. %)	Inflammation temperature (°C)
8.0	10	18.0	45	30
3.9	15	18.9	21	30
2.2	15	17.2	13	170

Mitsubishi 3.6 microns

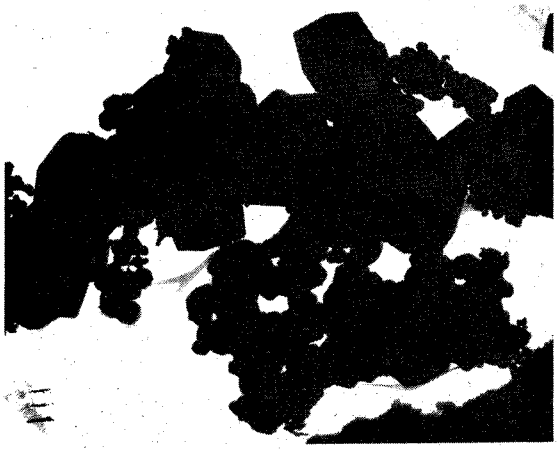

Kanto Kagaku

Mitsubishi 1.25 microns

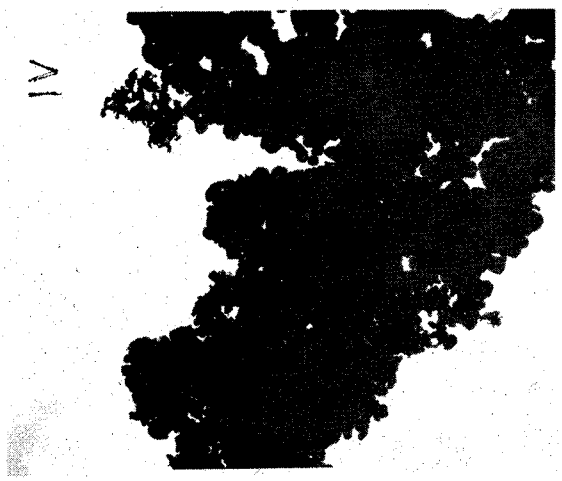

Kanto Kagaku, heat-treated in hydrogen

x 7000

Fig. I-3. Electron microphotographs of tungsten powders.

1, Mitsubishi Kinzoku, 3.6 microns.[a)]

2, Kanto Kagaku.

3, Mitsubishi Kinzoku, 1.25 microns.[a)]

4, Kanto Kagaku, heated to 800°C for 1 hour in a stream of hydrogen.

a) measured by Fisher's sub-sieve sizer in Mitsubishi Kinzoku.

In order to know the reaction behavior more quantitatively, the weight change of sample during fluorination was measured with the automatic thermobalance. From 350 to 400 mg sample was set in the thermobalance. The fluorine diluted with nitrogen was allowed to flow and the temperature was raised gradually. Fig. I-4 shows the temperature dependence of the weight change. At lower temperatures, in the early stage of each experimental run, no change in the sample weight occurred. With increase in the temperature, a small weight decrease began to take place, and the rise of temperature was accelerated, because of generation of the reaction heat; finally, the temperature rose rapidly up to 200°C for the powder sample and up to 300°C for the rods. At these temperatures, the weight of sample began to decrease rapidly. As seen in Fig. I-4, the reaction behavior was not influenced by fluorine concentration, but it depended largely upon the state of sample, i.e., powder and rod in the present case. The reaction rate was very small below 200°C for the powder sample and below 300°C for rod sample, and even if the inflammation occurred in these temperature range, the reaction did not proceed continuously. At the temperature of 200°C (for powder sample) and of 300°C (for rod sample), the reaction rate increased rapidly with self-inflammation. There were some drawbacks in the thermobalance; low degree of its evacuation, the hexafluoride depositing on the weighing mechanism, and the disintegration of the hexafluoride deposit to lower fluorides. Therefore, the reactor shown in Fig. I-1 was mainly used for the study; the reaction rate was measured by intermittent weighing of the sample, set in the reactor. In typical experiments, the fluorine concentration was 13 volume %, and the total gas flow rate was 23 l/h. After the reaction for 5 minutes, the gas supply was stopped, the reactor was cooled to room temperature under a flow of nitrogen, and the sample was taken out from the reactor and weighed. Figure I-5 shows the change in the reaction rate vs. the time. The reaction rates of various powders were different in the early stage of the reaction, but their values tended to converge to certain values with the advance of the reaction. The powder from Kanto Kagaku, reduced with hydrogen before use, was apparently the most finest in particle size as shown in Fig. I-3, but its reaction rate was the lowest. Consequently, the rate does not seem to be related with the particle size. On the contrary, it was found that the adsorption surface area of sample powder is almost in a linear relationship with the reaction rates as shown in Fig. I-6. This relationship may be applied for measuring in advance the powder's reactivity for the fluorination.*

* A similar relationship was also found for the fluorination of U_3O_8 powders, as will be described in Chapter II.

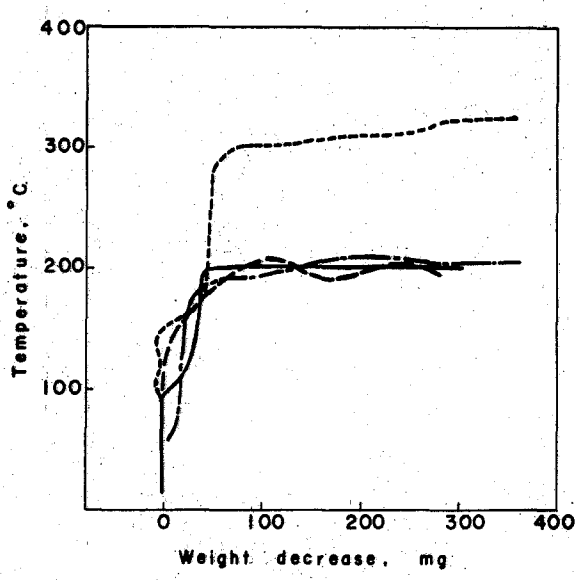

Fig. I-4. Temperature dependence of the weight decrease in the fluorination of tungsten.

F_2 flow rate	kinds of sample
——, 0.7 l/h – – –, 1.4 l/h — · —, 2.1 l/h	tungsten powder from Kanto Kagaku;
----, 2.1 l/h	tungsten rod, 2 mm in dia., 3 mm in length.

Fluorine was diluted with nitrogen, 5.0 to 6.0 l/h in flow rate.

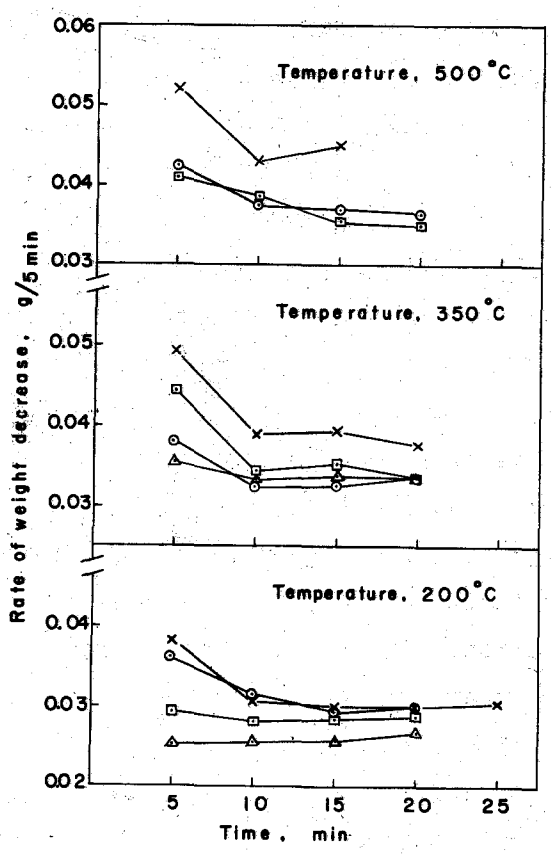

Fig. I-5. Change in reaction rates with reaction time.
×, Mitsubishi 1.25 microns;
⊙, Mitsubishi 3.6 microns;
⊡, Kanto Kagaku; △, Kanto Kagaku, heat-treated in hydrogen. Fluorine concentration, 13 vol. %; total gas flow rate, 23 l/h; diluting gas, nitrogen.

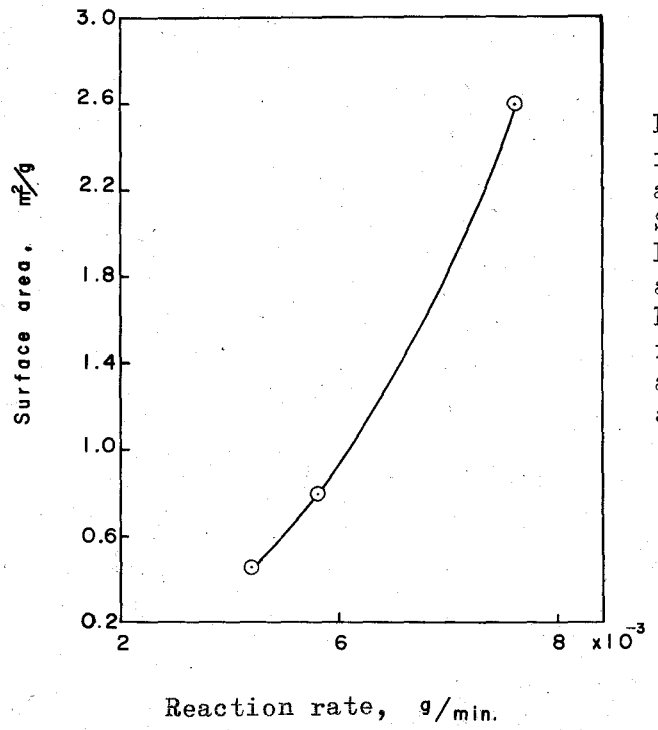

Fig. I-6. Relationship between fluorination rate and surface area of tungsten.
Surface area was measured by B.E.T. method; nitrogen was adsorbed at -195.8°C.
Reaction rates were calculated from the plots at 5 minutes after the start of the reaction at 200°C in Fig. I-5.

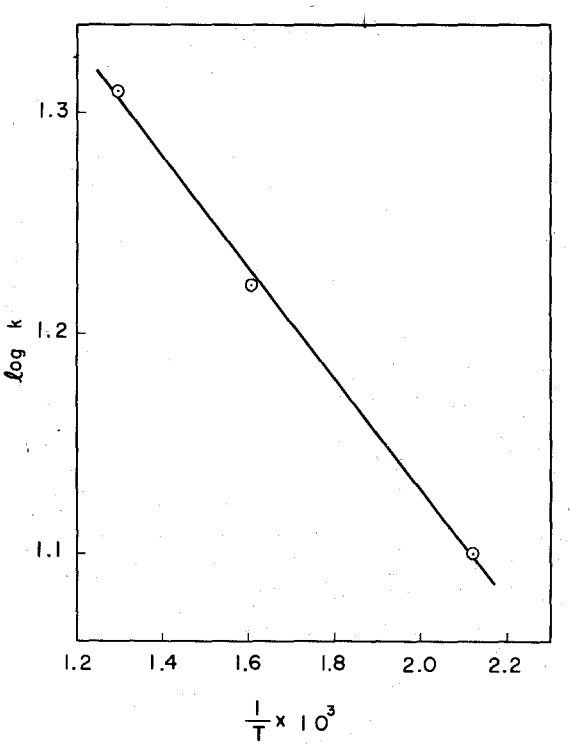

Fig. I-7. Temperature dependence of the reaction rate in the fluorination of tungsten powder.
Sample, Mitsubishi 3.6 microns; flow rate of nitrogen, 20 l/h; flow rate of fluorine, 3 l/h.

There was no evidence for the formation of solid intermediates in the appearance during the reaction of the solid samples. Electron diffraction patterns also confirmed non-formation of intermediates. The apparent activation energy of the reaction was 0.5 kcal/mole for the sample of 3.6 microns in particle size, using the values of the reaction rates at the time of 10 minutes in Fig. I-5; as the reaction rate became almost constant after 10 minutes, the values at 10 minutes were considered to be reliable. Fig. I-7 shows the Arrhenius plot of these reaction rates.

2. Fluorination of uranium metal

The uranium metal chips were used as the sample, because of the ease of obtaining in pure metal, and of the safety of their handling. Uranium metal powder was not used, because uranium metal powder with a large surface area is readily inflammable in air with a mechanical shock and, if not so, it gradually oxidizes in air at room temperature to a considerable degree. There was no essential difference in the experimental method between the fluorination of tungsten and that of uranium, except more cautious operation necessary in the latter.

2.1 Experimental method

Most of the apparatus and experimental procedure were similar to those used in the fluorination of tungsten metal. The sample was placed in an alumina boat, hanged at the tip of the thermocouple sheath. The uranium hexafluoride produced was trapped by chemisorption in a sodium fluoride bed kept at about 100°C. Thus, the amount of uranium hexafluoride produced during the run was traced by measuring the weight increase of this trap intermittently. The typical reaction conditions were as follows:

fluorine concentration, 12 volume %;
fluorine flow rate, 1.4 l/h;
argon flow rate, 10.0 l/h;
total gas flow rate, 11.4 l/h;
reaction temperatures, 100° ~ 400°C;
initial sample weight, 1.5 ~ 2.0 grams.

Materials

Uranium metal chips, 0.2 mm thick, 5 mm long, and 3 mm wide, were used. The purity of the metal was over 99.9 weight %. The impurities were: B, < 0.25; P, 62; Mn, 8; Cr, < 8; N, < 100; Cu, 23; Ag, 0.8; Si, 20; Fe, < 100; Mo, < 4; V, < 10; Cd, 0.5 —— in ppm.

Argon gas was used for most of the experiments as the diluting gas of fluorine, because it is completely inert for fluorine at any conditions. Nitrogen was used also as diluting gas in some experiments, to compare the reaction behaviors in both cases. Argon and nitrogen were purified by the method described in section 1.1 in this chapter. Fluorine gas was used after purification by the method described in section 7, Appendix I.

2.2 Results and discussion

Figure I-8 shows the weight change curves at given temperatures. In 100°C, the weight increase was a little, and the fluorination up to uranium hexafluoride was not observed. In 160°C, the metal chips were largely pulverized to a greyish black powder, and the hexafluoride was a little formed. With above 210°C inclusive, the fluorination to UF_6 took place and the sample weight decreased to 10% in about one hour.

Soon after fluorine gas was introduced in the reactor, the reaction temperature began to rise and then one to three peaks in temperature rise were observed. The reproducibility in the peak form or in the number of peak was not good. The figures I-9, I-10, and I-11, each, show the change in sample weight, the cumulative amount of hexafluoride produced during the reaction, and the deviation in reaction temperature from the initially-set temperature, In Fig. I-10 and I-11, there are two peaks in temperature rise, and in the curves for the weight change and the hexafluoride production, induction periods are seen: during this period, the weight of sample increased a little, whereas the hexafluoride was not much formed. The first peak of temperature rise is evidently found in the region of the induction period, which indicates that the first peak is attributed to the reaction heat to form non-volatile reaction intermediates. The second peak seems to correspond to the fluorination step of the intermediates to uranium hexafluoride; in the region of the second peak, a rapid decrease of sample weight takes place. In the fluorination at 160°C (Fig. I-9), three peaks are seen; the correspondence between peak and reaction step is vague. The reaction intermediates formed differed in color with the reaction temperature and also with the reaction time, as summarized in Table I-2. By X-ray analysis, it was confirmed that the green intermediate was UF_4 and the white one UO_2F_2, At temperatures from 100° to 160°C, a black intermediate was generally formed. From this result, the formation of black fluoride, UF_3, may be assumed, but its X-ray diffraction pattern was an unknown one. Towards the end of the reactions at high temperatures, the white intermediate, UO_2F_2, was produced on the layer of green intermediate, UF_4. Oxygen, contained in the fluorine

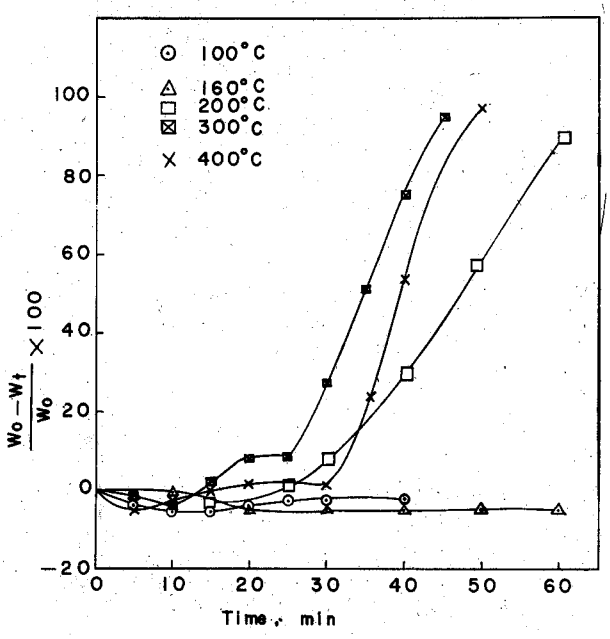

Fig. I-8. Weight change in the fluorination of uranium metal at different temperatures. Fluorine concentration, 12 vol. %; total gas flow rate, 11.4 l/h; diluting gas, argon; W_o, initial weight weight of sample; W_t, sample weight ~~at~~ at time t.

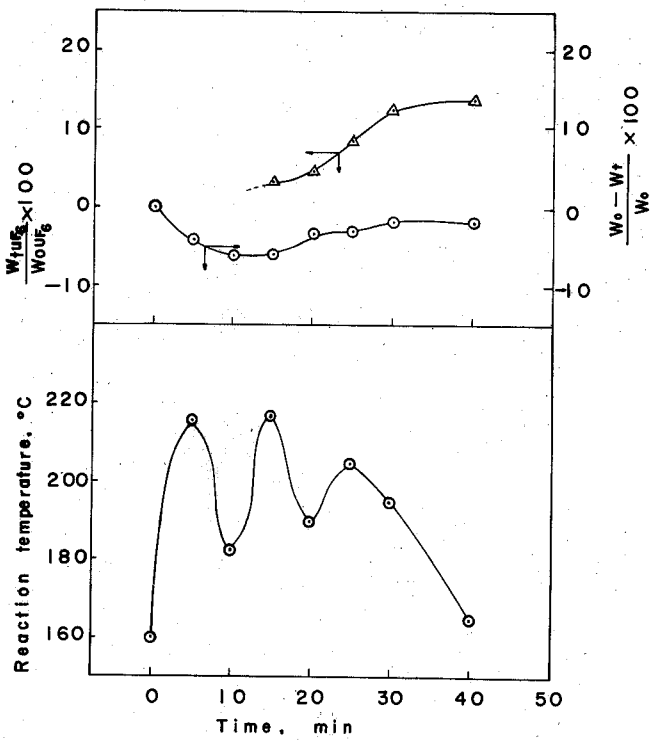

Fig. I-9. Percentage of UF_6 produced, percentage of change in the sample weight, and change in the reaction temperature during the fluorination of uranium metal. Initially-set temperature, 160°C; fluorine concentration, 12 vol. %; diluting gas, argon; total gas flow rate, 11.4 l/h; W_o, initial weight of sample; W_t, sample weight at time t; $WtUF_6$; total weight of UF_6 produced during the reaction time t;

$$W_{oUF_6} = \frac{\text{mol. weight of } UF_6}{\text{atomic weight of U}} \times W_o.$$

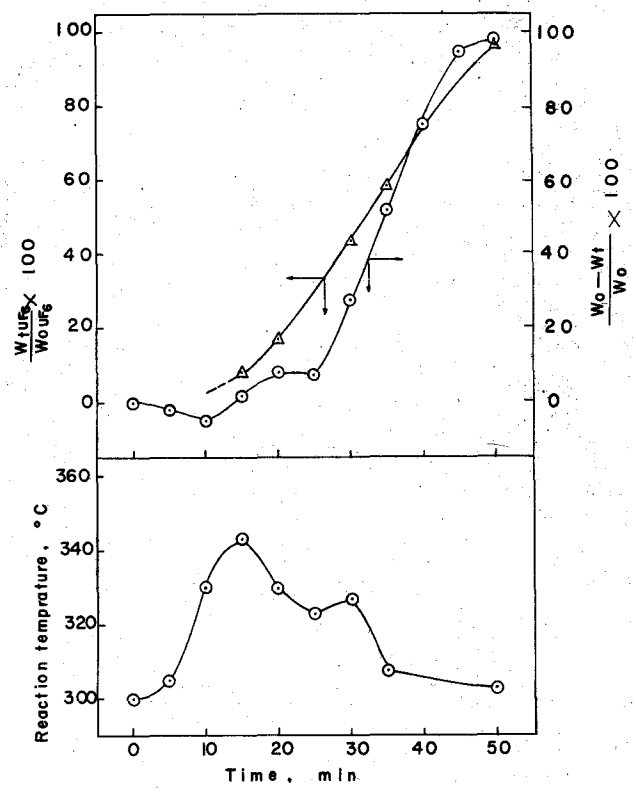

Fig. I-10. Percentage of UF_6 produced, percentage of change in the sample weight, and change in the reaction temperature during the fluorination of uranium metal. Initially-set temperature, 300°C; other reaction conditions and units of the ordinates are the same with those in Fig. I-9.

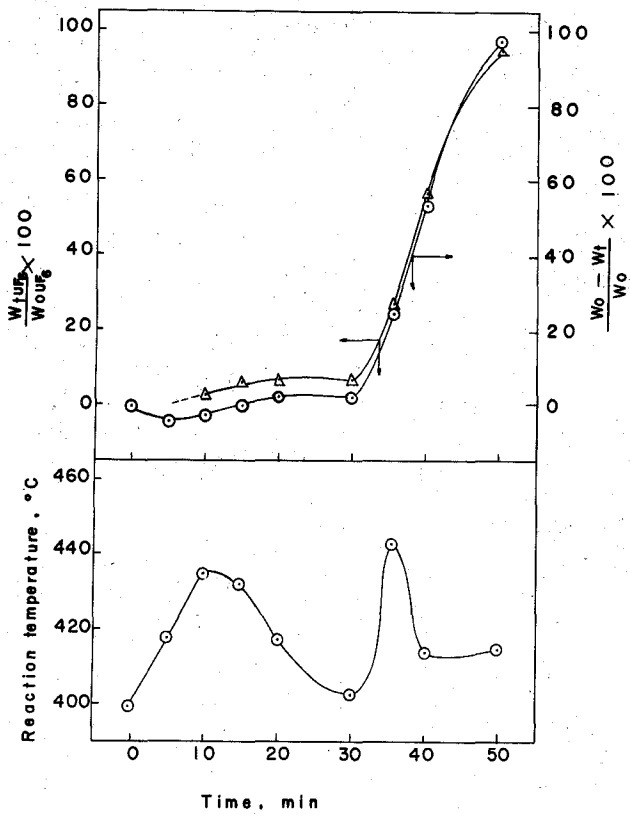

Fig. I-11. Percentage of UF_6 produced, percentage of change in the sample weight, and change in the reaction temperature during the fluorination of uranium metal. Initially-set temperature, 400°C; other reaction conditions and units of the ordinates are the same with those in Fig. I-9.

Table I-2. Colors of reaction intermediates.

Temp.(°C) \ Time(min.)	10	20	30	40	50
100	black 0.5*	black 5	black 5	black, partly green 5	
160	green 6.1	black, partly white 3.4	greyish black 2.1	greyish black 2.8	
300	green 4.5	green partly white 8.0	greenish yellow 27.5	white 75	white 98

* Numerical values: percent in weight-change.

gas and also in the sample itself as an oxide or adsorbed gas, may be the source for the oxygen in the intermediate, UO_2F_2.

The effect of fluorine concentration on the reaction rate is shown in Fig. I-12. It shows that with high fluorine concentration, the induction period becomes short, but there is no difference in the rate of weight decrease after the induction periods.

From the results described above, the following consecutive steps may be assumed:

$$U + F_2 \longrightarrow UF_3 \text{ to } UF_{4-x} \qquad (1)$$

$$UF_3,\ UF_{4-x} + F_2 \longrightarrow UF_4 \qquad (2)$$

$$UF_4 + F_2 \longrightarrow UF_6 \qquad (3)$$

The curves in Fig. I-12 indicate that the rate of steps (1) and (2) is more dependent on the fluorine concentration than that of step (3). The reaction behavior is so complicated, as shown in Fig. I-8, that the measurement of each reaction rate in the above steps is difficult, and the rate determining step for the overall process cannot be clarified.

In several experiments, nitrogen was used as diluting gas. The reaction behavior was similar to that in the case of dilution with argon.

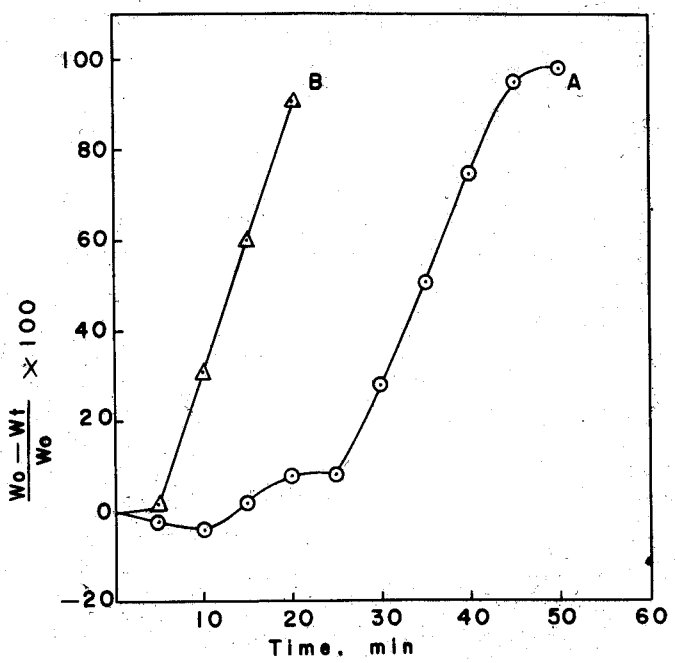

Fig. I-12. Effect of fluorine concentration on the fluorination of uranium metal.
Initial set temperature, 300°C; total gas flow rate, 11.4 l/h; fluorine concentration, 12 vol. % for A and 23 vol. % for B; W_o, initial weight of sample; W_t, sample weight at time t.

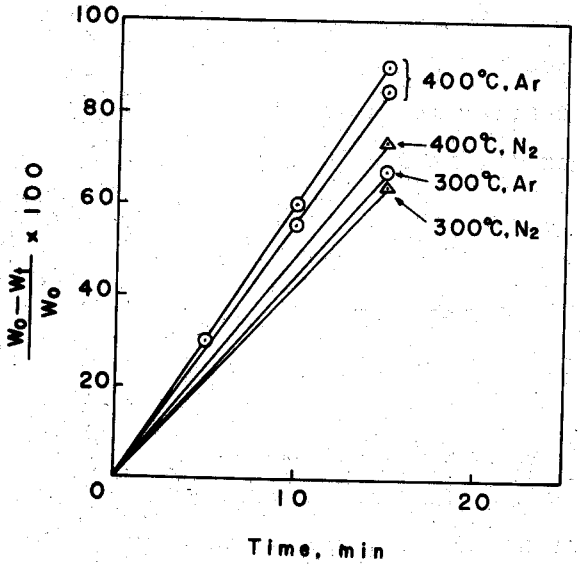

Fig. I-13. Effect of diluting gas on the rate of fluorination reaction of uranium metal.
Fluorine concentration; 23 vol. %; total gas flow rate, 13 l/h; W_o, initial weight of sample; W_t, sample weight at time t; ⊙, diluted with argon; △, diluted with nitrogen.

However, the production rate of UF_6 at 300° and 400°C was a little smaller when fluorine was diluted with nitrogen than when diluted with argon. The amount of UF_6 produced vs. time is plotted in Fig. I-13 for the cases at 300° and 400°C. This result suggests that fluorine may be partly consumed to form nitrogen fluoriders*, and also to form nitrogen oxyfluorides** when oxygen is contained in the reaction system as an impurity.

3. Summary

Fluorination of tungsten to tungsten hexafluoride

Powder or rod smaples, 300 ~ 500 mg in each run, was fluorinated by fluorine diluted with nitrogen.

1) Temperature dependence of the reaction
   Below 60°C: the reaction did not proceed.
   Between 100° and 180°C: the reaction rate became increasingly larger; for powder samples, the reaction began to proceed rapidly at 200°C, with inflammation, whereas for rod samples, this temperature was 300°C.
2) The reaction rate was nearly proportional to the adsorption surface area of a sample.
3) The formation of solid intermediate was not observed.
4) The reaction rate was not much influenced by fluorine concentration.

Fluorination of uranium to uranium hexafluoride

Uranium chips, 1.5 ~ 2.0 g in each run, were fluorinated by fluorine diluted with argon (in some experiments, diluted with nitrogen).

1) Temperature dependence of the reaction
   Between 100° and 160°C: the reaction proceeded somewhat, but uranium hexafluoride was not formed.
   Between 200° and 400°C: the fluorination to hexafluoride proceeded rapidly after an induction period.
2) Occurrence of the induction period was due to the formation of intermediates such as UF_3 (assumed from the color of intermediates, but not confirmed by X-ray analysis), UF_4, and UO_2F_2 (oxygen seemed to be supplied as an impurity).
3) The induction period decreased with increasing fluorine concentration.

---

* NF_3, NF_2, N_2F_2, and N_3F are known.

** FNO, and FNO_2 are known.

4) When fluorine was diluted with nitrogen, the reaction rate decreased a little; this result suggests that a nitrogen-fluorine compound is partly formed during the fluorination.

References

1) Simons, J. H., Fluorine Chemistry, Vol. I, p. 113, Academic Press, Inc., New York (1950).

2) Mitsubishi Kinzoku Kogyo Co., Instruction Manual for Tungsten Powders, Sept. (1960).

3) Kemmit, R. D. W., Sharp, D. W. A., Advances in Fluorine Chemistry, edited by Stacey, M., Tatlow, J. C., Sharpe, A. G., Vol. 4, pp. 189 ~ 196, Butterworths, London (1965).

Chapter II

Fluorination of uranium oxides by fluorine*

Uranium oxides, UO_2, U_3O_8, and UO_3, are fluorinated to UF_6 by fluorine.[1] The fluorination of uranium dioxide pellets by fluorine was investigated in an engineering scale in the United States, and when 20 to 30 weight % of initial charge of UO_2 pellets was fluorinated to UF_6, the formation of a small amount of UO_2F_2 was observed.[2,3,4] In the experiments by the authors, all the fluorination of uranium oxides to UF_6 were found to proceed through the intermediate, UO_2F_2. Thus, the overall reactions appear to consist of the following two steps:

$$\left.\begin{aligned} &UO_2 + F_2 \longrightarrow UO_2F_2 + 140 \text{ kcal/mole}, \\ &\tfrac{1}{3}U_3O_8 + F_2 \longrightarrow UO_2F_2 + \tfrac{1}{3}O_2 + 114 \text{ kcal/mole}, \\ &UO_3 + F_2 \longrightarrow UO_2F_2 + \tfrac{1}{2}O_2 + 107 \text{ kcal/mole}, \end{aligned}\right\} \quad \text{(a)}$$

$$UO_2F_2 + 2F_2 \longrightarrow UF_6 + O_2 + 106 \text{ kcal/mole}. \quad \text{(b)}$$

This chapter reports in details the fluorination of the uranium oxides in powder and then that of oxides in pellets. In the Appendix IV, the physical properties of uranium oxides and uranyl fluoride are summarized.

1. Fluorination of uranium oxide powders by fluorine

1.1 Reaction between gas and solid in powder

The behavior of the gas-solid reaction will largely depend on the state of solid materials, especially on the surface state. Since the powder substance consists of fine particles, very complicated in shape, distribution of size, and surface state, its reaction behavior cannot strictly be expressed in simple mathematical equation. In the reaction systems of ordinary experiments, the particles of powder are in a mass. In this case, the reaction behavior may be treated by the following two points of view: that is, macroscopic view of the reaction —— the reaction is treated as that of a collective mass of fine particles; and microscopic view —— it is concerned with single particles.

---

* Published in J. Inorg. Nucl. Chem., 26, 1853 (1964), 26, 1863 (1964), and J. Nucl. Mat., 25, 216 (1968).

1.1.1 Macroscopic view of the reaction

When the powder is placed in the form of a layer, in the reaction system for example, the assumed steps involved in the reaction between gas and the powder are:

(s-1) transport of the reacting gas to the surface of the powder layer;

(s-2) transport of the reacting gas into the powder layer;

(s-3) chemical reaction with the particles of powder;

(s-4) transport of the gaseous reaction products away from the powder layer.

Of these steps, only the step of (s-3) is related to the chemical change, whereas the others to physical processes, such as transfer or diffusion of materials.

Each step listed above will be affected by some of the following factors:

(f-1) properties of solid powder;

(f-2) temperature;

(f-3) concentration of reacting gas;

(f-4) flow rate of reacting gas.

By allowing the reacting gas to flow sufficiently and by minimizing the thickness of the powder layer, the differences in the reacting gas concentration at outer and inner parts of the powder layer are reduced and the effect of diffusion in the transport processes of steps (s-1) and (s-2) on the overall reaction rate is diminished. Consequently, the reaction rate is not affected by factor (f-4) and may be expressed by the following equation which contains only the factors (f-1), (f-2), and (f-3).

$$r = A \exp\left(-\frac{E}{RT}\right) p^n, \qquad (1)$$

where r is the reaction rate, A is the term related to the properties of solid powder and frequency factor, E is the apparent activation energy, p is the partial pressure of reacting gas, and n is a constant.

In general, the solid-gas reaction occurs on the reacting surface which moves into the inner part of the solid phase leaving the reaction products behind on the reacting surface. The rate of movement of the reacting surface is usually used to measure the rate of reaction. The amount of this movement of the reacting surface is usually used to measure the rate of reaction. The amount of this movement can be calculated from the weight of solid sample; the calculation method for solid particles will be given below.

1.1.2 Microscopic view of the reaction ——the models of the reaction between single particle and gas

Several investigators have presented the models of the reaction of solid particles, related to the chemical change of step (s-3) in the preceding section.[5,6,7] In all the cases, the following assumptions have been made to simplify the mathematical treatment:

(a) particle is spherical;

(b) particle has the same radius;

(c) reaction proceeds from the surface of particle to the center of particle;

(d) reaction proceeds at the surface of unreacted core in the particle.

Then, the reaction in a solid particle can schematically be shown by Fig. II-1; the reacting surface moves into the solid particle, leaving behind converted materials, and radius of the unreacted core r_t decreases with the reaction.

For the reaction in a particle also, steps similar to those listed in the preceding section, will occur consecutively, and therefore step (s-3) mentioned in the previous macroscopic view of the reaction is further divided into the following steps.

(s-3-1) penetration and diffusion of reacting gas through the products layer (B phase in Fig. II-1) to the surface of the unreacted core (C in Fig. II-1);

(s-3-2) chemical reaction on the surface of the unreacted core;

(s-3-3) diffusion of gaseous reaction products through the products layer back to the surface of the solid particle.

If the reaction is irreversible, step (s-3-3) does not contribute directly to the reaction rate, and step (s-3-1) or (s-3-2) controls the overall reaction; that is, called diffusion control or chemical reaction control.

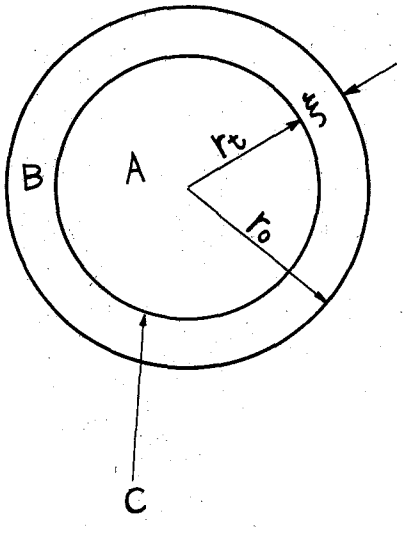

Fig. II-1. Sectional view of spherical particle during reaction.
A, unreacted core; B, layer of solid product; C, reacting surface; r_o, initial radius of the particle; r_t, radius of the unreacted core at time t; ξ, thickness of the product layer.

Diffusion control

In the reaction between fluid and solid plane, if the reaction rate is controlled by the diffusion of the reactant through the product layer, the kinetic equation, called the parabolic law,[5] is derived as described below.

When a reacting gas diffuses into the product layer under a steady state, the difference in concentration of the reactant between the outside bulk atmosphere and the inner reaction surface becomes constant, so that the rate of formation of the product layer is given by

$$\frac{d\xi}{dt} = k_1 \frac{\Delta C_g}{\xi} \qquad (2)$$

where ΔC_g is the difference in concentration of the reacting gas between the both sides of the product layer, ξ is the thickness of the product layer, k_1 is the reaction rate constant, and t is the reaction time. By integrating equation (2),

$$\xi^2 = k_2 t, \qquad (3)$$

where $k_2 = 2 k_1 \Delta C_g$. Jander applied equation (3) for the reaction of spherical particles in the manner of approximation.[5] When the fraction F is defined by the following equation,

$$F = \frac{v_o - v_t}{v} = \frac{r_o^3 - r_t^3}{r_o^3}, \qquad (4)$$

the thickness of the product layer ξ shown in Fig. II-1 is given by

$$\xi = r_o - r_t = r_o \left[1 - (1-F)^{1/3} \right], \qquad (5)$$

where v_o is the initial volume of the particle, v_t is the volume of the unreacted core at time t, r_o is the initial radius of the particle, and r_t is the radius of the unreacted core at time t. From equations (3) and (5),

$$\left[1 - (1-F)^{1/3} \right]^2 = k_3 t^{*}, \qquad (6)$$

where $k_3 = k_2 / r_o^2$. Since all the particles have the same radius, F can be calculated by the following equation:

$$F = \frac{m_o - m_t}{m_o (1-\alpha)} = \frac{M_o - M_t}{M_o (1-\alpha)}, \qquad (7)$$

where m_o is the initial weight of the particle, m_t is the weight of the particle at time t, M_o is the initial weight of the sample, M_t is the weight of sample at time t, and

---

* Equation (6) is called Jander's equation, and the kinetics expressed by eq. (6) is called parabolic law.

$$\alpha = \frac{\text{molecular weight of the solid product}}{\text{molecular weight of the original solid}} .$$

Strictly speaking, diffusion through a plane layer differs from that through a spherical layer; in the latter case under steady state, instead of equation (2) the rate of the formation of product layer must be expressed by

$$\frac{d\xi}{dt} = k_1 \, r_t \, r_{out} \, \frac{\Delta C_g}{\xi} \qquad (8)$$

where r_{out} is the radius of the product layer at the outer surface.[8] When the kinetic equation is derived by using equation (8), its form becomes complicated. To the contrary, the Jander's equation is simple and useful for practical problems.

Chemical reaction control

In the case of the chemical reaction control, shrinkage rate of the unreacted core (phase A in Fig. II-1) becomes constant:

$$\frac{dr_t}{dt} = k_4 . \qquad (9)$$

Therefore, decreasing rate in the volume of the unreacted core is given by

$$\frac{dv_o}{dt} = k_4 S_t = k_4 \, 4\pi r_t^2 , \qquad (10)$$

where S_t is the surface area of the unreacted core at time t and k_4 is the shrinkage rate of the unreacted core. When v_t and r_t are expressed by the fraction F,

$$\frac{d\frac{4}{3}\pi r_o^3 (1-F)}{dt} = -k_4 \, 4\pi r_o^2 (1-F)^{2/3} \qquad (11)$$

By integrating equation (11),

$$1 - (1-F)^{1/3} = k_5 \, t , \qquad (12)$$

where $k_5 = k_4 / r_o$. The reactions expressed by equation (12), are said to follow the linear law.[6] If the products are all gaseous and the solid products layer is not formed on the particle,

$$F = \frac{v_o - v_t}{v_o} = \frac{m_o - m_t}{m_o} . \qquad (13)$$

As each particle has the same radius by the assumption described previously,

$$F = \frac{M_o - M_t}{M_o} \qquad (14)$$

The reaction rate constants k_s and k_b in equations (6) and (12) may be expressed in a similar form to equation (1), i.e.,

$$k_s \text{ or } k_b = A_s \exp\left(-\frac{E}{RT}\right) p^n$$

where A_s is a constant related to the state of reacting surface.

Application to the fluorination reactions of uranium oxides

In the fluorination reaction of uranium oxides to UF_6, the final reaction products are all gaseous, so that the fraction F can be calculated by equation (14). The plot of $(1 - F)^{1/3}$ vs. t will give a linear relationship, and the reaction rate k_5 will be calculated from the slope of the straight curve. Labaton and Johnson observed that the fluorination reaction of UF_4 to UF_6 with fluorine follows the linear law.[9] Jarry and Baker reported that the fluorination of U_3O_8 also proceeds with the linear law.[10]

The fluorination reactions of uranium oxides to UF_6, however, are not simple in actuality, because the solid intermediate, UO_2F_2, is produced. A deviation from the linear law will occur according to where the rate determining step is. Even in this case, by analyzing qualitatively the form of deviation, the true mechanism of the reaction may be deduced, with the aid of the results from X-ray or chemical analysis of the solid residue, and a more suitable equation than equation (12) may be derived for expressing the reaction behavior.

1.2 Apparatus and experimental method

1.2.1 Apparatus

A thermobalance with a silica spring, mounted in a pyrex glass mantle, was used for measuring the weight change during the fluorination reaction. The view of the whole system, the thermobalance, the monel reactor, and the sample vessel, are shown in Figs. II-2, II-3, II-4, and II-5, respectively.

The cautions taken in construction of the apparatus were:

(i) gas tightness of the apparatus;

(ii) accuracy in the measurement of sample weight during the reaction,

(iii) accuracy in the measurement of reaction temperature of sample.

(i) Tightness of the apparatus

Gas tightness of the apparatus is necessary for avoiding the hydrolysis of UF_6 in the apparatus. In the parts where fluorine and UF_6 were kept near room temperature, the pyrex glass tubes and the ordinary vacuum glass cocks with a fluorogrease were used. To connect a metal tube to a glass tube, the method of Wilson seal with a packing of fluorocarbon-elastomer was used, as shown in Fig. II-4. The apparatus could be evacuated to the order of 10^{-5} mmHg.

(ii) Measurement of sample weight

The weight change of sample was measured by a silica spring, of which elongation was measured with a cathetometer. The silica spring was of about 100 turns and 15 mm in its diameter, and could bear a weight up to 7 grams. Its sensitivity was about 0.03 g/mm-elongation; the weight change of 0.003 g could be measured. The temperature around the spring was always near room temperature without being affected by the temperature of the reactor, so that the change in sensitivity of spring seemed to be negligible. At room temperature, the spring was resistant to fluorine gas.

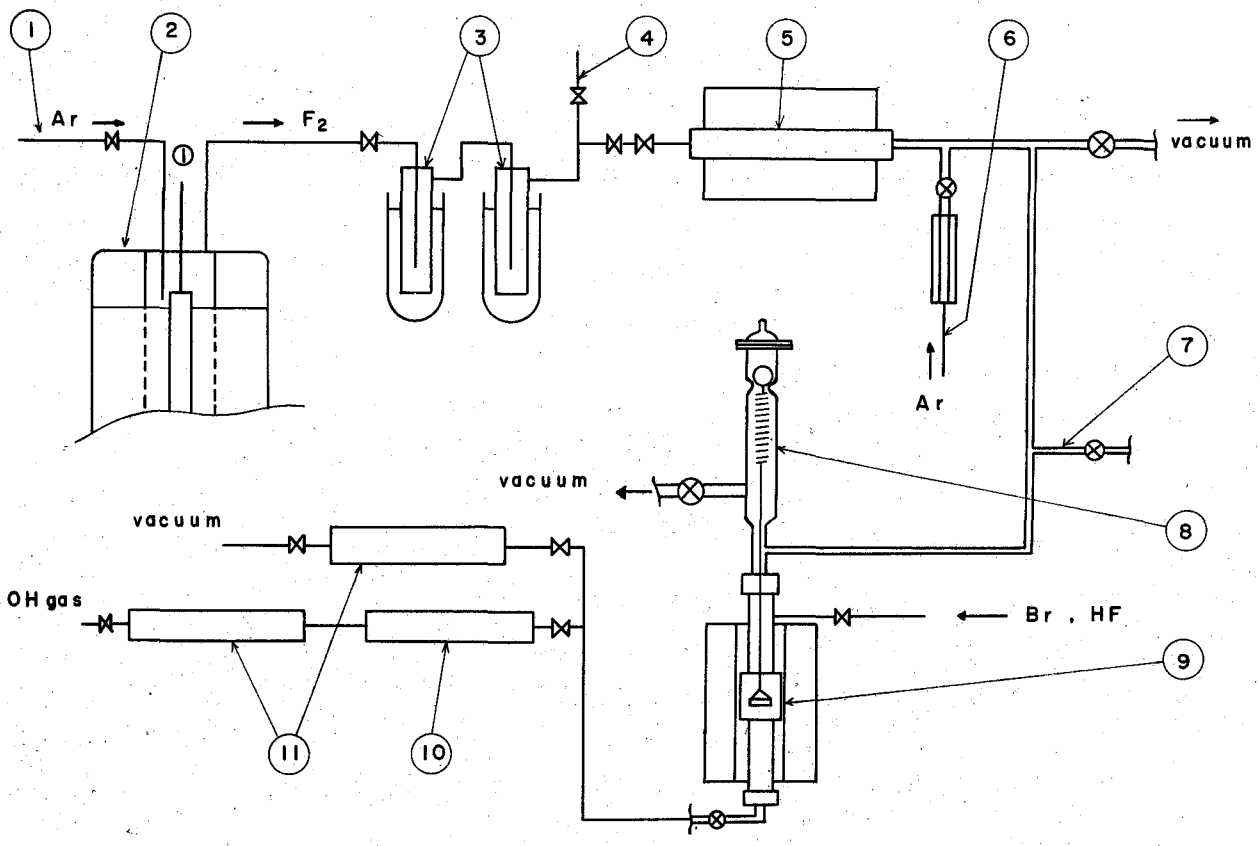

Fig. II-2. Schematic diagram of system used for the fluorination by fluorine gas.
(1), line for purging the cell chamber with inert gas; (2), fluorine cell; (3), traps cooled to -80°C with dry ice and trichlorethylene; (4), outlet of fluorine gas; (5) sodium fluoride bed for adsorbing hydrogen fluoride; (6), line for introducing argon as diluent; (7), line to manometer; (8), glass column for mounting silica spring; (9), monel reactor; (10), sodium fluoride bed for adsorbing uranium hexafluoride; (11), soda-lime bed for adsorbing fluorine in exhaust gas.

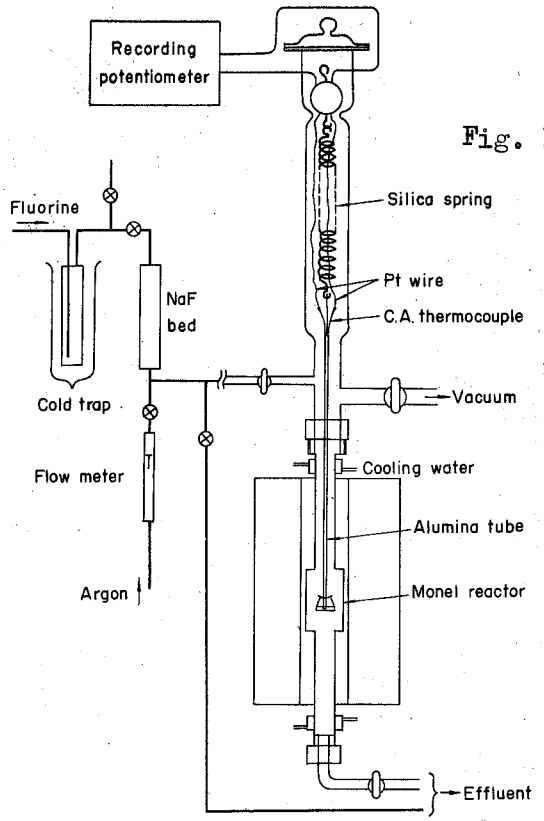

Fig. II-3. Schematic diagram of thermobalance.

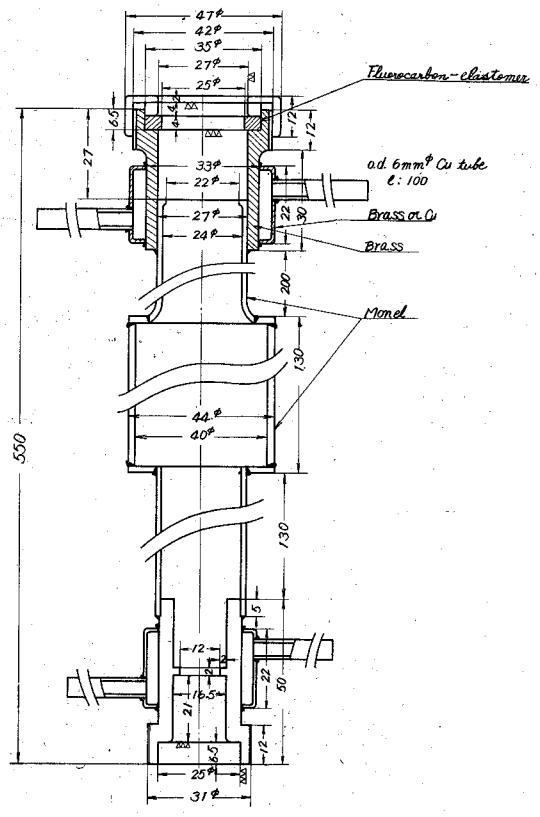

Fig. II-4. Sectional view of monel reactor.

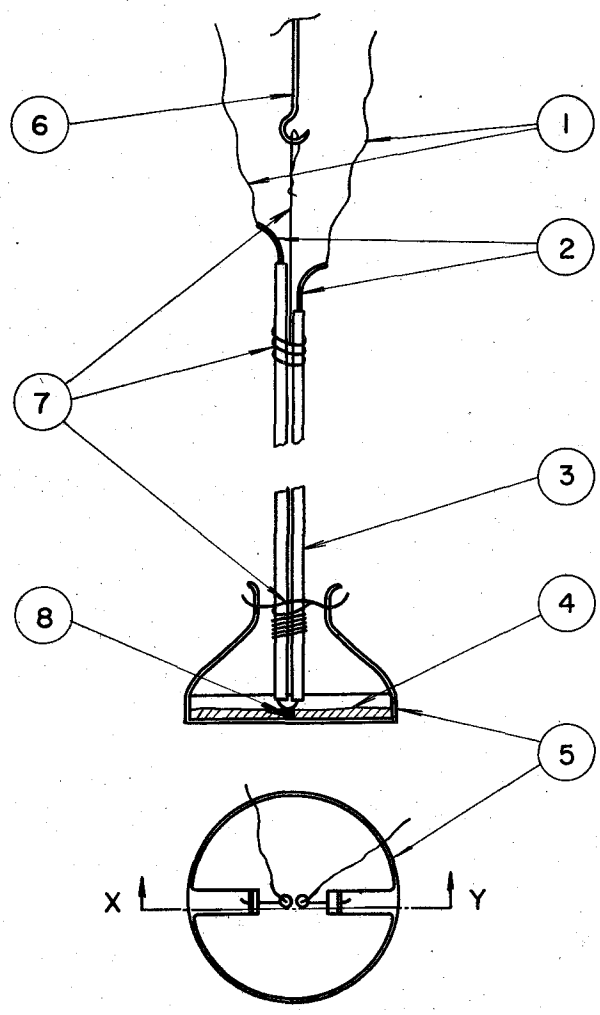

Fig. II-5. Detailed view of sample pan and thermocouple. (1) Pt wires, (2) thermocouple wires, (3) alumina sheath, (4) sample powder, (5) sample pan, (6) silica hook, (7) nickel wires, (8) thermocouple tip.

(iii) Measurement of the reaction temperature

The reaction temperature of sample powder was measured by a chromel-alumel thermocouple of which the tip was uncovered and touched directly the center of the sample pan (see Fig. II-5). This method of temperature measurement was applied to closely measure the temperature of samples and to control the reaction temperature accurately. The chromel-alumel thermocouple was not much corroded by fluorine gas even at the temperatures above 500°C and could be used for the experimental runs of several tens. Alumina tubes, 0.5 and 1.0 mm in inner and outer diameter, and above 99.9% in purity, were used as insulating sheaths of the chromel and alumel wires. To eliminate the influence of the thermocouple lead-wires upon the sensitivity of spring, it was made of a platimum wire, of diameter 0.02 mm.

1.2.2 Experimental method

The fluorination reaction generally proceeds rapidly and a large amount of the reaction heat is produced at the same time, so that the concentration of fluorine gas and the amount of sample must be suitably provided in order to control the reaction temperature and the reaction time. In typical experiments, about 100 mg of sample powder (100 ~ 150 mesh) and 20 ~ 40 vol.% in fluorine gas concentration were employed. The sample was placed on the pan and then lowered into the vertical tubular reactor (Fig. II-3). After evacuating the reactor below 5×10^{-5} mmHg, the reactor was filled with argon and then set to a reaction temperature. Finally, the fluorine gas, diluted with argon, was allowed to flow through the reactor.

1.3 Uranium oxides in powder

UO_2 powders used were supplied from the research group in Mitsubishi Kinzoku Kogyo Co., while U_3O_8 and UO_3 powders were prepared in our laboratory, excepting one U_3O_8 powder from Spencer Chemical Co.

Preparation of U_3O_8 and UO_3 powders

In the fluorination of tungsten powder, it was found that the reactivity of powder is nearly proportional to its adsorption surface area. In order to know whether this proportionality exist also for uranium oxides, the powder samples having different surface areas were prepared.

Ammonium diuranate $(NH_4)_2U_2O_7$*, uranyl nitrate $UO_2(NO_3)_2$, and uranyl

* The chemical form of the precipitate of ammonium diuranate is not so simple as the chemical formula noted above. The recent studies revealed the precipitate to be in ternary system with the components of NH_3, and H_2O and be in a mixture of two compounds, $3UO_3.NH_3.5H_2O$ and $2UO_3.NH_3.3H_2O$, above pH 7.[11] These results were obtained by the study on the equilibrium state among three compoments, after aging for several days. But, actual precipitate is generally far from the equilibrium state, and the chemical form of precipitate rapidly produced is not exactly clarified.

peroxide $UO_4.2(\text{or } 4)H_2O$, are all converted to UO_3 or U_3O_8 by calcinating them in air at suitable temperatures. In this study, ammonium diuranate was used for preparing the uranium oxides, because it is widely used as raw material for the large scale production of the oxide fuel, and therefore, the procedure has been established relatively in detail.

Ammonium diuranate was precipitated from the solution of uranyl nitrate by adding conc. ammoniac water. It has been known that the properties of produced oxide powder depend largely on the properties of the precipitate. The main factors, influencing the properties of the precipitate, are as follows.[12)]

(i) Concentration of uranyl nitrate

This is the most important factor for controlling the size of the precipitate. The size of the precipitated particles decreases with lowering the concentration of uranyl nitrate in aqueous solution.

(ii) Concentration of ammoniac water

It is preferable to use concentrated ammoniac water to obtain the precipitate with good properties for its sedimentation and for its filtration.

(iii) Final value of pH in the precipitation process

The precipitation begins to occur above pH 3.5 and is completed at pH 4.0.[11)] But, at such low pH values, the precipitation proceeds very slowly, so that pH value must be raised above 6 in practice for the complete and rapid precipitation from uranyl nitrate solution.

The oxide powders having different surface areas were prepared by the procedure shown in Fig. II-6. Uranyl nitrate hexahydrate* was dissolved in 3 N nitric acid to the concentration of 106, 53, and 13 g/l. Conc. ammoniac water was added rapidly to the solution under continuous stirring until pH of the solution reaches 7. After filtering and drying the precipitates, they were crushed roughly and then calcinated in air. The chemical changes during the calcination are believed to be as follows:

$$(NH_4)_2U_2O_7 \xrightarrow[\text{in air}]{300^\circ \sim 550^\circ C} 2\,UO_3 + H_2O + 2\,NH_3$$

$$3\,UO_3 \xrightarrow[\text{in air}]{\geq 600^\circ C} U_3O_8 + \frac{1}{2}\,O_2$$

The temperature range of each reaction has been clarified thermogravimetrically.[12)]

* Guaranteed reagent, made by Yokozawa Chemical Co. Ltd., assay minimum, 99%.

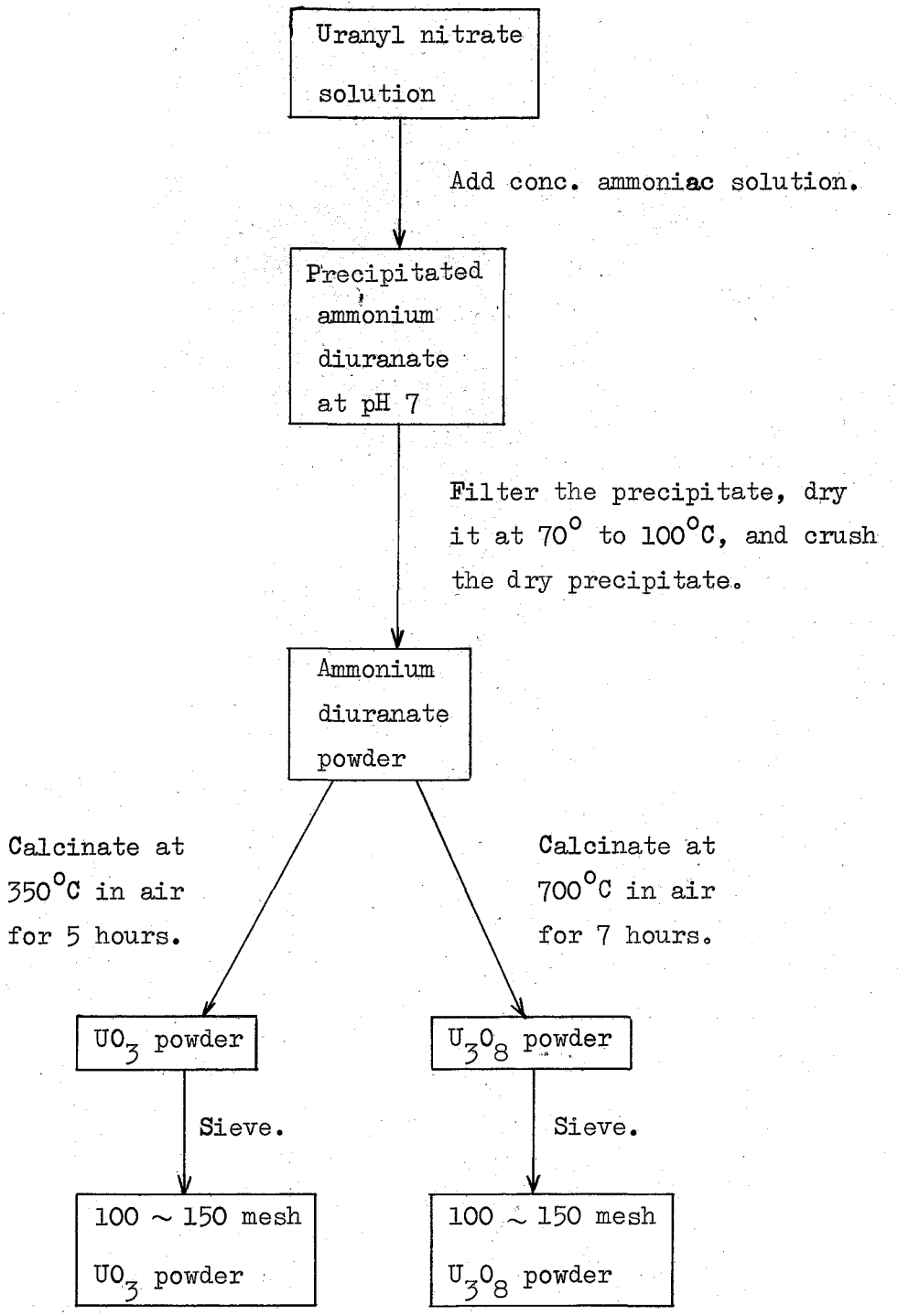

Fig. II-6. Flow sheet for preparation of U_3O_8 and UO_3.

In this work, the precipitates were calcinated at 350°C or 700°C. X-ray patterns of the powders produced by calcination at 350° and at 700°C showed the formation of amorphous UO_3 and orthorhombic U_3O_8, respectively. All the powders were sieved and the part from 100 to 150 meshes was used as sample. Table II-1 shows their surface areas which were measured by BET method using krypton as adsorbate.

Table II-1. Relationship between concentration of uranyl nitrate and surface area of resulted powders.

Compound	U_3O_8			UO_3	
Sample No.	A-1	A-2	A-3	B-2	B-3
Concentration of uranyl nitrate (g/l)	106	53	13	106	53
Surface area[a] of produced powder[b] (m^2/g)	1.2	1.6	2.0	3.3	6.3

a) Kr was used as adsorption gas.

b) from 100 to 150 mesh.

UO_2 powders

Two kinds of powders, active and inactive, were supplied from Mitsubishi Kinzoku Kogyo Co. The active and inactive powders were made by reducing U_3O_8 powder at 900° and 1500°C, and have surface areas of 4.4 and 0.17 m^2/g (determined by krypton adsorption) respectively.[13]

1.4 Chemical analysis of solid residue

The solid residue, taken out halfway in the process of fluorination, contained fluorine in addition to uranium and oxygen. In order to know the F/U ratio (as a degree of the fluorination of these materials), the content of fluorine and of uranium were determined by the method consisting of pyrolysis and colorimetry.[14,15,16] The chemical analyses were made with the aid of analytical section.[15] Figure II-7 shows the flow sheet of analytical procedure, consisting of three parts; (1) separation of fluorine and uranium by pyrolysis* (2) quantitative analysis of fluorine by colorimetry,

* The direct analyses of fluorine and uranium which co-exist in a solution are unsuccessful, because they are combined to each other to form a strong complex ion in the solution; they must be separated prior to the chemical analysis of each component.

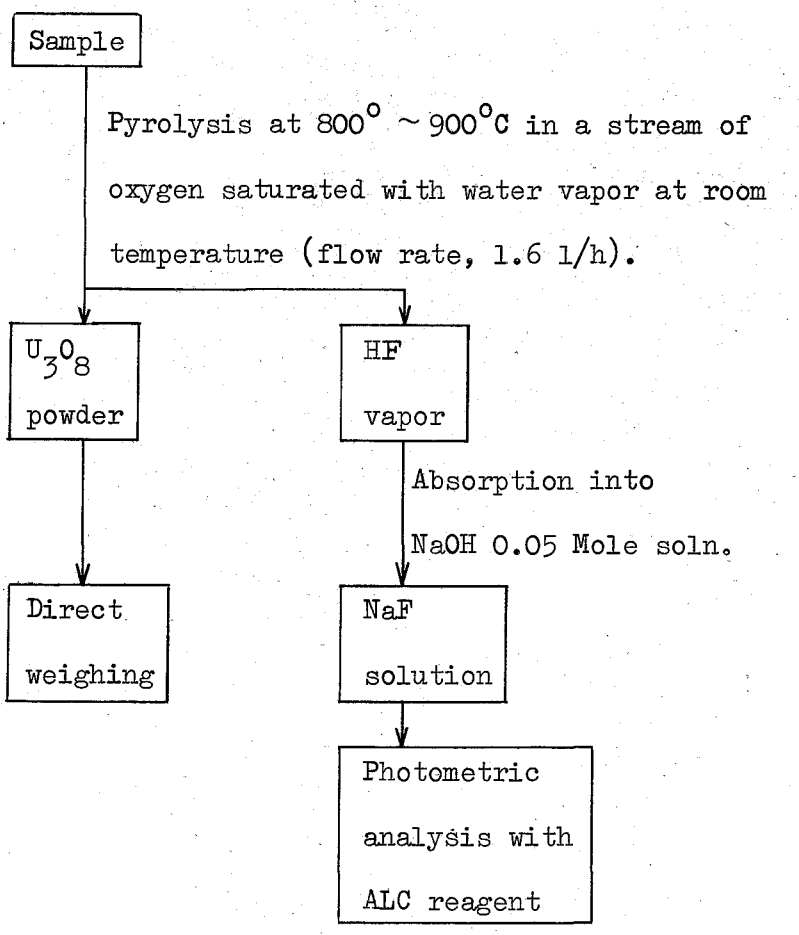

Fig. II-7. Flow sheet of procedure in the chemical analysis of uranium and fluorine in the sample.

(3) quantitative analysis of uranium.

(1) Separation of fluorine and uranium

Willard and Winter developed a method to separate the fluorine in solid material as hydrofluosilicic acid, H_2SiF_6, by distillation in H_2SO_4.[18] The various modification of this method have been reported, but a long time is necessary for the complete separation by this method. Warf et al developed a new method, named pyrohydrolysis,[17] in which the fluorine contained in a solid sample is distilled off as hydrofluoric acid, HF, in a short time by the hydrolysis in a stream of steam at high temperature. As a modification of Warf's method, Powell and Menis succeeded in reducing the volume of distillate by using a stream of moist oxygen instead of steam; this method is called pyrolysis.[19]

This pyrolysis was used to separate the fluorine in the intermediate of uranium oxyfluoride. The sample for the analysis was placed on a platinum boat, 10 mm wide, 70 mm long, and 5 mm deep, which was inserted into a reactor made of silica tube. After the reactor was heated to 800°C, a stream of oxygen saturated with water was passed for 15 minutes. The distillate HF was absorbed in a 0.05 mole sodium hydroxide solution. The uranium in the sample remained in the form of U_3O_8.

(2) Analysis of fluorine

In the early stage of the experiment, the quantity of fluorine was determined by titrating with thorium nitrate solution with the indicator of alizarin sulfonate, but it was difficult to know the end point of the titration because the change in colour is faint with this indicator.

Belcher et al found that fluoride ion forms a blue complex with cerous chelate of alizarin complexone, Ce-ALC (1, 2-dihydroxyanthraquinone-3yl-NN-(methylamine-)diacetic acid), and applied this phenomenon to the colorimetry of fluoride ion.[20] The blue complex contains fluoride ion and the chelate in 1:1 mole ratio.[21] This colorimetry is useful for the analysis of fluorine in micro to semi-micro quantity, so that the sample in this work was analyzed after diluting it less than 160 mg/100 ml in fluorine concentration. Here, another type chelate, La-ALC —— the behavior to fluoride ion is similar to Ce-ALC[22] —— was used.

(3) Analysis of uranium

After separating fluorine by pyrolysis, the uranium is in the form of U_3O_8. The quantity of uranium was determined by weighing the residual U_3O_8.

1.5 Fluorination of UO_2 powders

1.5.1 Kinetics and mechanism of the reaction

The reaction was very slow below 300°C, although it was observable. The $(1 - F)^{1/3}$ is plotted against the time in Figs. II-8 and II-9. The active UO_2 reacted mainly according to the linear law, except at the beginning of the reaction (see Fig. II-8). To the contrary, in the case of the inactive UO_2, the reaction curve consists of two straight lines (see Fig. II-9); the cause of this result is not yet clarified. X-ray analysis showed that in both cases all the UO_2 powder had been changed to UO_2F_2 at the very beginning of the reaction and most of the reaction period shown in Figs. II-8 and II-9 was the second step reaction from UO_2F_2 to UF_6. The initial rise of reaction temperature which took place explosively when the fluorine was added to UO_2 powder, is shown in Fig. II-10. For the inactive UO_2, in contrast to the case of U_3O_8 (see section 1.6 in this chapter), a large temperature rise of 30°C was observed in spite of the extremely small surface area (0.17 m^2/g). The weight change vs. the time is plotted in Fig. II-11; the curve for UO_2 pellet, 2 mm thick, 6 mm in diameter, and 96% of theoretical density, was added for comparison. The reaction rate was determined from the slopes of the straight parts of the curves in Figs. II-8 and II-9, which appears after the bendings at the early stage of each line; the obtained data are listed in Table II-2 and II-3.

Table II-2. Effect of temperature on reaction rate constant
Sample, UO_2 powders, active and inactive; total gas flow rate, 13.7 l/h; total pressure, 760 mmHg; partial pressure of fluorine, 170 mmHg.

Reaction temp. (°C)	Rate constant, k_2 (min^{-1})			
	Active UO_2		Inactive UO_2	
	measured	calcd.[a]	measured	calcd.[a]
350	0.0024	0.0043	0.0031	0.0034
370	0.0079	0.0077	0.0053	0.0056
390	0.0132	0.0134	0.0092	0.0087
410	0.0260	0.0222	——	——
430	0.0305	0.0354	0.0210	0.0224

a) calculated by equations for UO_2 in section 1.9.

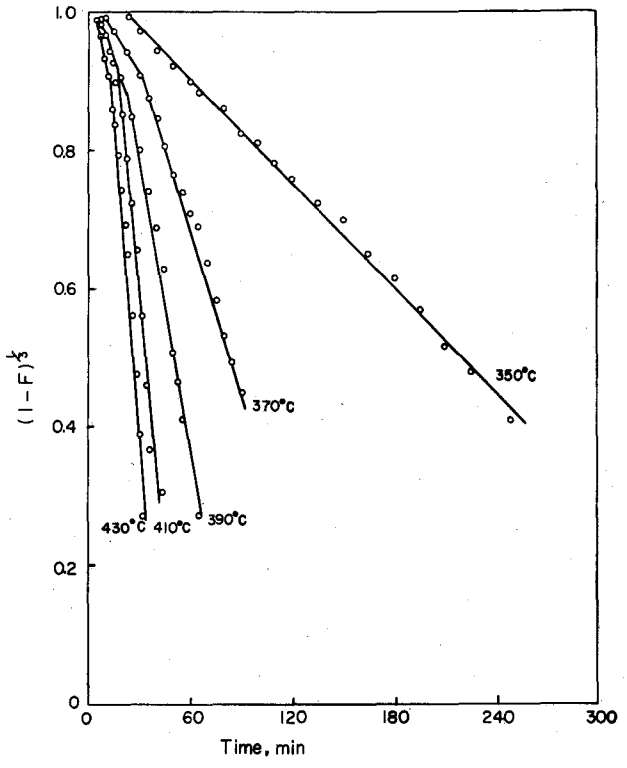

Fig. II-8. Relations between $(1 - F)^{1/3}$ and time at different temperatures.
Sample, active UO_2; initial weight of sample, 100 mg; total gas flow rate, 13.7 l/h; partial pressure of fluorine, 170 mmHg; total pressure, 760 mmHg.

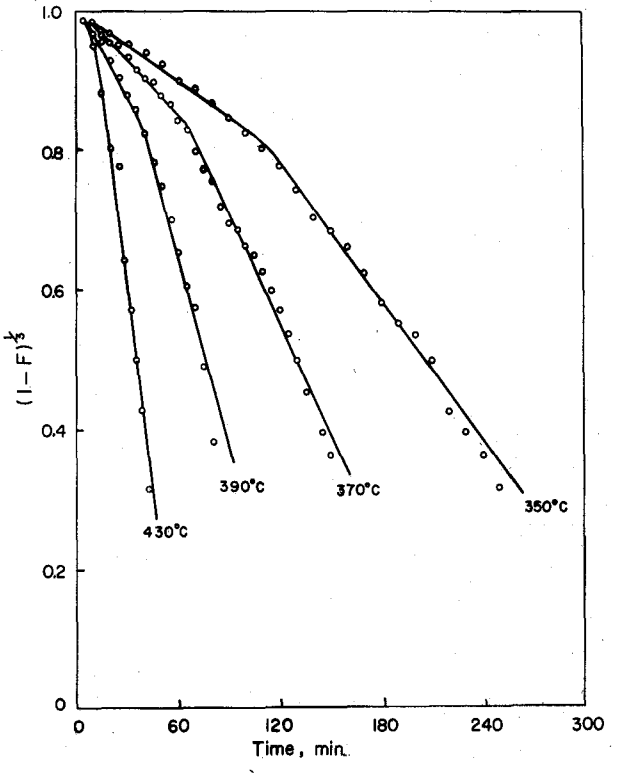

Fig. II-9. Relations between $(1 - F)^{1/3}$ and time at different temperatures.
Sample, inactive UO_2; initial weight of sample, 100 mg; total gas flow rate, 13.7 l/h; partial pressure of fluorine, 170 mmHg; total pressure, 760 mmHg.

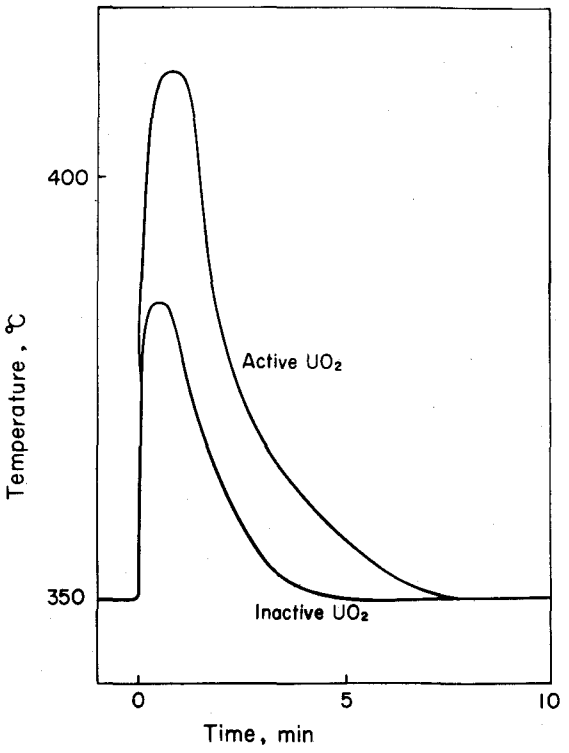

Fig. II-10. Temperature rise at the beginning of reaction. Sample, UO_2 powder; initial setting temperature, 350°C; initial weight of sample, 100 mg; total gas flow rate, 13.7 l/h; partial pressure of fluorine, 170 mmHg; total pressure, 760 mmHg.

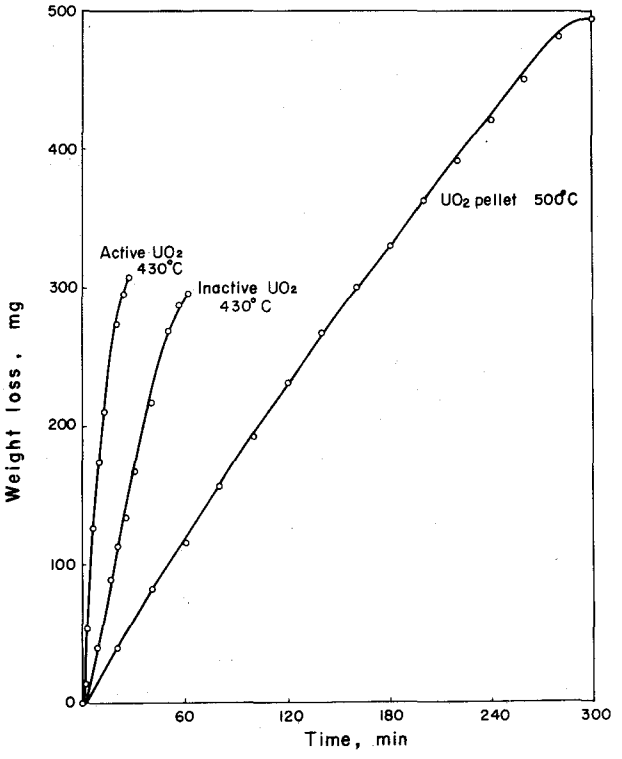

Fig. II-11. Weight loss vs. time for various UO_2 powders. Initial weight of UO_2 powder, 300 mg; initial weight of pellet, 560 mg; total gas flow rate, 13.7 l/h; partial pressure of fluorine, 170 mmHg; total pressure, 760 mmHg.

Table II-3. Effect of initial surface area of sample on reaction rate constant.
Sample, UO_2 powder; total gas flow rate, 13.7 l/h; total pressure, 760 mmHg; partial pressure of fluorine, 170 mmHg.

Reaction temp. (°C)	Material	Surface area (m^2/g)	k_2 (min^{-1})
370	Active UO_2	4.4	0.008
370	Inactive UO_2	0.17	0.005
430	Active UO_2	4.4	0.031
430	Inactive UO_2	0.17	0.021

The difference in the reaction rate between the active and the inactive UO_2 was somewhat smaller than that expected from the difference in the surface area between them. This result indicates that the UO_2 particles are destroyed rapidly when fluorine attacked the samples, and so the effect of the initial surface area on the reaction rate becomes small. The apparent activation energies for the second step were determined to be 23.0 and 20.7 kcal/mole for the active and inactive UO_2 respectively; those values may be considered to be approximately the same.

1.5.2 Effect of fluorine concentration and total gas flow rate on the reaction rate for active UO_2 powder

In order to know the effect of fluorine concentration on the reaction rate, the experiments were made at different partial pressures of fluorine under constant gas flow rate 13.7 l/h, and constant temperature 430°C. From the slope of the curve of the rate constant vs. the partial pressure of fluorine, the exponent factor "n" in equation (1) was found to be near 1.0; the rate constants at different partial pressure of fluorine are shown in Table II-4. Three experiments were made in which the partial pressure of fluorine and the reaction temperature were kept at 170 mmHg and 430°C, respectively. But the total gas flow rate was varied; Table II-5 lists the data from these experiments. It was seen that the change in gas velocity had no effect on the rate constant.

Table II-4. Effect of partial pressure of fluorine on reaction rate constant.
Sample, active UO_2 powder; temperature, 430°C; total gas flow rate, 13.7 l/h; total pressure, 760 mmHg.

Partial pressure of fluorine (mmHg)	k_2 (min^{-1})	
	measured	calcd. a)
85	0.0085	0.021
170	0.031	0.035
255	0.046	0.046
340	0.064	0.057

a) calculated by the equation for active UO_2 in section 1.9.

Table II-5. Effect of gas flow rate on reaction rate constant.
Sample, active UO_2 powder; temperature, 400°C; partial pressure of fluorine, 170 mmHg; total pressure, 760 mmHg.

Total gas flow rate (l/h)	k_2 (min^{-1})
13.8	0.016
10.3	0.016
6.9	0.018

1.6 Fluorination of U_3O_8 powders

1.6.1 Effect of the surface area of the powder on the reaction rate

Fig. II-12 shows the typical curves of the weight change vs. the time for the samples having different surface areas. From the slope of the linear part of the curves, the rates of weight loss were calculated. Table II-6 summarizes those values. The rates of weight loss of U_3O_8 powders against the Kr adsorption areas are plotted in Fig. II-13, where a considerable proportionality is seen. At the beginning of the reaction, the temperature always rose sharply for 2 or 3 minutes; the peak heights are shown in Fig. II-14. In this initial stage, the weight decrease was negligibly small and at times a slight increase in weight was observed; X-ray pattern of the sample taken at a given time in this stage showed the formation of an intermediate UO_2F_2, as described later. The peak height of the

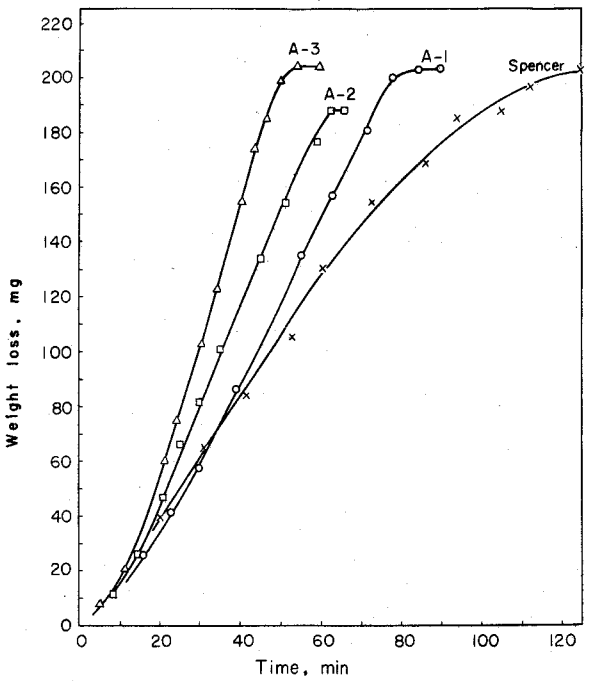

Fig. II-12. Weight loss vs. time for U_3O_8 powders having different surface areas. Temperature, 440°C; total gas flow rate, 13.7 l/h; partial pressure of fluorine, 170 mmHg; total pressure, 760 mmHg.

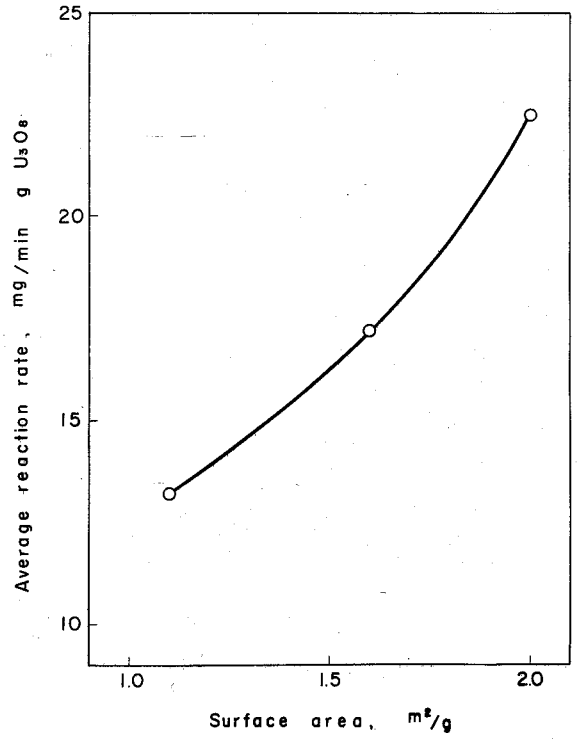

Fig. II-13. Dependence of reaction rate on the surface area for U_3O_8 powders.

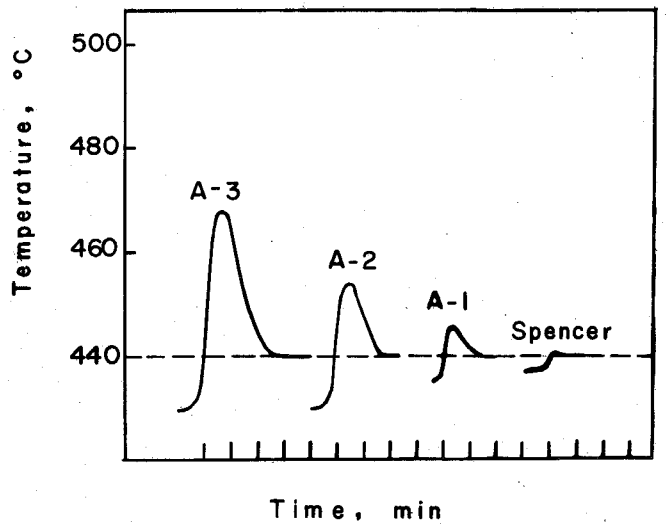

Fig. II-14. Temperature rise at the beginning of reaction. Sample, U_3O_8 powders; initial setting temperature, 440°C; initial weight of sample, 100 mg; total gas flow rate, 13.7 l/h; partial pressure of fluorine, 170 mmHg; total pressure, 760 mmHg.

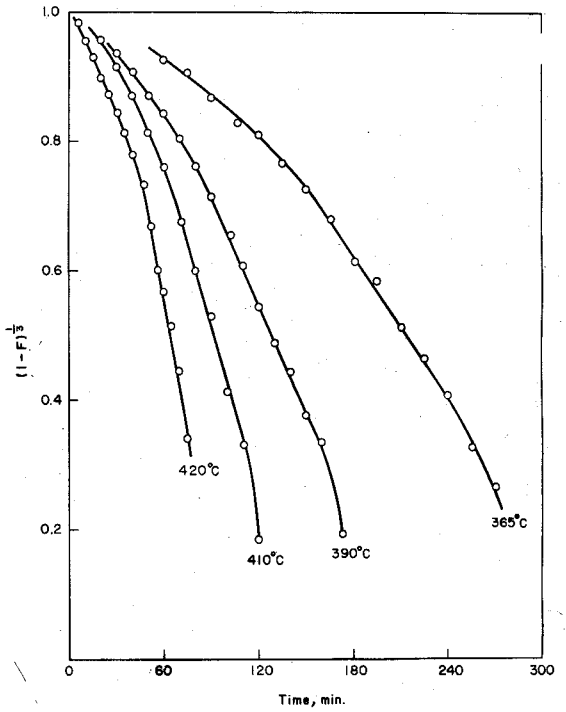

Fig. II-15. Relations between $(1 - F)^{1/3}$ and time at different temperatures.
Sample, U_3O_8 (A-2); initial weight of sample, 100 mg; total gas flow rate, 13.7 l/h; partial pressure of fluorine, 170 mmHg; total pressure, 760 mmHg.

Table II-6. Surface area of U_3O_8 powder and reaction behavior. Temperature, 440°C; initial weight of sample, 100 mg; total gas flow rate, 13.7 l/h; partial pressure of fluorine, 170 mmHg; total pressure, 760 mmHg.

Sample	Surface area[a] (m^2/g)	Reaction rate per surface area[b] (mg. min^{-1}. m^{-2})	Temperature rise at the beginning of the reaction (°C)
(A-1)	1.2	11.2	5
(A-2)	1.6	10.7	13
(A-3)	2.0	11.5	28
Spencer	1.2		Negligible

a) measured by BET method using Kr as adsorbing gas.

b) calculated by using Kr adsorption surface area.

initial temperature rise is nearly proportional to the surface area of the sample of U_3O_8. This indicates that the initial reaction spreads rapidly over the whole surface of the particles, forming UO_2F_2.

1.6.2 Reaction behavior

The plots of $(1 - F)^{1/3}$ vs. the time are shown in Fig. II-15. While the reaction deviates from the linear law in the beginning half, the reaction follows the linear law for a significant part of the time. X-ray analyses of the samples taken throughout the run show that, during the first part of the run, the residue was a mixture of U_3O_8 and UO_2F_2. The fraction of U_3O_8 in the residue decreased as the reaction proceeded and in the period corresponding to the linear part of the curves in Fig. II-15, the pattern of U_3O_8 sometimes disappeared. Hence, the reaction consists of the following two steps similar to the case of UO_2:

$$\frac{1}{3} U_3O_8 + F_2 \longrightarrow UO_2F_2 + \frac{1}{3} O_2 \qquad (a)$$

$$UO_2F_2 + 2 F_2 \longrightarrow UF_6 + O_2 \qquad (b)$$

The initial deviation of the reaction from the linear law can be explained as follows. If the first step is simply the first order homogeneous reaction in the solid phase, the change in concentration of UO_2F_2 in the solid particles is expressed by the equation,

$$-\frac{d(a - x)}{dt} = k_1 (a - x), \qquad (15)$$

where k_1 is the rate constant of the first step reaction, a is a constant, and x is the concentration of UO_2F_2 at the time t in the solid phase of the particles. By integrating equation (15),

$$x = a\left[1 - \exp(-k_1 t)\right] . \qquad (16)$$

In the chemical change from U_3O_8 to UO_2F_2 in the first reaction, the weight change is much smaller than that in the chemical change from UO_2F_2 to UF_6 in the second step, so that the weight change of the overall reaction may be considered to depend only on the second step. If the rate of the second step reaction is proportional to the UO_2F_2 concentration on the surface of the particles, then the rate of reduction in mass of the single particle is given by

$$-\frac{dm}{dt} = k_2' S_t x \qquad (17)$$

where k_2' is the rate constant of the second step reaction and S_t is the surface area of the particle at time t. By inserting equation (16) into equation (17) and when the particle is assumed to be spherical, equation (17) becomes

$$-\frac{dm}{dt} = k_2' 4\pi r_t^2 a\left[1 - \exp(-k_1 t)\right], \qquad (18)$$

where r_t is the radius of the particle at time t. From equations (4) and (18), $(1 - F)^{1/3}$ is obtained as a function of t, namely

$$(1-F)^{1/3} = \left(1 + \frac{k_2}{k_1}\right) - k_2 t - \frac{k_2}{k_1}\exp(-k_1 t), \qquad (19)$$

where $k_2 = a k_2'/r_0\rho$, and ρ is the density of the particle. When $k_1 \gg k_2$ ($k_2/k \simeq 0$), equation (19) becomes

$$(1 - F)^{1/3} = 1 - k_2 t. \qquad (20)$$

Equation (20) has the same form with equation (12). The value of the last exponential term in equation (19) becomes smaller when t increases, and therefore at large t,

$$(1-F)^{1/3} \cong \left(1 + \frac{k_2}{k_1}\right) - k_2 t. \qquad (21)$$

When $(1 - F)^{1/3}$ is plotted against t, equation (21) gives the asymptote for the curve of equation (19).

Equation (19) shows a slightly convex curve, similar to the initial half of the experimental curves in Fig. II-15. In the actual reaction, however, the decreasing rate of $(1 - F)^{1/3}$ will be lower than the rate obtained from equation (19), because of the increase in weight by the first step reaction,

of which the effect was not considered in derivation of the equation. This lower rate of the reaction appears to be the reason of the fact that each curve in Fig. II-15 has an inflexion before reaching the linear part. The value of k_2 can be measured from the slope of the straight part appearing in the latter half of the curves in Fig. II-15. The value of k_1 can be calculated from this k_2 value and the value of $(1 + k_2/k_1)$ which can be obtained from the extraporated value of ordinate, of the straight part of the curves. Table II-7 is the list of k_1 and k_2 values.

Table II-7. Effect of temperature on reaction rate constant. Sample, U_3O_8 powder (A-2); total gas flow rate, 13.7 l/h; partial pressure of fluorine, 170 mmHg; total pressure, 760 mmHg.

Reaction temp. (°C)	k_1 (min^{-1}) measured	k_2 (min^{-1}) measured	k_2/k_1	k_2 (min^{-1}) calcd. [a]
365	0.026	0.0035	0.134	0.0035
	0.028	0.0036	0.128	
390	0.052	0.0041	0.079	0.0055
	0.049	0.0038	0.078	
410	0.060	0.0088	0.147	0.0094
420	0.070	0.0112	0.160	0.0117
			0.120 (av.)	

a) calculated by the equation for U_3O_8(A-2) in section 1.9.

The Arrhenius plot of k_1 values did not show the good linear relationship, and so the activation energy could not be determined exactly; its value, however, appears to be a little smaller than the value for second step reaction.

The U_3O_8 from Spencer Chemical Co. showed a somewhat different mechanism of the reaction which did not follow the linear law at any period of the reaction (see Fig. II-18 in section 1.8). Microscopic observations revealed that the original particles have well-developed crystalline surfaces and formation of the intermediate predominates at edges and kinks on the crystalline surfaces without spreading over the whole surfaces throughout the reaction. X-ray patterns showed the formation of a small amount of UO_2F_2. These results indicate that the reaction rate is controlled by a nucleation process of UO_2F_2 at the active sites on the surfaces. This slowdown of the first step reaction is probably due to the well-developed crystalline state

of each particle and the small surface reactivity. When the synthsized U_3O_8 (A-2) was calcinated at 1000°C for 3 hours in air to reduce the surface reactivity and was fluorinated, a similar nucleation of the intermediate UO_2F_2 was observed. This is in good agreement with the assumption on the relation between the reaction behavior and the crystalline state.

1.6.3 Effect of fluorine concentration and total gas flow rate on the reaction rate

In several experiments, the reactions were made at different partial pressures of fluorine under the constant temperature 410°C and the constant gas flow rate 13.7 l/h; the results are shown in Table II-8.

Table II-8. Effect of partial pressure of fluorine on reaction rate constant.
Sample, U_3O_8 powder (A-2); temperature, 410°C; total gas flow rate, 13.7 l/h; total pressure, 760 mmHg.

Partial pressure of fluorine (mmHg)	k_2 (min^{-1}) measured	calcd.[a]
80	0.004	0.0047
170	0.009	0.0094
250	0.012	0.0135
	0.013	
360	0.016	0.0187
	0.017	

a) calculated by the equation for U_3O_8(A-2) in section 1.9.

From the slope of the plot of the logarithm of the rate constant vs. the partial pressure of fluorine, the exponent factor n for the concentration term of equation (1) was determined to be about 0.9 for A-2 sample; this value indicates that the reaction rate is nearly proportional to the partial pressure of fluorine. It was seen that the change in gas velocity had no effect on the rate of reaction (see Table II-9).

Table II-9. Effect of gas flow rate on reaction rate constant.
Sample, U_3O_8 powder (A-2); temperature, 410°C; partial pressure of fluorine, 170 mmHg; total pressure, 760 mmHg.

Total gas flow rate (l/h)	k_2 (min^{-1})
6.8	0.009
10.3	0.009
13.7	0.0095

1.7 Fluorination of UO_3 powders

At the beginning of the reactions, the temperature always rose sharply as in the case of fluorination of UO_2 and U_3O_8 powders. The peak found with one UO_3 sample (B-3) was much higher than those of U_3O_8, which appeared to be due to its large surface area 6.3 m^2/g. After the peak of temperature rise, the UO_3 had been almost completely converted to UO_2F_2, which was then gradually fluorinated to UF_6; Fig. II-16 shows that the great part of the reaction follows the linear law with a short initial deviation. These results show the rapid formation of intermediate UO_2F_2 at the early stage of the reaction. Table II-10 summarizes the rate constants of second step which were calculated from the slope of the linear part in the curves in Fig. II-16.

Table II-10. Effect of temperature on reaction reaction rate constant. Sample, UO_3 powder (B-3); total gas flow rate, 13.7 l/h; partial pressure of fluorine, 170 mmHg; total pressure, 760 mmHg.

Reaction temp. (°C)	k_2 (min^{-1})	
	measured	calcd.[a]
350	0.0027	0.0028
380	0.0063	0.0061
400	0.0109	0.0103
420	0.0160	0.0163

a) calculated by the equation for UO_3(B-3) in section 1.9.

The surface area of powder did not influence on the reaction rate as shown in Fig. II-17; although there is no experimental result to explain this fact, it may be assumed that the initial state of UO_3 powder is completely converted into a new state of UO_2F_2, which is independent of the original state of the powder because of the unstable crystalline state of UO_3 assumed from the amorphous pattern of X-ray diffraction.

1.8 Comparison between the various reaction types

The fluorination of uranium oxides, UO_2, U_3O_8, and UO_3, to UF_6 consisted of two steps; in the first step, each oxide was converted to UO_2F_2 and in the second step, UO_2F_2 was converted to UF_6. However, there were seen some differences between their reaction behaviors. Figure II-18 shows various forms of the curve $(1 - F)^{1/3}$ vs. the time; the occurrence of these forms may be explained from the following relationships between the rate constants k_1 and

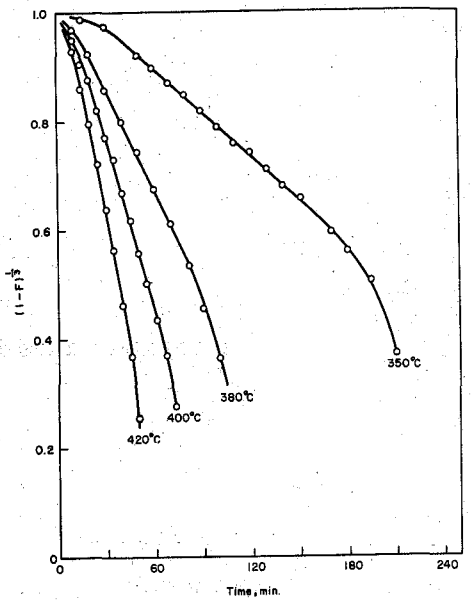

Fig. II-16. Relations between $(1 - F)^{1/3}$ and time at different temperatures.
Sample, UO_3 (B-3); initial weight of sample, 100 mg; total gas flow rate, 13.7 l/h; partial pressure of fluorine, 170 mmHg; total pressure, 760 mmHg.

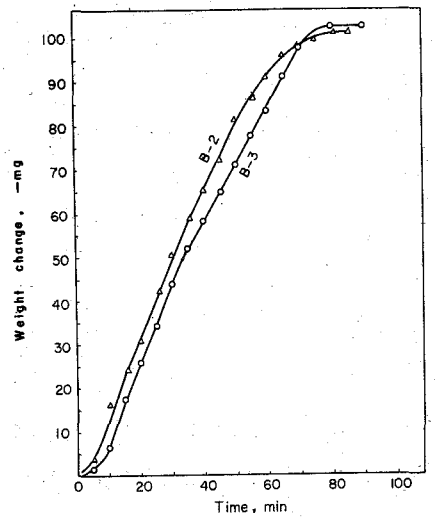

Fig. II-17. Weight loss vs. time for UO_3 powders.
Temperature, 400°C; total gas flow rate, 13.7 l/h; partial pressure of fluorine, 170 mmHg; total pressure, 760 mmHg; surface area of (B-2) and (B-3), 3.3 and 6.3 m^2/g respectively.

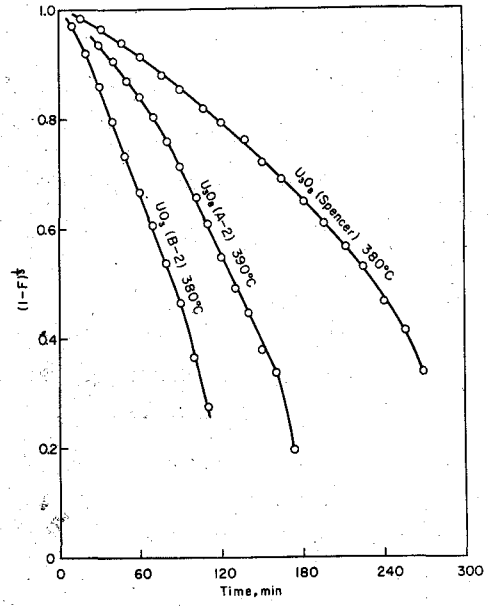

Fig. II-18. Various forms of the plot between $(1 - F)^{1/3}$ and time.
Total gas flow rate, 13.7 l/h; partial pressure of fluorine, 170 mmHg; total pressure, 760 mmHg; initial weight of sample, 100 mg.

k_2 for various uranium oxides:

$k_1 \gg k_2$ for UO_2 and UO_3 powders,

$k_1 \gtrsim k_2$ for U_3O_8 powders (A-1 ~ 3), and

$k_1 \lesssim k_2$ for U_3O_8 powder (Spencer);

temperature range, 350° ~ 430°C.

These relationships are also derived from the observation of residual sample powders, which were taken out from the reactor after stopping the reaction at a given time. Figure II-19 shows the microphotographs of these samples. Table II-11 summarizes the characteristics of those various residues.

Table II-11. Change in the appearance of powder samples during fluorination.

Powder sample	UO_2	U_3O_8 synthetized	U_3O_8 Spencer	UO_3 Amorphous
color of original sample	(dark) brown	dark brown	black	orange
Change in color during reaction	whitish yellow (UO_2F_2)	greyish yellow (U_3O_8 + UO_2F_2)	orange spots (U_3O_8 + slight UO_2F_2)	whitish yellow (UO_2F_2)

In the fluorination of UO_3, the first step reaction proceeds rapidly throughout the solid particle and the great part of the reaction time following linear law is for second step reaction. However, in the case of U_3O_8 (Spencer), the first step reaction proceeds partly on the solid surface with neither spreading over the whole surface nor progressing into the solid particle. Consequently, the first and second step reactions coexist at any time during the reaction; this may be the reason that all the part of the reaction does not follow the linear law. The reaction behavior of U_3O_8 (A-2) appears to be between the above two cases.

All the powders of various oxides, except the powder of Spencer U_3O_8, were in the form of agglomerate lumps of which the sizes were arranged in the range between 100 and 150 meshes by sieving. Microscopic observations revealed that these lumps were not broken throughout the reaction, while

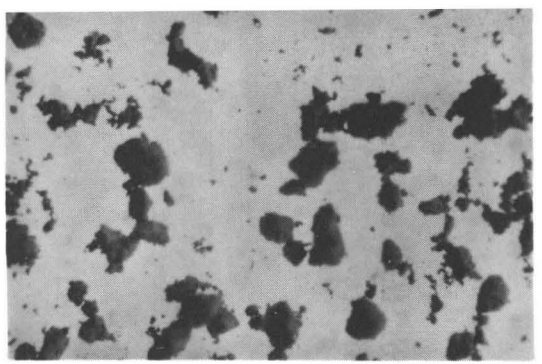

U_3O_8 (A−2)

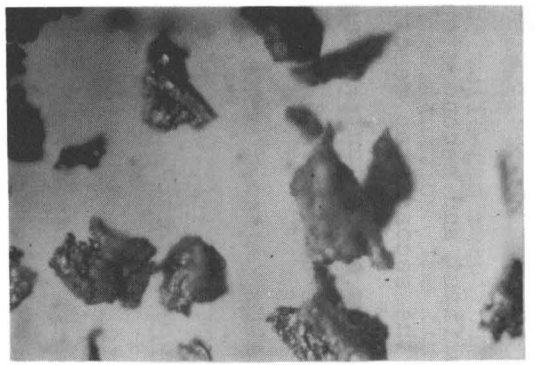

U_3O_8 (Spencer)

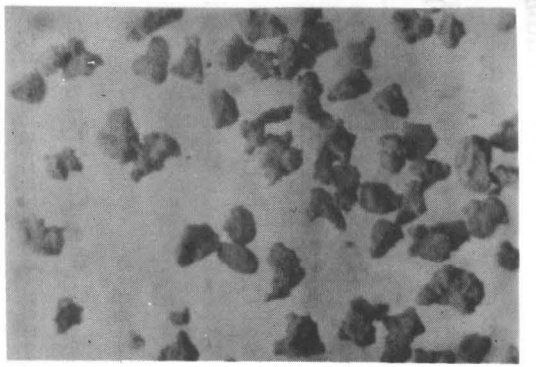

UO_3 (B−2)

U_3O_8 (A−2) weight loss 70%

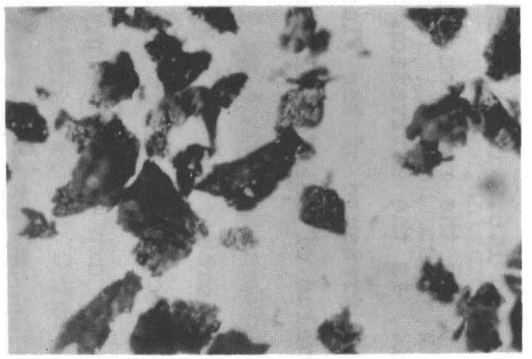

U_3O_8 (Spencer) weight loss 60%

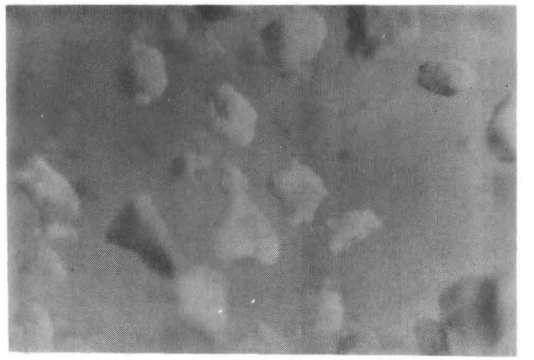

UO_3 (B−2) weight loss 30%

Fig. II-19. U_3O_8 and UO_3 powders converted by fluorination.

they changed in color and size as the reaction proceeded. Figure II-19 shows some of these changes in the appearance; that is, the original lumps were converted rapidly (for UO_2 and UO_3) or rather slowly (for U_3O_8) to UO_2F_2 lumps. Decrease in $(1 - F)^{1/3}$ appears to be related to the shrinkage of these lumps.

The Spencer U_3O_8 powder is not agglomerated and the nucleation of UO_2F_2 on the particle seems to be rate determining step of the fluorination reaction. This is probably due to the well-developed crystalline state of each particle and the small surface reactivity.

1.9 Equations for claculating the reaction rate constants .

Using the diminishing sphere model, the kinetics of the fluorination reactions between uranium oxides in power and fluorine may be expressed by

$$(1 - F)^{1/3} = (1 + k_2/k_1) - k_2 t - k_2/k_1 \exp(-k_1 t)$$

$$k_2 = A \exp\left(-\frac{E}{RT}\right) p^n$$

(see sections 1.1 and 1.6.2 in this chapter),

where k_1 and k_2 (min^{-1}) are the rate constants for the first and second step reactions, E (kcal/mole) is the activation energy for the second step reaction, p (mmHg) is the partial pressure of the fluorine, and n is a constant; n was found to be near the value of one for all the oxides. The derived equations are as follows.

Active UO_2

$$(1 - F)^{1/3} = 1 - k_2 t,$$

$$k_2 = 2.7 \times 10^3 \exp\left(-\frac{23000}{RT}\right) p.$$

Inactive UO_2

$$(1 - F)^{1/3} = 1 - k_2 t,$$

$$k_2 = 3.3 \times 10^2 \exp\left(-\frac{20700}{RT}\right) p.$$

U_3O_8 (A-2)

$$(1 - F)^{1/3} = 1.20 - k_2 t - 0.20 \exp(-k_1 t)$$

$$= 1.20 - k_2 t \text{ (in the latter half of the reaction)},$$

$$k_2 = 5.5 \times 10^2 \exp\left(-\frac{21300}{RT}\right) p^{0.9}.$$

UO_3 (B-3)

$$(1 - F)^{1/3} = 1 - k_2 t,$$

$$k_2 = 2.8 \times 10^2 \exp\left(-\frac{22000}{RT}\right) p^{1.2}.$$

2. Fluorination of uranium oxides in pellets by fluorine

2.1 Introduction

It was shown that the fluorination of the uranium oxides in powder to UF_6 proceeds in two steps; (1) uranium oxides to UO_2F_2, and (2) UO_2F_2 to UF_6. In general, the fluorination of UO_2F_2 to UF_6 is the rate controlling step, while the formation of UO_2F_2 in the first step proceeds rapidly. Since the large reaction heat is produced for the short period of the first step, the control of the reaction temperature is difficult; in the experimental runs, the reaction temperature rose sharply in the beginning of the reaction and so the reaction rate could not be measured, and moreover even the velocity of the second step reaction became too large at temperature above 450°C to measure it accurately.

These difficulties in measuring the reaction rate may be avoided by using the sample in the form of disc pellets; the reasons are (1) lower chemical reactivity due to the smaller reacting surface area and (2) ease of the analysis in the solid-gas reaction due to the simple and uniform shape of the solid pellets. In this situation the fluorination of pelletized oxides was studied.

2.2 Pellets of uranium oxides

2.2.1 UO_2 pellets[23)]

Uranium dioxide pellets, 2 ± 0.2 mm in thickness, 6 ± 0.2 mm in diameter, and 10.53 ± 0.11 g/cm^3 in density —— 96% of the theoretical density of UO_2, 10.95 —— were made by Mitsubishi Atomic Power Industries Inc. The outline of manufacturing processes are as follows. The UO_2 powder was mixed with organic binders, pressed at 3 tons/cm^2, and sintered at 900°C in CO_2 atmosphere for 1 hour (preliminary sintering) and then at 1450°C in vacuum for 2 hours. The concentrations of major impurities (in ppm) are as follows ; Fe, 220; Si, 110; C, 39; Mo, 21; Ca, < 20; N, 16; Ti, <15; Al, <14, Ag, B, Cd, Mg, Ni, Pb, Sh, and V, <5.

2.2.2 U_3O_8 pellets[24)]

U_3O_8 pellets, 2.00 to 2.40 mm in thickness, 6.10 to 6.25 mm in diameter and 6.39 to 8.0 in apparent density were made by Sumitomo Denki Kogyo Co. The outline of manufacturing processes are as follows. The U_3O_8 powder was pressed at 3 tons/cm^2 and sintered at 1200°C for 2 hours in air. The concentrations of major impurities are as follows; B, 0.2; Ag, 0.2; Cl, 5; F, 10; C, 20; Si, 40; Al, 15; Fe, 35 (in ppm).

The values of the pellet density are much lower than the theoretical value, 8.38. The pellets were classified according to their densities as

follows:

densities	number of the pellets
7.5 to 8.0	28
7.0 to 7.5	54
6.5 to 7.0	16
6.0 to 6.5	2

The pellets with densities of 7.0 to 7.5 were used in the experiments.

2.3 Experimental method

The experimental apparatus and procedures were similar to those described in section 1.2. The pellet was placed on a support which was put on a nickel pan. This support, made of nickel, ensured a smooth flow of fluorine over all the pellet surface. In all the experimental runs, the total gas flow rate was kept at 20 l/h; the reaction was not much affected by the gas flow rate, when it was near 20 l/h.

2.4 Method of calculation

For cylindrical specimen, if the shrinkage rate of the unreacted solid core in gas-solid reaction is the same at any surface, the following equations can be derived.

$$\frac{dr_t}{dt} = \frac{dl_t}{dt} \tag{22}$$

$$r_o - r_t = l_o - l_t \tag{23}$$

where r_o is the initial radius of the pellet, r_t is the radius at time t (in the range of $2 \leq r_t \leq 3$ mm), l_o is half of the initial length of the pellet, and l_t is half of the length at time t (in the range of $0 \leq l_t \leq 1$ mm). By using equation (23), the weight of unreacted core remaining at time t, M_t, is given by,

$$M_t = 2\pi r_t^2 l_t \rho = 2\pi r_t^2 (r_t + l_o - r_o) \rho \ , \tag{24}$$

where ρ is the apparent density of the pellet. Then, the rate of weight change is given by

$$\frac{dM_t}{dt} = 2\pi r_t^2 \rho \frac{dl_t}{dt} + 4\pi r_t l_t \rho \frac{dr_t}{dt} \ , \tag{25}$$

or by using equation (22),

$$\frac{dM_t}{dt} = \frac{dr_t}{dt} \rho (2\pi r_t^2 + 4\pi r_t l_t)$$

$$= \frac{dr_t}{dt} \rho S_t, \quad \text{or} \quad \frac{dl_t}{dt} \rho S_t \ , \tag{26}$$

where S_t is the surface area of the unreacted core at time t. When an overall reaction between gas and solid is controlled by a chemical process on the solid surface, the value of dM_t/dt is proportional to the available surface of the unreacted core, therefore,

$$\frac{dr_t}{dt} = \frac{dl_t}{dt} = -k, \tag{27}$$

and by integrating equation (27),

$$r_o - r_t = l_o - l_t = k\,t \tag{28}$$

Equation (28) shows the kinetics of the pellet shrinkage.

If the uranium oxides are fluorinated to gaseous UF_6 without forming solid intermediate, M_t can be measured experimentally, and then r_t and l_t are calculated by using equations (24) and (23). The rate of surface reaction is usually measured by a weight change per unit surface area, which is a more useful value for measuring chemical change than the above shrinkage rate. From equations (26) and (28),

$$-\int_o^t \frac{1}{S_t}\,dM_t = \rho\,(r_o - r_t) = \rho\,(l_o - l_t) = k\,\rho\,t. \tag{29}$$

Equation (29) shows the kinetics of the weight loss per unit surface area of the uranium oxide pellets.

When the reaction is not governed by a surface process, the plot of the experimentally obtained $(r_o - r_t)$ or $\rho\,(r_o - r_t)$ with the time will deviate from the linear relation. By analyzing the form of these plots, the reaction mechanism can be deduced.

2.5 Fluorination of UO_2 pellets

2.5.1 Experimental results

Fig. II-20 shows the weight change of the pellets during the fluorination at temperatures from 360 to 540°C. The curves at the temperatures above 460°C show nearly a linear change in weight, whereas the curves below 400°C are in a sigmoidal form; this difference indicated a change in the reaction mechanism. No experiments were performed below 300°C where the reaction proceeds very slowly.

Reaction in the temperature range from 300° to 400°C (Type I)

A thick layer of pulverized intermediate was always formed on the unattacked pellet core throughout the reaction. The layer changed its color from yellow at the outer surface to dark green at the inner surface, which indicated that the layer is not homogeneous. X-ray diffraction patterns showed the formation of UO_2F_2 as only definite intermediate. The apparent

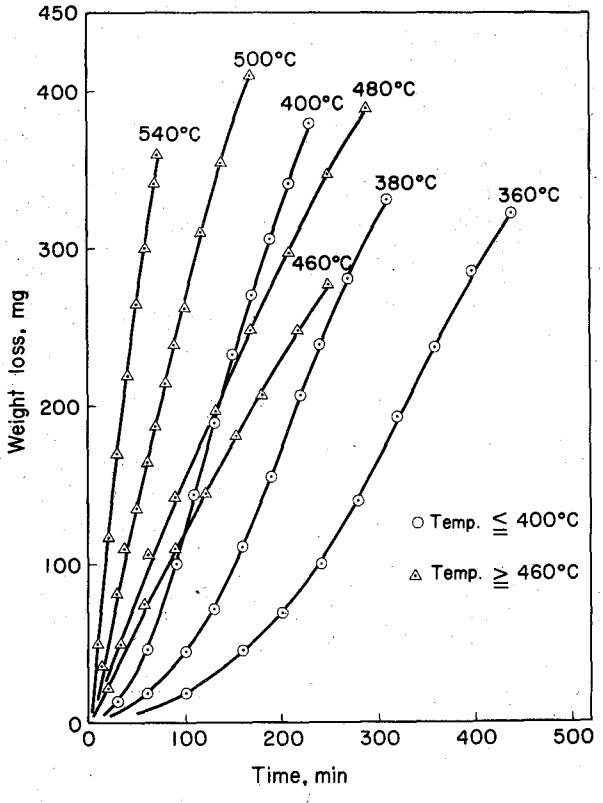

Fig. II-20. Weight loss vs. time at different temperatures. sample, UO_2 pellet; total gas flow rate, 20 l/h; partial pressure of fluorine, 150 mmHg (20 vol. %); total pressure, 760 mmHg.

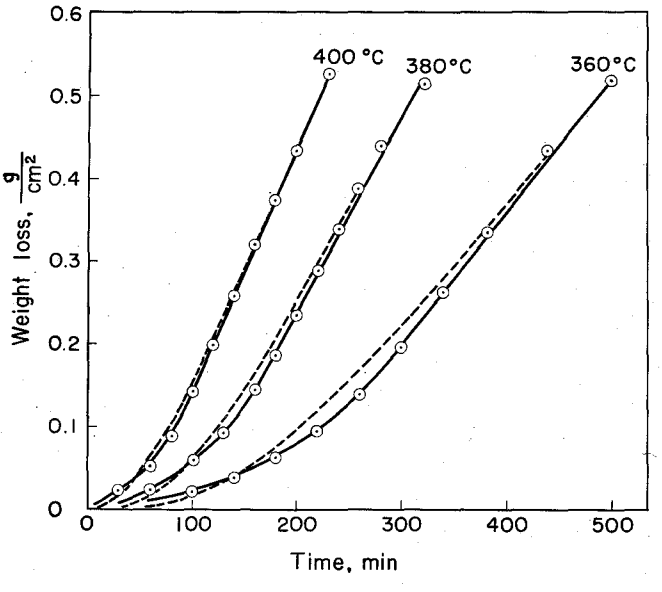

Fig. II-21. Weight loss per unit surface area of UO_2 pellet. Temperature, 360° to 400°C; total gas flow rate, 20 l/h; partial pressure of fluorine, 150 mmHg (20 vol. %); total pressure, 760 mmHg. Dotted lines: calculated from equation (40).

weight change per unit area, calculated by substituting the sample weight during reaction in equation (24) and then using equation (29), is presented in Fig. II-21. Since the actual reaction proceeds successively at the surface of the unreacted core, the intermediate layer, and the outer surface of the intermediate layer, its kinetics are not so simple as those expressed by equation (29). The observed induction period in Fig. II-21 is evidently due to the formation of an intermediate layer. After removing the intermediate scale, the weight of the unreacted core was measured. Fig. II-22 shows that the rate of core shrinkage, calculated from equation (24), is constant with the exception of a short induction period. By the above calculating method and by measuring directly the core size, it was confirmed that below 400°C, the core shrinks linearly. When the fluorine concentration was varied from 7 to 40 volume %, curves similar to those in Figs. II-21 and II-22 were obtained. The reaction rate, determined from the slopes of their straight parts, are plotted in Fig. II-23.

Reaction in the temperature range from 430° to 540°C (Type II)

In this temperature range, the quantity of intermediate formed was generally smaller at any time during the reaction than that of Type I. Fig. II-24 shows the weight loss per unit area at different fluorine concentrations, where the reaction temperature of 480°C was selected as an example in this range. The effect of temperature on the weight change is shown in Fig. II-25.

Above 20% in fluorine concentration, the reaction on the pellet surface proceeded with the formation of a slight amount of white intermediate. The straight lines in Figs. II-24 and II-25 with no induction period, indicate a linear decrease in the pellet size. The reaction rate, determined from the slopes of the straight lines in Fig. II-24, is plotted in Fig. II-23 which shows a linear relationship between the rate and the fluorine concentration in this region.

Below 12% in fluorine concentration, the plots in Fig. II-24 deviate from a linear relationship. In this case, a pulverization of the reacting pellet surface under the white intermediate described above forms a rather thin layer of black powder. The accelerated increase of weight loss shown in Fig. II-24 can be explained by this pulverization which increases the reacting surface on the pellet. The apparent reaction rate increases with the time in the range between the initial and final slopes for each curve. The shaded region in Fig. II-23 corresponds to this range.

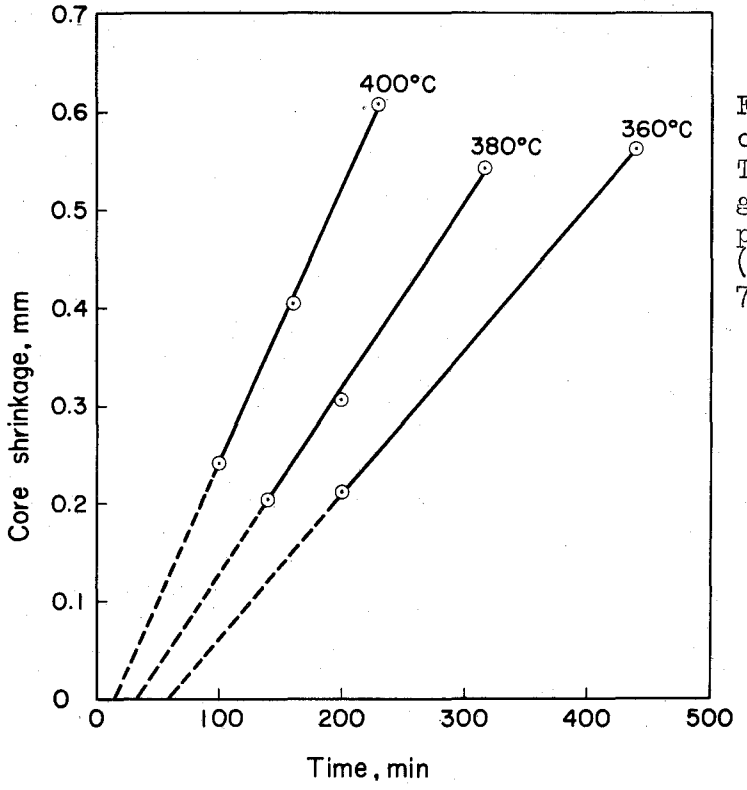

Fig. II-22. Shrinkage of unreacted core of UO_2 pellet. Temperature, 360 to 400°C; total gas flow rate, 20 l/h; partial pressure of fluorine, 150 mmHg (20 vol. %); total pressure, 760 mmHg.

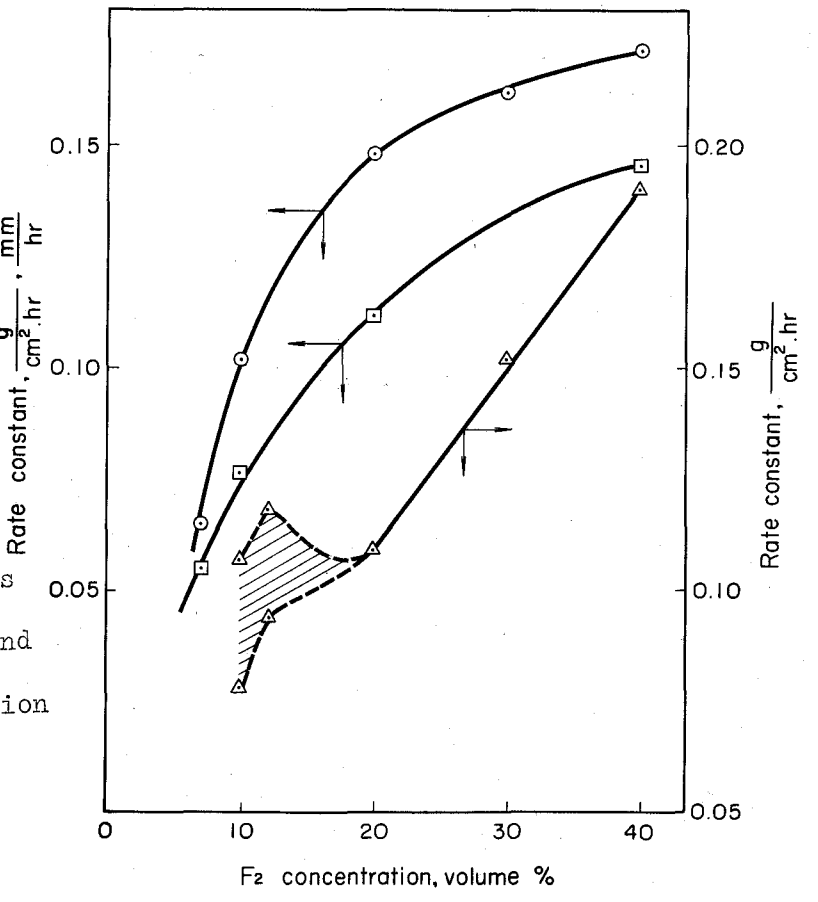

Fig. II-23. Effect of fluorine concentration on rate constant. Sample, UO_2 pellets; ⊙, rate of overall reaction (g/cm^2h) at 380°C, calculated from the slopes of the straight part in curves similar to those in Fig. II-21 and corresponding to k_4 in equation (40); △, rate of overall reaction (g/cm^2h) at 480°C; ⊡, core shrinkage rate (mm/h) at 380°C.

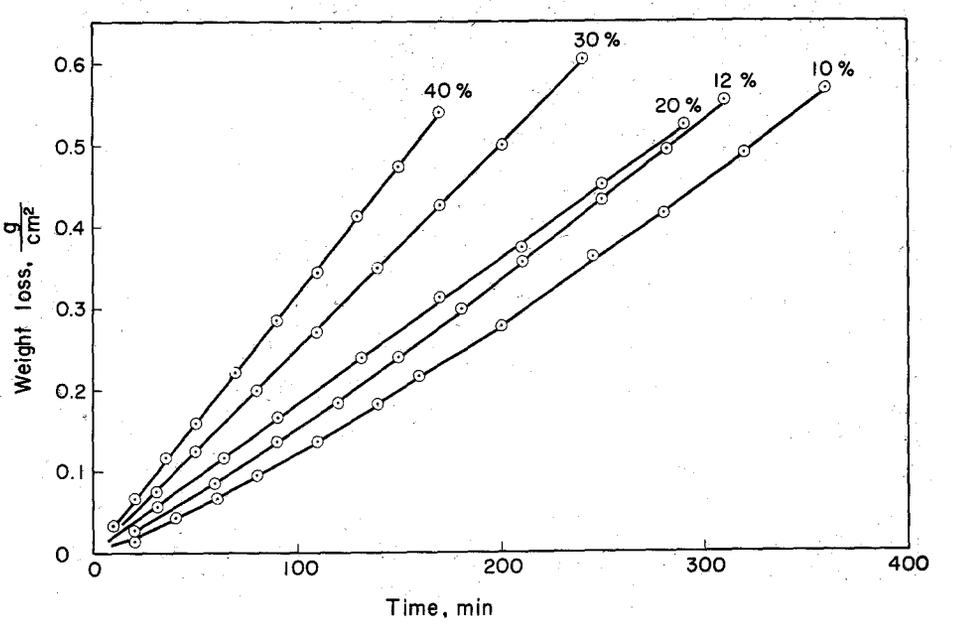

Fig. II-24. Weight loss per unit surface area of UO_2 pellet at different fluorine concentrations.
Temperature, 480°C; fluorine concentrations, 10 to 40 vol. % (76 to 300 mmHg in partial pressure of fluorine); total pressure, 760 mmHg; total gas flow rate, 20 l/h.

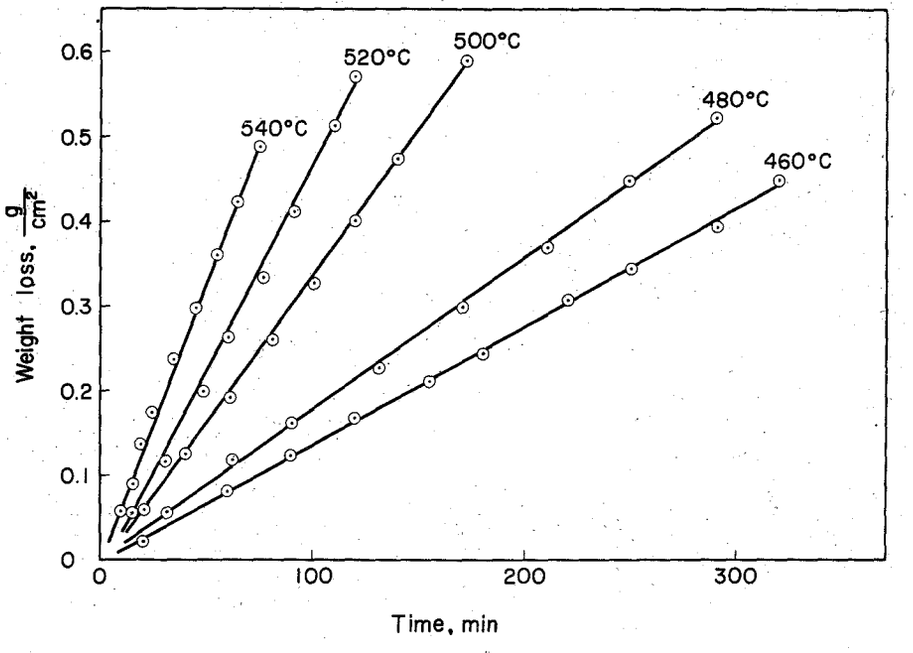

Fig. II-25. Weight loss per unit surface area of UO_2 pellet at different temperatures.
Partial pressure of fluorine, 150 mmHg (20 vol. %); total pressure, 760 mmHg; total gas flow rate, 20 l/h.

2.5.2 Derivation of two types reaction

The fluorination process of the UO_2 pellet was classified into two types of reaction according to the temperature as shown in Fig. II-26. Table II-12 summarizes the properties of various intermediates.

Table II-12. Analysis of reaction residue in the fluorination of UO_2 pellet.

Reaction	Type I	Type II	Type II (dev.)	Type I or II
Intermediate and unreacted core	Greenish yellow powder[a]	White powder[b]	Black powder[c]	Unreacted pellet core
F/U[d]	1.74 to 1.80	2.07[e]	1.35[f]	0.04 to 0.08
X-ray pattern	UO_2F_2	UO_2F_2	Unknown[f]	UO_2
Amount formed[g] (mg)	50 to 100	1	5 to 13	

a, the intermediate formed at reaction temperatures below 400°C and with fluorine concentrations of 5 to 40 volume %.

b, the intermediate formed at reaction temperatures above 430°C and with fluorine concentrations of 7 to 40 volume %.

c, the intermediate formed at the reaction temperature of 480°C and with fluorine concentrations of 7 to 12 volume %.

d, calculated from the results of chemical analysis.

e, average value for the white intermediates formed with fluorine concentrations of 20 to 40 volume %.

f, with fluorine concentration of 7 volume %.

g, formed when 60 to 70% of original pellet weight is lost.

The facts that the atom ratio of fluorine to uranium in the intermediates is usually less than that of stoichiometric UO_2F_2, indicates the formation of a partly fluorinated intermediate in the initial step. It was supposed that the process is started by selective fluorination at the grain boundaries which breaks the pellet into powder partly fluorinated on the surface. Thus, the following consecutive processes may be considered as a simplified model.

$$UO_2 \text{ pellet} \xrightarrow{\text{step 1}} UO_2 \text{ powder (partly fluorinated)}$$

$$\xrightarrow{\text{step 2}} UO_2F_2 \text{ powder} \xrightarrow{\text{step 3}} UF_6.$$

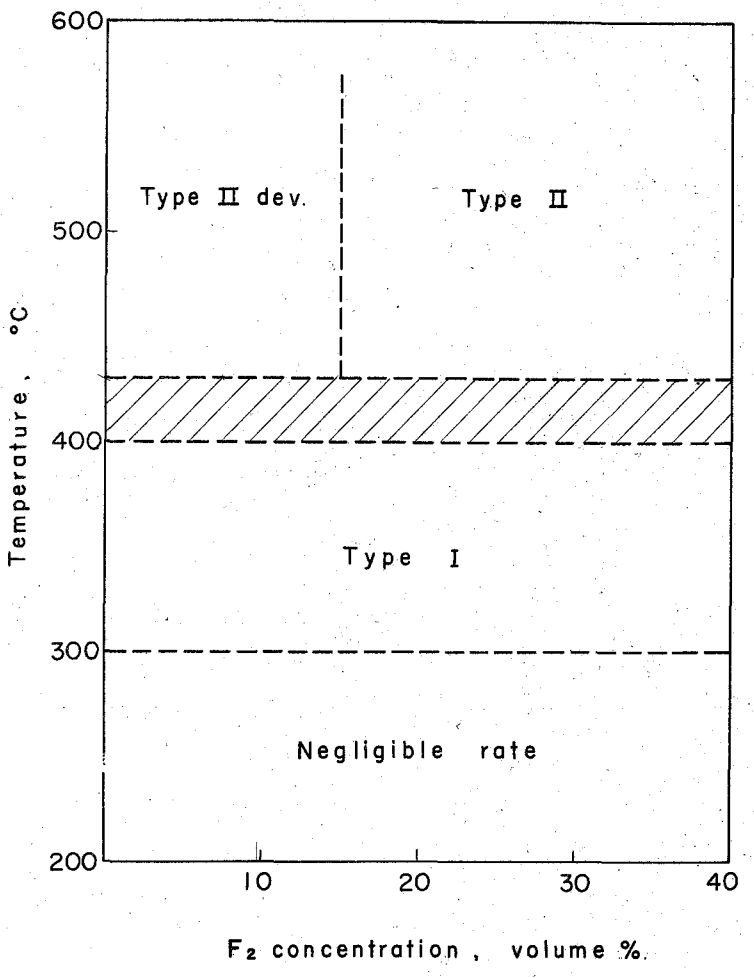

Fig. II-26. Region of two types of reaction. Shaded region is boundary between each type. Type I: temperature, 300° to 400°C; fluorine concentration, 5 to 40 vol. %. Type II: temperature, 430° to 540°C; fluorine concentration, 7 to 40 vol. %.

Step 1 and step 3 are the surface reactions which proceed on the interface between the pellet core and the intermediate layer, and on the outer surface of the intermediate layer respectively, whereas step 2 proceeds throughout the intermediate layer. The rate of step 2 can be measured by the weight change per unit area of an arbitrary surface which is parallel to the core surface or the outer surface of the intermediate layer. Therefore, the reaction rate can be expressed by a common unit of surface reaction. If all steps are simply first order reactions of solid reactants, the reaction rate of i th step is given by

$$r_i = k_i C_i , \qquad (30)$$

where k_i is the reaction rate constant of i th step, measured by a common dimensional unit, r_i is the reaction rate of i th step, and c_i is the fraction of solid reactant of i th step.

In the reaction Type I, it was found that the core shrinkage (step 1) proceeds always linearly independent of the formation of the intermediate layer. If the diffusion of fluorine gas through the intermediate layer controlled the step 1 process, the shrinkage should deviate from the linear

relationship. Therefore, even in the innermost part of the reaction layer, the fluorine gas appears to penetrate sufficiently. Thus, the effect of gaseous fluorine was neglected in equation (30).

The occurrence of two types of reaction may be explained by assuming the following relations among the rate of each step.

Type I, $k_1 > k_2 \gg k_3$, $r_1 > r_2 \gg r_3$ at 300 to 400°C;

Type II, $k_1 \ll k_2 < k_3$, $r_1 \approx r_2 \approx r_3$ at 430 to 540°C.

A large amount of the pulverized intermediate was formed in Type I, while in Type II the amount was generally smaller than that of Type I. These facts cause their inequalities to be in opposite directions. In Type I, since the intermediate powder has relatively high values of F/U ratio, 1.74 to 1.80 (see Table II-12), the relation $k_2 \gg k_3$ can be deduced. In Type II, the relation $k_1 \ll k_2$ is derived from the results that the formation of intermediate is very slight in the region above 15% fluorine, whereas the relation $k_2 < k_3$ is derived by considering that the intermediate of UO_2F_2 is formed even though its amount is very slight. Since step 1 in Type II controls the overall reaction rate, the rates of the other steps (r_2, and r_3) become equal to r_1.

In the region of Type II, it is clearly shown in Fig. II-24 that the form of the reaction begins to change below the vicinity of 15 to 20% fluorine. If the reaction above 20% fluorine is classified as typical of Type II, the reaction at lower fluorine concentrations may be classified as another type of reaction. But, in this case, the change in the appearance of the reaction residue was small as described in section 2.5.1 and not as distinct as that seen between Types I and II. From these facts, it was considered that in the region above 430°C, there is essentially one type of reaction of which the typical form is shown above 20% fluorine and the reaction at lower fluorine concentrations may be regarded as a deviated form. Although it is difficult to express the deviation in a formula, a detailed discussion will appear in the next section.

2.5.3 Mechanism of the reaction

In the preceding section, it was proposed that step 1 (UO_2 pellet $\longrightarrow$ UO_2 powder, partly fluorinated) should be added to the other consecutive steps. In this section, its probable mechanism is discussed.

Taking account of the inequalities for Types I and II in section 2.5.2, the rate of step 1 at different temperatures was evaluated from the slopes of Figs. II-22 and II-25, and listed in Table II-13. Fig. II-27 shows the

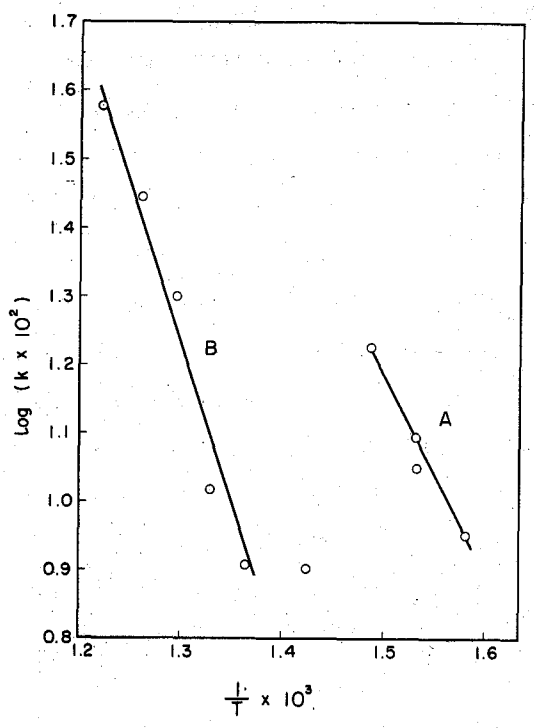

Fig. II-27. Arrhenius plot. Sample, UO_2 pellet; A; 360° to 400°C; B; 460° to 540°C; partial pressure of fluorine, 150 mmHg (20 vol. %); total pressure, 760 mmHg; total gas flow rate, 20 l/h.

Arrhenius plot of these k_1 values, where the plot is divided into separate lines, A and B. The activation energies were calculated as 14.0 kcal/mole in the region below 400°C and 23 kcal/mole above 460°C.

Table II-13. Reaction rate constants for the fluorination of UO_2 pellets Partial pressure of fluorine, 150 mmHg (20 vol. %); total pressure, 760 mmHg; total gas flow rate, 20 l/h.

Temperature (°C)	k_1 a) (mm/h)	k_2 b) (l/min)	k_4 c) ($g/cm^2.h$)
360	0.089	1/185	0.094
380	0.125	1/108	0.146
400	0.167	1/53	0.178
460	0.081 d)	——	0.085
480	0.104 d)	——	0.109
500	0.200 d)	——	0.210
520	0.278 d)	——	0.292
540	0.380 d)	——	0.400

a) refer to equation (31); b) refer to equations (32) and (40); c) refer to equation (40); d) k_1 (mm/h) was calculated by the equation, k (mm/h) = 1/1.05 k ($g/cm^2.h$), which was derived from equations (28) to (31). The values of k_4 were determined from the slopes of lines in Fig. II-24.

If step 1 were always controlled by the same mechanism, the reaction rate should always increases with increase of temperature by following the Arrhenius type relationship. The occurrence of the anomalous region between 400° and 460°C, which apparently has a negative activation energy, appears to be due to some change in the mechanism of the step 1 process. The following causes may be suggested: (1), formation of a protective film which restricts the transport of fluorine or reaction product; (2), occurrence of a side reaction which consumes fluorine; (3), effects of impurities, etc. But, by considering the experimental conditions and results, assumptions (1) and (2) cannot be recognized as reasonable causes. For (3), it may be considered that oxygen, contained as an impurity, or generated in the fluorination, acts to pulverize the pellet. But Peakall and Antill have reported that the rate of pulverization of UO_2 pellets by oxidation is rather slow below 400°C and accelerates above 450°C.[25] A similar change in the rate of pulverization with increase of temperature was observed for the pellets used in this experiments for oxidation in air or oxygen. These results are inconsistent with the k_1 values in Table II-12 which show a maximum at 400°C.

On the contrary, the plots between the reaction rate and fluorine concentration in Fig. II-23 show a marked difference in their forms, from which the cause of the change in reaction mechanism may be deduced. The linear relation at 480°C, above 20% in fluorine concentration, may well be explained by a simple collision process, whereas, at 380°C, the plot for the step 1 process resembles the chemisorption isotherm. It may be further postulated that the fluorine gas should be adsorbed in a monolayer without dissociating to atoms, by examining the fit of the k_1 values to the expression for the isotherm at the corresponding fluorine concentration. This fact is suggestive of the following reaction process in the region below 400°C. First, the fluorine is chemisorbed rapidly at the active sites on the solid surface when it is in equilibrium with the partial pressure of fluorine in the gas phase. By supposing that this chemisorbed fluorine acts as the main reactant for further fluorination and that the rate is controlled by its reaction with the solid reactant, the relationship between the rate and fluorine concentration will become similar to the curve of the chemisorption isotherm as shown in Fig. II-23. Since the active sites will be concentrated at the grain boundaries, pulverization of the pellet progresses as a result of the selective fluorination at these places. A decrease in the value of k_1 in the

temperature range from 400 to 430°C corresponds to a decrease in the amount of chemisorbed fluorine, which is generally explained by the exothermic nature of chemisorption. This state of adsorbed fluorine may be regarded as a metastable state in the reaction processes, so that it seems difficult to observe directly such a state which would soon change to a following state. The increase in the rate again above 460°C may be attributed to another reaction process in which a collision mechanism becomes predominant.

In the region of lower fluorine concentration for Type II, pulverization of the pellet surface seems to occur and a layer of black powder was observed as described in section 2.5.1. The F/U ratio, 1.35, of this powder is relatively low, as compared with the value, 1.74 to 1.80, for the intermediate in Type I, as shown in Table II-12. This result indicates that in the type II region, the general relation $k_1 \ll k_2$ seems to have a tendency to be changed to the inverse relation $k_1 > k_2$ with decreasing fluorine concentration. As possible causes of this, the following reasons may be supposed: First, if the possible reaction processes are limited to the three steps described in section 2.5.2, the rate of steps 1 and 2 must have different dependences on the fluorine concentration in this region in order to produce the above tendency in the relation between k_1 and k_2. Steps 1 and 2 are essentially similar as regards the formation of the intermediate UO_2F_2, but step 1 is a corrosive process on the surface of the UO_2 pellet, whereas step 2 is a gas-solid reaction between fluorine and a UO_2 powder partly fluorinated. This difference in the physical aspects of the reaction suggests the possibility that k_1 and k_2 have different dependences on the fluorine concentration. Secondly, the effect of oxygen is considered as another possible cause, since pulverization of the UO_2 pellet progresses rather rapidly above 450°C. In this case, it may be supposed that the oxidation always takes place concurrently with the fluorination, but that in the higher fluorine concentrations, the fluorination processes predominate, so that the effect of oxidation cannot be observed.

2.5.4 Derivation of expressions for the reaction rate

In Type I, each step proceeds in relatively separate zones, so that the numerical relationship between each step can be determined. The results in Fig. II-22 show that the first step reaction, which occurs at the interface between the pellet core and the intermediate layer, corrodes the core linearly, i.e.,

$$l_o - l_t = k_1 t , \qquad (31)$$

where k_1 is the rate constant of the first step reaction. If the second step

is a first-order homogenous reaction which proceeds in the pulverized intermediate, the rate of the second step reaction in a zone of thickness $d\xi$ at an arbitrary point P (Fig. II-28) is expressed by

$$\frac{dx_\xi}{dt'} = k_2 (1 - x_\xi), \qquad (32)$$

where k_2 is the rate constant of the second step reaction,* x_ξ is the mole fraction of UO_2F_2 at the elemental zone, and t' is the time from the start of the second step given by

$$t' = t - \frac{\xi}{k_1} . \qquad (33)$$

Then, the solution of equation (32) is

$$x_\xi = 1 - \exp \left[-k_2 \left(t - \frac{\xi}{k_1} \right) \right] . \qquad (34)$$

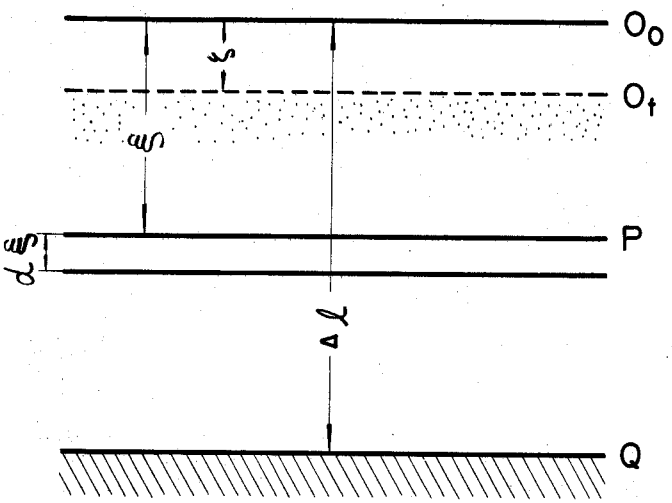

Fig. II-28. Cross sectional view of the intermediate layer during fluorination of UO_2 pellet. O_o, original pellet surface; O_t, surface of the intermediate layer at time t; Q, surface of the unreacted core.

---

* k_2 in this section and k_2 in section 2.5.2 differ in their units. In equation (32), the dimension of k_2 is $time^{-1}$, which is derived by considering the rate of step 2 at an arbitrary point in the intermediate at a given reaction time. In section 2.5.2, k_2 was defined as having a dimension $g/cm^2.h$ in order to compare the rate of step 2 with that of steps 1 and 3. The dimension of $g/cm^2.h$ in step 2 may be considered as a cumulative rate over the whole intermediate layer at a given reaction time.

In the elemental zone, the weight gain per unit area at time t' (dm) is given by

$$dm_{\xi} = \rho (\alpha - 1) x_{\xi} \quad d_{\xi} , \tag{35}$$

where

$$\alpha = \frac{\text{molecular weight of } UO_2F_2}{\text{molecular weight of } UO_2}, \text{ and}$$

ρ = the density of the original pellet.

The total weight gain per unit area, Δm_{ti}, is given by integrating equation (35):

$$\Delta m_{ti} = \int_0^{k_1 t} dm_{\xi} = \rho (\alpha - 1) k_1 \{ t - \frac{1}{k_2} [1 - \exp (- k_2 t)] \} . \tag{36}$$

By assuming that the third step reaction proceeds on the external surface of the intermediate layer and that its rate is proportional to the mole fraction of UO_2F_2 on the surface, the following equation is obtained:

$$\frac{d\zeta}{dt} = \beta k_3 \{ 1 - \exp [- k_2 (t - \frac{\zeta}{k_1})] \} \tag{37}$$

where ζ is the coordinate of the external surface and k_3 is the rate constant of the third step reaction. The outer surface of the pulverized layer is rather rough and the actual reaction of step 3 occurs partly in from the surface. The factor β was used to relate this complex process to a simple surface reaction.

Since the relationship of $r_1 \gg r_3$ leads to $k_1 t \gg \zeta$, the following approximation is given:

$$\frac{d\zeta}{dt} \approx \beta k_3 [1 - \exp(-k_2 t)] . \tag{38}$$

The weight loss per unit area, Δm_{td}, in the third step reaction is given by:

$$\Delta m_{td} = \beta \alpha \rho k_3 \{ 1 - \frac{1}{k_2} [1 - \exp(-k_2 t)] \} \tag{39}$$

Then, the total weight loss per unit area, Δm_t, can be represented by:

$$\Delta m_t = \Delta m_{td} - \Delta m_{ti} = \rho [\alpha \beta k_3 - (\alpha - 1) k_1] \{ t - \frac{1}{k_2} [1 - \exp (- k_2 t)] \}$$

$$= k_4 \{ t - \frac{1}{k_2} [1 - \exp (- k_2 t)] \} . \tag{40}$$

The dotted lines in Fig. II-20 are calculated from equation (40). The values of k_4 and k_2 were determined from the slopes of straight parts of the curves in Fig. II-21 and from the intercepts of those lines with abscissa. The reaction time was measured from the intercepts of the straight lines with the abscissa in Fig. II-22.

In the Type II reaction above 20% fluorine, since the first step reaction is rate-controlling, the overall reaction rate is represented by the simple linear relationship of equation (29) as shown in Fig. II-25. An Arrhenius type plot of the reaction rate, determined from the slope of the straight parts in Figs. II-21 and II-25, gives apparent activation energies of 23 kcal/mole above 460°C and 16.6 kcal/mole below 400°C. A series of k_2 values also yields an activation energy of 26.6 kcal/mole. Table II-13 summarizes the values of several rate constants.

2.6 Fluorination of U_3O_8 pellets

2.6.1 Effect of pellet density on the reaction rate

The densities of U_3O_8 pellets were from 6.0 to 7.5 g/cm^3 much lower than the theoretical value of 8.38, and so the pellets has relatively large porosities distributed over a wide range. Consequently, the effect of the pellet porosity on the reaction rate must be clarified. For the pellet with a large porosity, fluorine gas will penetrate readily into the pellet and the fluorination will proceed not only at the outer surface but also in the interior of the pellet. The kinetic equation (28) and (29) in section 2.4 were derived by assuming that the reaction always proceeds at the outer surface of the pellets. However, when the reaction occurs in the interior, a deviation from the linear relationship of equation (28) or (29) will occur. Figure II-29 shows the shrinkage of the pellets with different densities. The deviation from the linear relationship of shrinkage of the unreacted core increases with decreasing pellet density. To express the degree of deviation, the following equation was derived by modifying the equation (28):

$$r_o - r_t = l_o - l_t = k\,(t)^x. \qquad (41)$$

When $x = 1$, equation (41) is in the same form as equation (28).

In Fig. II-30, $r_o - r_t$ (or $l_o - l_t$) vs. t are plotted on a logarithmic scale; from the slopes of each curve, the values of x were calculated as follows:

Range of pellet density (g/cm^3)	x
7.5 to 8.0	1.03
7.0 to 7.5	1.2
6.5 to 7.0	1.3
6.0 to 6.5	1.4

Above 7.5 in the pellet density, the pellet shrinks linearly, since x = 1, whereas, for the pellets having the densities below 7.5, the reaction deviated from the linear relationship. All the curves in Fig. II-29, however, have the same slope at the early stage of the reaction. Therefore, the rate of shrinkage of the pellet can be measured from the slope of the asymptote for the curves at the beginning, irrespective of the difference in pellet density. In the present work, the pellets with densities from 7.0 to 7.5 were mainly used.

2.6.2 Kinetics and mechanism of the reaction

Fig. II-31 shows the plots of the weight change per unit area vs. the time at different temperature; at higher temperatures, the linear relationships are obtained, while below 430°C deviations take place. When the sample weight became 40 ~ 70% of the initial weight, the reaction was suspended to observe the residual pellet. At any temperatures, a slight amount of whitish yellow intermediate UO_2F_2 was found on the surface of the residual pellet.

In order to determine the amount of this UO_2F_2 formed, the residual pellet was immersed in a warm water at about 60°C, and the UO_2F_2 was removed by dissolution into water, and finally the undissolved residue was dried and

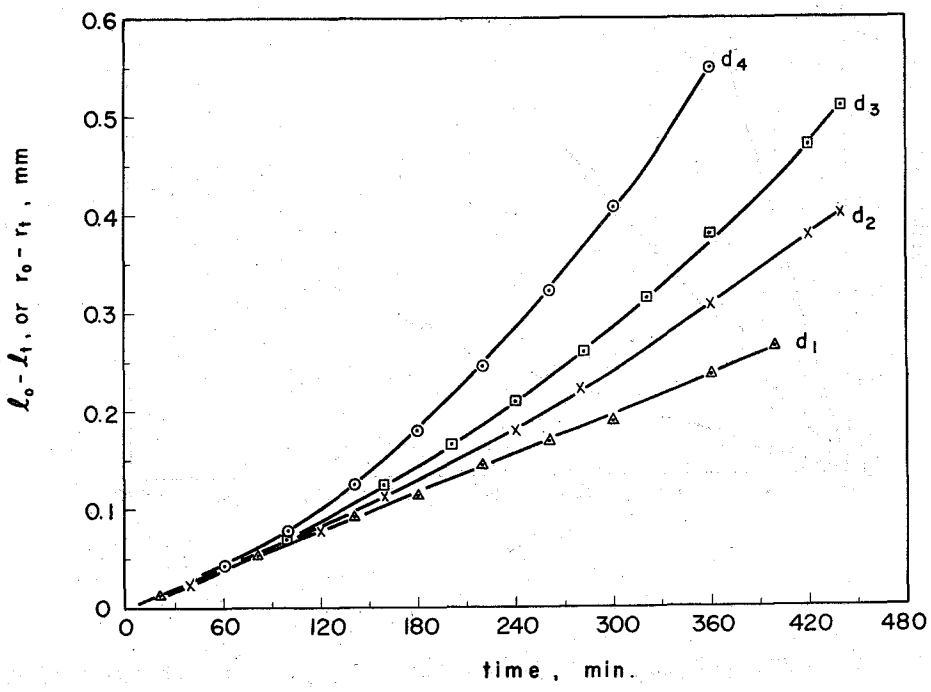

Fig. II-29. Core shrinkage of U_3O_8 pellets with different densities.
Temperature, 430°C; partial pressure of fluorine, 150 mmHg (20 vol. %); total pressure, 760 mmHg; total gas flow rate, 20 l/h; d_1: 7.5 to 8.0, d_2: 7.0 to 7.5, d_3: 6.5 to 7.0, d_4: 6.0 to 6.5 in pellet density(g/cm^3).

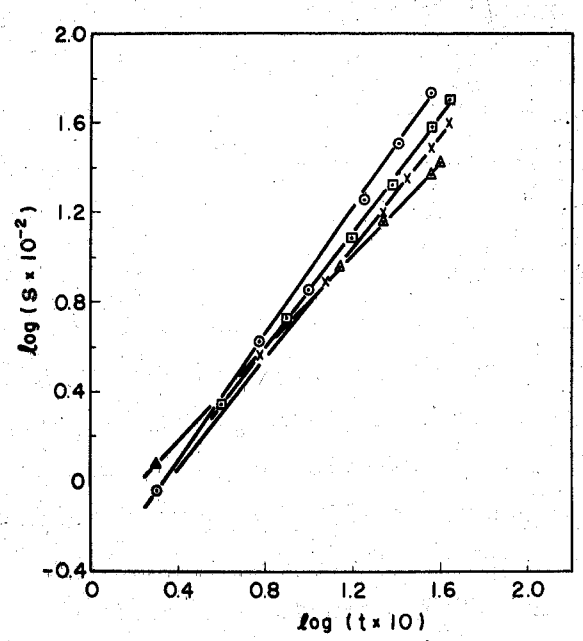

Fig. II-30. Logarithmic plot of core shrinkage vs. time for U_3O_8 pellets with different densities. Notations of d_1 to d_4 are the same with those in Fig. II-29; $s = l_o - l_t$ or $r_o - r_t$.

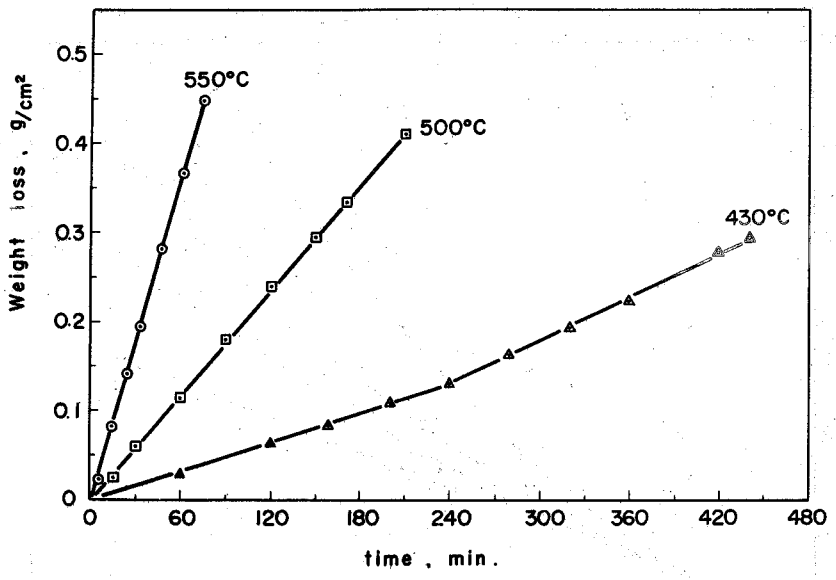

Fig. II-31. Weight loss per unit surface area of U_3O_8 pellet at different temperatures.
Partial pressure of fluorine, 150 mmHg (20 vol. %); total pressure, 760 mmHg; total gas flow rate, 20 l/h.

weighed. The weights of the reaction residue before and after this immersion are shown in Table II-14. At the reaction temperature of 500°C, the amount of intermediate UO_2F_2 was slight, while at 430°C, its amount was large and the residual pellet was broken into pieces during the immersion in the warm water. These results indicate that the intermediate UO_2F_2 is formed at the inner part of pellet at 430°C but not at 500°C. To the contrary, little difference appeared in the form of the weight loss curves in Fig. II-31 or in the appearance of the residual pellets, for the fluorinations at 430° and 500°C. A layer of the intermediate was not formed, unlike the case of the fluorination of UO_2 pellets below 430°C. From the slopes of the curves in Fig. II-31, the overall reaction rate was determined, and the Arrhenius plot was obtained as shown in Fig. II-32; the activation energy was calculated to be 23 kcal/mole. The good linearity in the Arrhenius plot appears to show that there is apparently no change in the reaction mechanism. However, the large difference between the amounts of UO_2F_2 formed at 430° and 500°C suggests that a change in the reaction mechanism similar to that assumed in the fluorination of UO_2 pellets occurs; that is, the simple collision mechanism at higher temperatures and the fluorine adsorption mechanism at lower temperatures. At temperatures below 430°C, the reaction velocity was too slow to analyze the mechanism of reaction.

The effect of the partial pressure of fluorine on the reaction rate were shown in Figs. II-33 and II-34 and the rate constants calculated from the slopes of the curves in Fig. II-33 are listed in Table II-15. The reaction rate is nearly proportional to the partial pressure of fluorine.

The reaction rate of the U_3O_8 pellet can be expressed by the following equations:

$$\frac{dM_t}{dt} = k\,S_t, \text{ or } \rho\,(l_o - l_t) = \rho\,(r_o - r_t) = kt,$$
$$k\left[\frac{g}{cm^2 h}\right] = 2.4 \times 10^3 \exp\left(-\frac{23000}{RT}\right) p, \qquad (42)$$

where k is the reaction rate constant, and ρ is the apparent density of pellet (7.25 g/cm^3), p is the partial pressure of fluorine; the other symbols have the same significance as those in section 2.4 in this chapter.

In Table II-15 and II-16, the rate constants obtained experimentally, and those calculated from equation (42), are listed.

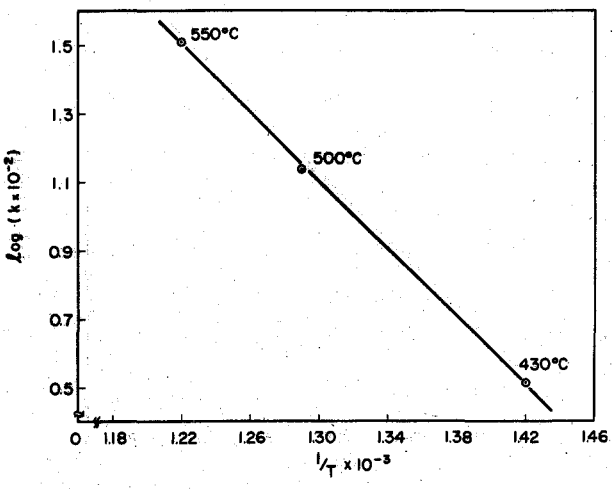

Fig. II-32. Arrhenius plot. Sample, U_3O_8 pellet; partial pressure of fluorine, 150 mmHg (20 vol. %); total pressure, 760 mmHg; total gas flow rate, 20 l/h.

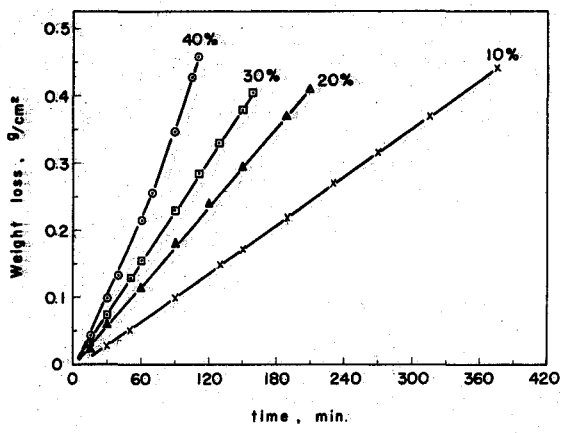

Fig. II-33. Weight loss per unit surface area of U_3O_8 pellet at different fluorine concentrations. Temperature, 500°C; total pressure, 760 mmHg; total gas flow rate, 20 l/h.

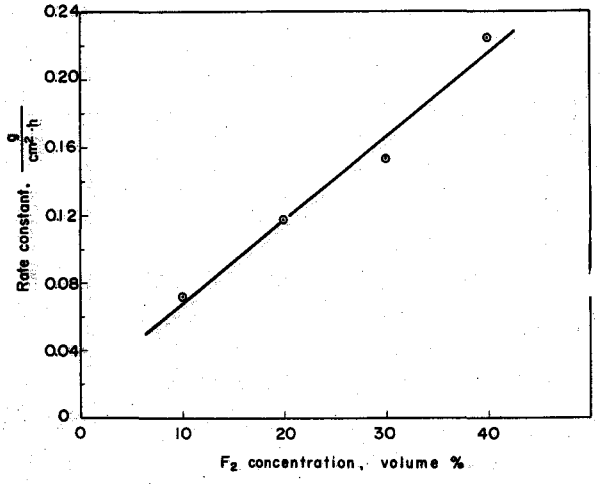

Fig. II-34. Effect of fluorine concentration on rate constant. Sample, U_3O_8 pellet; temperature, 500°C; total pressure, 760 mmHg; total gas flow rate 20 l/h.

Table II-14. Imersion test of the residual U_3O_8 pellet.

Reaction temperature (°C)	Pellet density	Weight of residue (mg)	Weight of insoluble residue (mg)	Weight decrease (mg)
430	6.5~7.0	172.4	75.1	98.3
430	7.0~7.5	212.4	125.6	86.8
500	7.0~7.5	187.4	181.1	6.3
500	7.0~7.5	147.1	140.0	7.1

Table II-15. Reaction rate constants for the fluorination of U_3O_8 pellet by fluorine —— effect of fluorine partial pressure. Temperature, 500°C.

Partial pressure of fluorine (mmHg)	Rate constants $(\frac{g}{cm^2.h})$	
	measured	calculated
76 (10 mole %)	0.072	0.062
150 (20 mole %)	0.117	0.122
230 (30 mole %)	0.153	0.187
300 (40 mole %)	0.234	0.244

Table II-16. Reaction rate constants for the fluorination of U_3O_8 pellet by fluorine —— effect of temperature. Fluorine partial pressure, 150 mmHg.

Temperature (°C)	Rate constants $(\frac{g}{cm^2.h})$	
	measured	calculated
430	0.032	0.028
500	0.117	0.122
550	0.361	0.300

3. Summary

I) Fluorination of UO_2, U_3O_8, and UO_3 in powders by fluorine

The reaction was investigated at temperatures from 350° to 430°C, and partial pressures of fluorine from 80 to 150 mmHg. All the reactions consisted of the following steps:

$$UO_2 + F_2 \xrightarrow{k_1} UO_2F_2$$
$$\frac{1}{3}U_3O_8 + F_2 \xrightarrow{k_1} UO_2F_2 + \frac{1}{3}O_2 \qquad \text{(a)}$$
$$UO_3 + F_2 \xrightarrow{k_1} UO_2F_2 + \frac{1}{2}O_2$$
$$UO_2F_2 + 2F_2 \xrightarrow{k_2} UF_6 + O_2 \qquad \text{(b)}$$

Except in the case of U_3O_8 powders, the first step proceeded much more rapidly than the second step. The reaction behaviors of the powders are as follows.

UO_2 powders

$k_1 \gg k_2$ for both the samples, active and inactive, which have the adsorption surface area of 4.4 and 0.17 m^2/g respectively; k_1 and k_2 are the rate constants of reactions (a) and (b). The reaction rate of the active sample was larger than that of the inactive sample.

U_3O_8 powders

The rate of overall reaction was nearly proportional to the surface area of powder sample.

$k_1 > k_2$ for U_3O_8 prepared by calcination of ammonium diuranate at 700°C.

$k_1 \lesssim k_2$ for U_3O_8 prepared by calcination of ammonium diuranate at 1000°C.

UO_3 powders

$K_1 \gg k_2$ for the samples prepared by calcination of ammonium diuranate at 350°C. The reaction rate was not affected by the adsorption surface area of samples.

II) Fluorination of UO_2 and U_3O_8 pellets fluorine

UO_2 pellets

The reaction was studied at temperatures from 300 to 540°C and at partial pressures of fluorine from 50 to 300 mmHg. Below 430°C, a thick layer of intermediate scale was formed on the unreacted pellet core. In this range, by surveying the relationship between the rate of reaction and the fluorine partial pressure, it was concluded that chemisorption of fluorine takes place.

Above 430°C, on the contrary, the intermediate was formed in small amounts. Although the formation of UO_2F_2 was confirmed by X-ray analysis, the atomic ratio of fluorine to uranium in the intermediate was usually less than that of stoichiometric UO_2F_2. From this result, the following consecutive reaction steps were considered:

$$UO_2 \text{ pellet} \xrightarrow{k_1} UO_2 \text{ powder (partly fluorinated)} \xrightarrow{k_2}$$

$$UO_2F_2 \text{ powder} \xrightarrow{k_3} UF_6.$$

The occurrence of the above two types of reaction was explained by the following relations between the rates of these steps:

$$k_1 > k_2 \gg k_3 \qquad \text{at } 300^\circ \sim 430^\circ C, \text{ and}$$

$$k_1 \ll k_2 < k_3 \qquad \text{at } 430^\circ \sim 540^\circ C,$$

where k_1, k_2, and k_3 are the rate constants of the above consecutive steps in order from initial to final one.

U_3O_8 pellets

The reaction was studied at temperatures from 430° to 540°C and at partial pressures of fluorine from 80 to 300 mmHg. Below 400°C, the reaction was too slow to measure the rate accurately. At 430°C, the intermediate UO_2F_2 was formed in large amounts at the inner part of pellet, but the formation of a thick layer of intermediate seen in the fluorination of UO_2 pellet at lower temperatures was not observed. At higher temperatures above 500°C, the amount of intermediate formed was very slight. However, considering also the results of the fluorination of U_3O_8 powder, it was concluded that the reaction consists of the following two steps:

$$U_3O_8 \text{ pellets} \xrightarrow{k_1} UO_2F_2 \xrightarrow{k_2} UF_6$$

where, $k_1 < k_2$ at temperatures above 500°C, and

$k_1 > k_2$ at temperatures below 430°C.

The reaction rate constant may be expressed by the following equation:

$$K\left[\frac{g}{cm^2 h}\right] = 2.4 \times 10^3 \exp\left(-\frac{23000}{RT}\right) p,$$

where T is the temperature (°K) of 700° to 810°K, p is the partial pressure of fluorine (mmHg), and t is the reaction time.

References

1) Katz, J. J., Rabinowitch, E., The Chemistry of Uranium, National Nuclear Energy Series, Division VIII, Vol. 5, pp. 396 ~ 403, Dover Publications, Inc., New York (1951).
2) Mecham, W. J., Jonke, A. A., Gabor, J. D., Wehrle, J., ANL-6145, p. 103 (1960).
3) Jonke, A. A., Mecham, W. J., Gabor, J. D., Kinzler, R., Raschinskas, A., Wehrle, J., ANL-6379, p. 159 (1961).
4) Jonke, A. A., Mecham, W. J., Gabor, J. D., Anastasia, L., Wehrle, J., Kinzler, R., Raschinskas, A., ANL-6543, p. 128 (1962).
5) Jander, W., Z. anorg. Chem., 163, 1 (1927).
6) Farrar, R. L. Jr., Smith, H. A., J. Phys. Chem., 59, 763 (1955).
7) Levenspiel, O., Chemical Reaction Engineering, pp. 333 ~ 357, John Wiley and Sons, Inc., New York (1962).
8) Crank, J., The Mathematics of Diffusion, Oxford at the Clarendon Press (1956).
9) Labaton, V. Y., Johnson, D. B., J. Inorg. Nucl. Chem., 10, 74 (1959).
10) Jarry, R. L., Baker, T. D., ANL-6725, p. 125 (1963).
11) Cordfunke, E. H. P., J. Inorg. Nucl. Chem., 24, 303 (1962).
12) Moriya, K., Private Communications (1962).
13) Moriya, K., Takashima, A., Private Communications (1963).
14) Motojima, K., Bunseki no Shishin, JAERI-memo 2102, F-1201-1 (1965).
15) Hashitani, H., Unpublished work (1967).
16) Harrington, D. E., Dorsett, R. S., DP-1004 (1965).
17) Warf, J. C., Cline, W. D., Tevebaugh, R. D., Anal. Chem., 26, 343 (1954).
18) Willard, H. H., Winter, O. D., Ind. Eng. Chem., Anal. Ed., 5, 7 (1933).
19) Powell, R. H., Menis, O., Anal. Chem., 30, 1546 (1958).
20) Belcher, R., Leonard, M. A., West, T. S., J. Chem. Soc., 3577 (1959).
21) Leonard, M. A., West, T. S., J. Chem. Soc., 4477 (1960).
22) Hashitani, H., Muto, H., Japan Analyst, 14, 1114 (1965).
23) Mitsubishi Atomic Power Industries, Inc., Specifications for the UO_2 pellets.
24) Sumitomo Denko Co., Specifications for the U_3O_8 pellets.
25) Peakall, K. A., Antill, J. E., J. Nucl. Materials, 2, 194 (1960).

Chapter III

Fluorination of uranium oxides by bromine trifluoride

1. Fluorination behavior of interhalogen fluorides

It is well known that halogen fluoride, ClF, ClF_3, BrF_3, and BrF_5, can fluorinate various uranium compounds to UF_6. Of these halogen fluorides, ClF, ClF_3, and BrF_5 have relatively low boiling points, so they are generally used as gaseous fluorinating reagents. BrF_3 has been used as the liquid fluorinating reagent since it has a suitable temperature range of liquid phase from the melting point 8.77°C to the boiling point 125.75°C.

Many investigations have been made on the gas-solid reactions between gaseous halogen fluorides and various uranium compounds.[1-6, 8-13] Labaton studied the details of the fluorination reaction of UF_4 with ClF_3 and found that it proceeded even at room temperature.[1] The fluorination of uranium oxides with ClF_3 to UF_6 have been studied by Schmets et al.[4-6] In all the cases, the reactions proceeded at much lower temperatures than the case for fluorine (the reaction with fluorine occurring above 300°C [7]). The activation energies were much lower (2 ~ 6 kcal/mole) than that for the reaction with fluorine (20 ~ 30 kcal/mole).

Jarry and Steindler investigated the fluorination reaction of UF_4, UO_2F_2, UO_2, U_3O_8, and UO_3 with gaseous BrF_5, which proceeded in a little higher temperature range, 200° to 300°C, with a little higher activation energies ranging from 8 to 17 kcal/mole.

The investigations so far published on the fluorination reactions with BrF_3 have all been made in liquid phase. Emeleus and co-workers have found that BrF_3 readily fluorinates uranium oxides to volatile uranium hexafluoride at temperatures below the boiling point of BrF_3.[10,11] It has also been found that uranium metal and its alloys are rapidly fluorinated to UF_6 in liquid BrF_3.[12,13] These results indicate that the reactivity of BrF_3 as a fluorinating reagent is as strong as that of ClF_3.

It was observed in the author's preliminary experiments that U_3O_8 powder reacted explosively with liquid BrF_3 at room temperature, whereas gaseous BrF_3 fluorinated the uranium oxides rapidly but at a controllable and measurable rate. Here, the reaction with gaseous BrF_3 are described.

2. Experiment

Materials

A commercial bromine trifluoride from Harshaw Chemical Co., was used.

The UO_2 and U_3O_8 samples were in pelletized form; their properties and preparation methods were the same with those described in Part II, section 2.2.

Experimental apparatus and procedure

The apparatus used is shown schematically in Fig. III-1. The liquid BrF_3 in a Daiflon vessel (4) was evaporated by bubbling it with a flow of argon gas at a constant rate and at a given temperature. The vessel (5) was filled with fluoro-oil (Daifloil) and its temperature was controlled to a value lower than that of the vessel (4), A Daiflon spiral tube was immersed in the fluoro-oil; in the tube, the excess of BrF_3 was condensed and the partial pressure of BrF_3 in the argon carrier-gas was held to the equilibrium pressure at the fluoro-oil temperature. A desired partial pressure of BrF_3 was obtained by adjusting the fluoro-oil temperature, its value being calculated from the experimental data of Oliver and Grisard.[14] Since BrF_3 severely corroded the glass, the thermobalance with silica spring and glass column employed for the experiments with fluorine could not be used for the experiments with BrF_3. In the thermobalance used in the present work, the spring column (6) was made of a Daiflon tube, and the sensing element was a nickel spring (7), the extension of which was measured by a differential transformer and recorded automatically.[15] In a monel reaction chamber (13), a nickel sample pan (14), 2 mm deep and 10 mm in diameter, was suspended by a nickel chain (10) below the nickel spring.

In most of the runs, the total flow rate of argon was about 15 l/h (55.4 cm/min in gas velocity) and the partial pressure of BrF_3 was 19 mmHg. The reaction rate was not affected by the gas flow rate, when it was near 15 l/h. The experiments were made in the temperature range from 100° to 250°C; the calculating method of the rate was the same with that described in Part II, section 2.4.

3. Fluorination of UO_2 pellets

The sample pellet was corroded without breaking into pieces. A slight amount of intermediate appeared to be formed on the surface of the residual pellet, but the X-ray pattern of the pellet surface by a diffractometer showed only the pattern of the original UO_2. Figures III-2 and III-3 show the

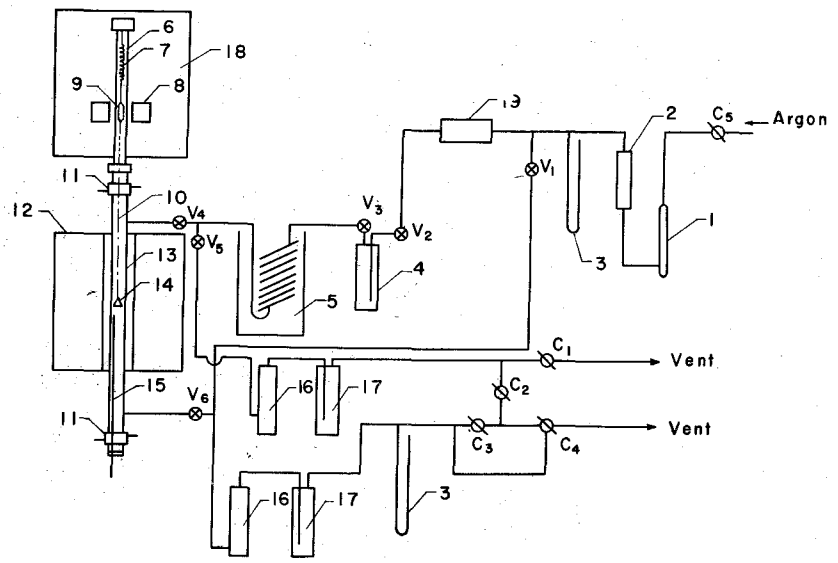

Fig. III-1. Apparatus for the fluorination by BrF_3 vapor.
1, vessel for absorbing moist; 2, flow meter; 3, Hg manometer; 4, vessel of liquid BrF_3; 5, thermostat; 6, teflon tube; 7, nickel spring; 8, differential transformer; 9, ferrite core sealed by teflon-100X tube; 10, nickel chain; 11, jacket for cooling water; 12, resistance furnace; 13, tubular reactor made of monel; 14, sample vessel made of nickel; 15, thermocouple sheath; 16, 17, cold traps; 18, thermostat to maintain the temperature around the weighing mechanism constant; 19, preheater of argon gas.

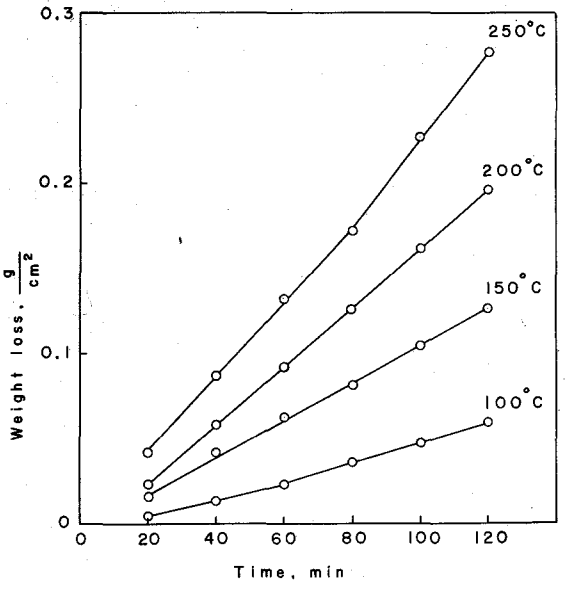

Fig. III-2. Relationships between weight loss per unit surface area of UO_2 pellet and time at different temperatures.
BrF_3 vapor pressure, 19 mmHg; total pressure, 760 mmHg; carrier gas flow rate, 15 l/h (55.4 cm/min).

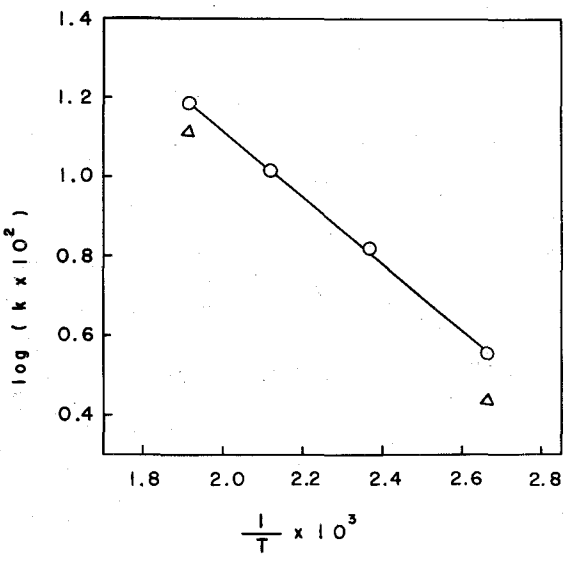

Fig. III-3. Arrhenius plot for the reaction between UO_2 pellet and BrF_3 vapor.
The reaction rates were calculated from the slopes of the curves in Fig. III-2. The marks ⊙, the rates calculated from the final slopes of the curves in Fig. III-2; △, the rates from the initial slopes of the curves at 100° and 250°C in the Fig. III-2.

temperature dependence of the reaction rate at temperatures from 100° to 250°C. Although a small deviation from the linear shrinkage is seen in the curves of 100° and 250°C in Fig. III-2, the pellet shrinkage proceeds almost linearly. From the slopes of the curves in Fig. III-2, the rate constant was calculated and plotted in Fig. III-3; the apparent activation energy was calculated to be 3.9 kcal/mole.

Figures III-4 and III-5 show the effect of the pressure of BrF_3 on the rate constant. The rate constant is proportional to the pressure of BrF_3.

In Table III-1 and III-2, the values of the rate constant are listed.

Table III-1. Rate constants for the fluorination of UO_2 pellet by BrF_3 vapor —— effect of temperature.
BrF_3 vapor pressure, 19 mmHg.

Temperature (°C)	Rate constants $(\frac{g}{cm^2.h})$ measured	calculated*
100	0.027[a)]	0.036
	0.036[b)]	
150	0.066	0.065
200	0.103	0.107
250	0.130[a)]	0.158
	0.153[b)]	

a) calculated from the slope of the initial part of the plot in Fig. III-2.
b) calculated from the slope of the latter part of the plot in Fig. III-2.

Table III-2. Rate constants for the fluorination of UO_2 pellet by BrF_3 vapor —— effect of BrF_3 vapor pressure. Temperature, 200°C.

BrF_3 vapor pressure (mmHg)	Rate constants $(\frac{g}{cm^2.h})$ measured	calculated*
10.5	0.062	0.059
19.0	0.103	0.107
33.0	0.200	0.186

* calculated by the equation in section 5.

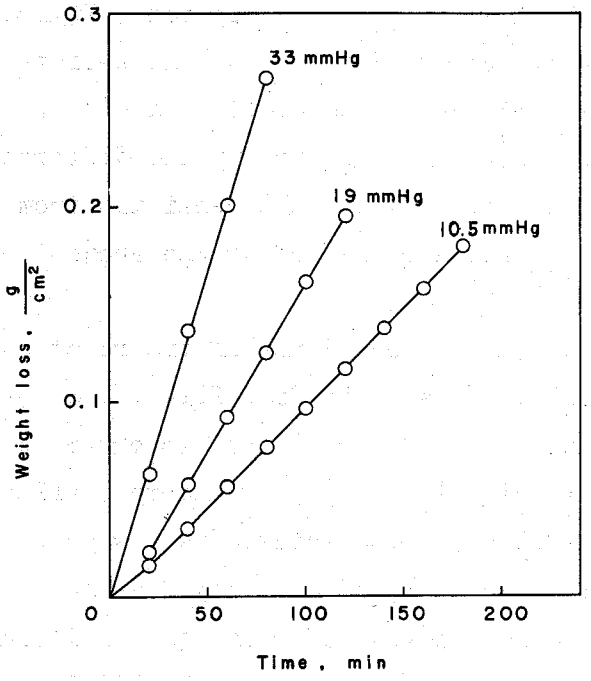

Fig. III-4. Relationships between weight loss per unit surface area of UO_2 pellet and time at different vapor pressures of BrF_3.
Temperature, 200°C; total pressure, 760 mmHg; carrier gas flow rate, 15 l/h.

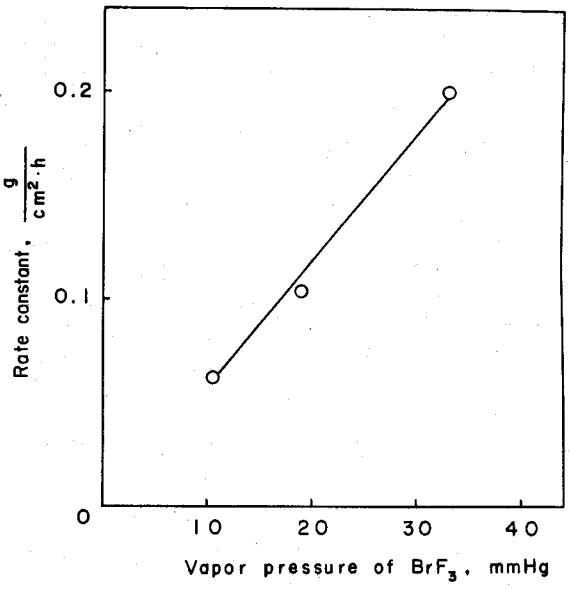

Fig. III-5. Relationships between rate constant of UO_2 pellet and BrF_3 vapor pressure.
The rate constants were calculated from the slopes of the curves in Fig. III-4.

4. Fluorination of U_3O_8 pellets

The pellets were corroded with a linear shrinkage, as seen in the fluorination of the UO_2 pellets. Since the densities of the pellets differed in a wide range from 6.0 to 8.0 g/cm^3 (see Part II, section 2.2), the effect of the pellet density upon the reaction rate was first investigated. Figure III-6 shows the results; it is seen that the reaction rates for the pellets with densities 7.12 and 7.85 g/cm^3 (85 and 94% of the theoretical density, respectively) are the same. In order to avoid the influence of the difference in pellet density on the reaction rate, the pellets with the densities from 7.0 to 7.5 g/cm^3 were used in the other experiments made after the above examinations.

Figures III-7 and III-8 show the temperature dependence of the reaction rate at the temperatures from 100° to 250°C. As seen in Fig. III-8, the Arrhenius plot shows a poor linearity, so that the linear line was obtained by the least-square method. The apparent activation energy was very small (0.9 kcal/mole). The formation of water-soluble solid intermediate was observed on the surface of residual pellets which were taken out from the reactor after stopping the reaction at a given time. The reaction conditions and the amounts of the intermediate formed are summarized in Table III-3.

Table III-3. Amounts of water-soluble solid intermediate formed on the residual pellets.

	UO_2 pellet		U_3O_8 pellet	
Reaction temperature (°C)	100	250	100	250
Vapor pressure of BrF_3 (mmHg)	19	19	19	19
Initial weight of pellet (mg)	565.3	565.5	440.7	448.4
Weight loss during reaction (mg)	49.2	218.6	192.2	243.2
Total weight of solid residue	516.1	346.9	248.5	205.2
Weight of water-soluble residue (mg)*	0.4	1.2	5.4	18.4
Wt. % of water-soluble residue**	0.08	0.35	2.2	9.0

* determined by the method of immersion in water, described in Part II, section 2.6.2.

** $\frac{\text{weight of water-soluble residue}}{\text{total weight of solid residue}} \times 100$

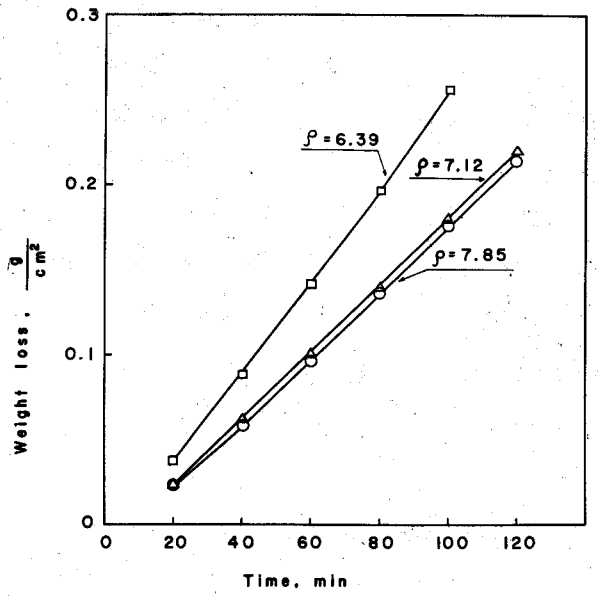

Fig. III-6. Relationships between weight loss per unit surface area of U_3O_8 pellet and time —— effect of pellet density, ρ (g/cm³).
BrF_3 vapor pressure, 19 mmHg; total pressure, 760 mmHg; temperature, 150°C; carrier gas flow rate, 15 l/h.

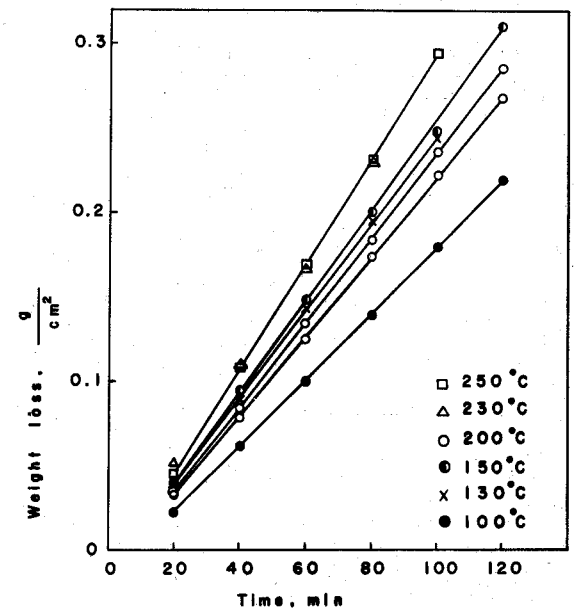

Fig. III-7. Relationships between weight loss per unit surface area of U_3O_8 pellet and time at different temperatures.
BrF_3 vapor pressure, 19 mmHg; total pressure, 760 mmHg; carrier gas flow rate, 15 l/h.

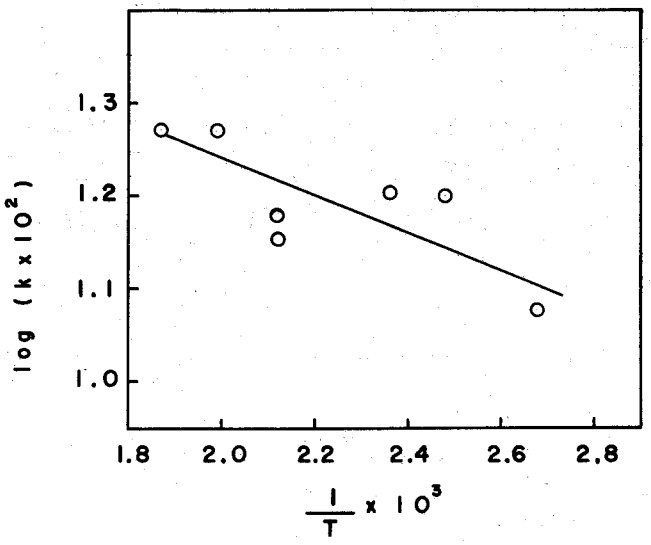

Fig. III-8. Arrhenius plot for the reaction between U_3O_8 pellet and BrF_3 vapor.
The reaction rates were calculated from the slopes of the curves in Fig. III-7.

The X-ray pattern for the pellet surface by a diffractometer showed only the pattern of the original material U_3O_8, as in the case of UO_2 pellet. Consequently, the intermediate appears to be of a poor crystalline state.

Figures III-9, III-10, and III-11 show the relationships between the vapor pressure of BrF_3 and the reaction rate. It is seen in Fig. III-11 that the reaction rate is nearly proportional to the BrF_3 vapor pressure.

In Tables III-4 and III-5, the values of the rate constant for the U_3O_8 pellets at different reaction conditions are listed.

Table III-4. Rate constants for the fluorination of U_3O_8 pellet by BrF_3 vapor —— effect of temperature.
BrF_3 vapor pressure, 19 mmHg.

Temperature (°C)	Rate constants $(\frac{g}{cm^2.h})$	
	measured	calculated*
100	0.120	0.127
130	0.160	0.139
150	0.160	0.149
200	0.143	0.168
	0.151	0.168
230	0.187	0.177
250	0.187	0.183

Table III-5. Rate constants for the fluorination of U_3O_8 pellet by BrF_3 vapor —— effect of BrF_3 vapor pressure.

BrF_3 vapor pressure (mmHg)	Rate constants $(\frac{g}{cm^2.h})$			
	at 200°C		at 100°C	
	meas.	calcd.*	meas.	calcd.*
10.5	0.103	0.093	0.069	0.071
19.0	0.143	0.168	0.120	0.127
	0.151			
33.0	0.264	0.292	0.191	0.222

* calculated by the equation in section 5.

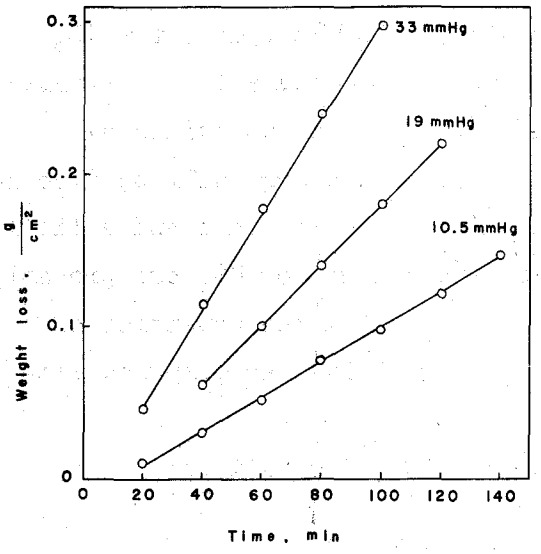

Fig. III-9. Relationships between weight loss per unit surface area of U_3O_8 pellet and time at different vapor pressures of BrF_3. Temperature, 100°C; total pressure, 760 mmHg; carrier gas flow rate, 15 l/h.

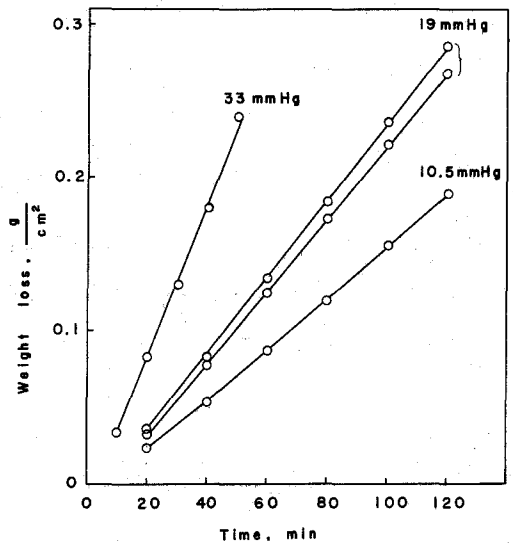

Fig. III-10. Relationships between weight loss per unit surface area of U_3O_8 pellet and time at different vapor pressures of BrF_3. Temperature, 200°C; total pressure, 760 mmHg; carrier gas flow rate, 15 l/h.

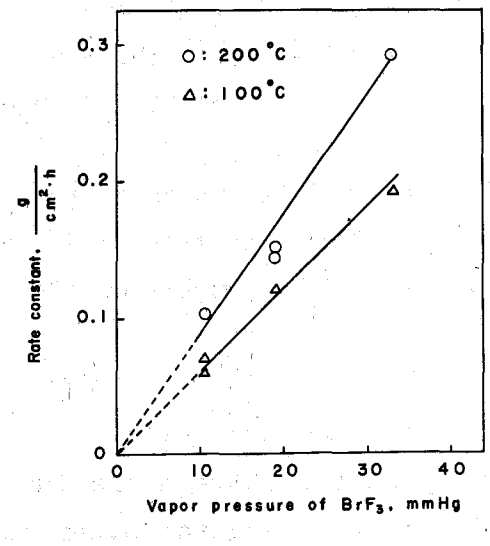

Fig. III-11. Relationships between rate constant of U_3O_8 pellet and BrF_3 vapor pressure.
The rate constants were calculated from the slopes of the curves in Figs. III-9 and III-10.

5. Derivation of kinetic equations

In the fluorination of UO_2 and U_3O_8 pellets with bromine tri-fluoride, the pellets shrinked linearly with formation of a relatively little amount of the intermediate. The apparent activation energies, 3.9 kcal/mole for UO_2 pellets, and 0.95 kcal/mole for U_3O_8 pellets, are much smaller than the values of 20 to 30 kcal/mole obtained for the fluorination of uranium oxides by fluorine. The reasons for the low values in activation energy will be discussed in next section. A little higher values in the reaction rate and a little lower values in the activation energy for U_3O_8 than those for UO_2 are probably due to the difference in the porosity of pellet; that is, the densities of U_3O_8 pellets are from 84 to 89% of its theoretical density, as compared with 94% of the theoretical density for UO_2 pellets.

The reaction rate can be expressed by the following equations:

$$\frac{dM_t}{dt} = k\, S_t, \text{ or } \rho\,(l_o - l_t) = \rho\,(r_o - r_t) = k\, t$$

$$k\left[\frac{g}{cm^2.h}\right] = 0.346 \exp\left(-\frac{3900}{RT}\right) p \quad \text{for } UO_2 \text{ pellets, and}$$

$$k\left[\frac{g}{cm^2.h}\right] = 0.024 \exp\left(-\frac{950}{RT}\right) p \quad \text{for } U_3O_8 \text{ pellets,}$$

where k is the reaction rate constant, ρ is the apparent density of pellets, i.e., 10.5 and 7.25 g/cm^3 for UO_2 and U_3O_8 pellets respectively, and p is the vapor pressure of BrF_3 (mmHg); the other symbols have the same significance as those in section 2.4 chapter II.

6. Mechanism of the fluorination reaction with BrF_3 —— compared with the reaction with F_2

The fluorination of uranium oxides to UF_6 with gaseous BrF_3 proceeded much more rapidly at lower temperatures than with F_2. In Table III-6, the rate constants in the fluorination of U_3O_8 with various fluorinating reagents are summarized.

The cause of the differences in the reaction rate may be analyzed from the following two points of view: one is the effect of the reaction products on the reaction mechanism, and the other is physico-chemical properties of the fluorinating reagents.

6.1 Effect of the reaction products on the reaction mechanism

Emeleus et al. found that the reaction products between uranium oxides and BrF_3 were UF_6, Br_2, and O_2.[11,16] However, several other compounds are known which are composed of bromine, oxygen, and fluorine, including Br_2O,

BrO_2, BrO_2F, and BrF; these are possible to be formed in the reactions. Of these compounds, bromine oxides and oxyfluorides are not stable at above room temperature,[17] so that they are not considered to be formed through the reaction. BrF also is not recognized as a stable compound, because it cannot be separated as a pure compound, but its existence has been confirmed in the gas phase which is in equilibrium with a liquid mixture of Br_2 and BrF_3.[18~21] In the author's experiments, an amorphous solid intermediate (hereafter, call intermediate (X)) was found to be formed. Thus, the following chemical reaction are considered to take place:

$$UO_2,\ U_3O_8 + BrF_3,\ (BrF) \longrightarrow \text{intermediate (X)} + O_2 + Br_2$$

$$\text{intermediate (X)} + BrF_3,\ (BrF) \longrightarrow UF_6 + O_2 + Br_2$$

Bromine monofluoride, BrF, may be formed by the reaction

$$Br_2 + BrF_3 \longrightarrow BrF, \qquad \triangle F = -1.2 \text{ kcal/mole.}^{20)}$$

Gaseous product

Bromine does not react with uranium oxides at low temperatures such as 50° to 250°C.[22] It has been observed that oxygen reacts with UO_2 pellets only at temperatures above 400°C.[23] It has also been reported that uranium metal is fluorinated to UF_6 by BrF_3 at room temperature, without oxygen in the reaction system. Consequently, the oxygen produced during fluorination will not further cause subsidary reactions which increase the overall reaction rate. The behavior of BrF will be discussed in the next section together with BrF_3.

Solid product

When UO_2 or U_3O_8 pellets were fluorinated with gaseous BrF_3, the amorphous intermediate (X) formed was not a compact layer, and appeared to be very reactive; the low value of the activation energy is considered to be related to the formation of this intermediate. When uranium oxides were fluorinated with fluorine, however, the stable intermediate UO_2F_2 was formed, and the overall reaction-rate was determined in general by the step of the fluorination of UO_2F_2 to UF_6. The differences in the chemical form of the intermediates and in the reaction behaviors between the fluorination by BrF_3 and that by F_2 will be further discussed from the differences in the properties of the fluorinating reagents.

6.2 Reaction behavior of BrF_3

If the fluorination reaction with BrF_3 proceeded through collision and instantaneous bond breaking, this reaction would proceed more slowly than

with F_2, because the values of the bond energy between Br and F are generally found to be 50 to 60 kcal/mole, whereas the dissociation energy of F_2 is 37 kcal/mole.[24,25] To explain this inconsistency and the difference in the nature of the intermediate formed in the fluorination with BrF_3 and with F_2, the behaviors of the fluorinating reagents during the reaction must be further clarified.

It is generally accepted that the reaction between fluorine and hydrogen or an organic compound is initiated with the formation of F radicals by breaking the F-F bond in the fluorine molecule.[26,27] Since the electronegativity of fluorine is extremely high, the dissociation of the fluorine molecule to negative and positive ions is unlikely because of the difficulty to form F^+ ion.

For all the interhalogen compounds containing fluorine, the F-X bonds have ionic characters which are associated with the high electronegativity of fluorine compared with the values of other halogen elements. Since the interhalogen compounds have generally large dipole moments, they are strong ionizing solvents in liquid state. In the case of BrF_3, in particular, Emeleus and Woolf postulated the following autoionization to explain the electroconductivity of liquid BrF_3 and the formation of many complex salts with metallic fluorides.

$$2\ BrF_3 \rightleftharpoons BrF_2^+ + BrF_4^-$$

They also gave the criteria for the ready reaction of an oxide with liquid BrF_3: the fluorinated product from the oxide must be volatile or soluble in liquid BrF_3. The explanations given above are all related to the reaction with gaseous BrF_3. However, the reaction with gaseous BrF_3 appears to proceed also with ionic character.

Sufficient data are not available to clarify the steps of reaction in the fluorination with gaseous BrF_3. The reaction behavior, however, may be roughly characterized as follows. The processes of reaction between uranium oxides and gaseous BrF_3 will begin with the adsorption of BrF_3; in this adsorption, the dipole moment of BrF_3 and the configuration of atoms and electrons in the molecule (see Fig. III-12) may have an important role in making a bond of the adsorption. BrF_3 is a strong complexing agent, so that its behavior as acid or base must be considered in the process after adsorption. The formation of complex salts possibly occurs in the reaction system of the original oxides-BrF_3 and intermediate-BrF_3. That BrF_3 and the solid reactant attract each other by adsorption and then by formation of complex compound, seems to be related to the experimental results such as the high reaction rate, low temperature range of the reaction, and low values of the

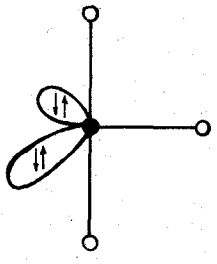

BrF_3

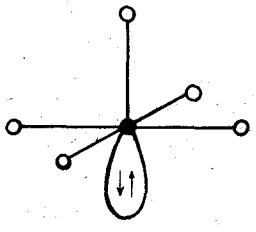

BrF_5

Fig. III-12. Lone pairs in BrF_3 and BrF_5.

● : Bromine , ○ : Fluorine

activation energy, compared with the fluorination with F_2.

In the fluorination of uranium oxides with fluorine, the first step reaction to form UO_2F_2 proceeded in general with higher rate than the second step reaction from UO_2F_2 to UF_6. This may also be explained by the formation of a combined state between the reactants; that is, in the first step, the chemisorption appeared to take place as described in Chapter II section 2.5.3, but there is no evidence of forming such a combined state in the second step.

Table III-6 summarizes the physical properties of bromine fluorides and elementary fluorine, and their characteristics in the reaction with U_3O_8 powder. The reaction rates and the activation energies are in the following relationships, respectively:

$$R(BrF_3) > R(BrF_5) > R(F_2), \text{ and } \quad E(BrF_3) < E(BrF_5) < E(F_2).$$

It is of interest that the sequence of the rate constant values is the same as that for the number of lone pair; it may be considered that the lone pairs in the bromine fluorides have some role in making chemical interactions. Rogers and Katz also described the role of lone pairs in forming intermediate complex between ClF_3 and HF.[33)]

7. Evaluation of BrF_3 as fluorinating reagent

As shown in Table III-6, gaseous BrF_3 fluorinates uranium oxide at much lower temperatures and partial pressures than fluorine; that is, the efficiency in using BrF_3 is very high, compared with the case of the elementary fluorine. The temperature dependence of the reaction rate is very low and the heat of reaction is about half that for the fluorine; the control of the reaction and the design of the fluorinating reactor are both favored by these facts. The boiling point of Br_2 and of BrF_3 are not much different from the sublimation point of UF_6, so that the separation of UF_6 from Br_2 and BrF_3 in the final product must be done by distillation.

Materials are usually converted with elementary fluorine to the fluorides of high valency. But, the free energy of BrF_3 is smaller than that of elementary fluorine, by 55 kcal/mole, and so BrF_3 may be used for selective fluorination by differences in the free energy changes between the materials to be fluorinated. Plutonium compounds are fluorinated with fluorine to volatile PuF_6, for example, while they are fluorinated with BrF_3 only to solid PuF_4; the application of this phenomenon is being studied for the separation of plutonium and uranium in an irradiated fuel.

Teflon and Diflon (Kel-F) are excellent materials for handling BrF_3 and they can be used at temperature below 100°C without corrosion. At higher temperatures, nickel and monel were usually used.

Table III-6. Physicochemical properties of fluorinating reagents and the kinetic data on the reaction with U_3O_8.

Fluorinating reagent	Boiling point (°C)	Dipole moment (Debye)	Number of lone pair[a), 30)]	Rate constant, k[b)] (min^{-1})	△ E (kcal/mole)
BrF_3	125.75	1.0[28)]	2	0.014~ 0.015 at 200°C and 10 mmHg BrF_3[31)]	0.9[31)]
BrF_5	40.76	1.51[29)]	1	0.015 at 200°C and 189 mmHg BrF_5[9)]	9.5[9)]
F_2	-187.99	0	0	No reaction below 300°C; 0.0088 at 410°C and 170 mmHg F_2[32)]	21.3[32)]

a) The lone pairs formed by hybridization of the electron orbitals in N shell.
b) The values of the rate constant were determined from eq. (12) in Part II, which derived from the diminishing sphere model in gas-solid reaction.

8. Summary

The fluorination of UO_2 and U_3O_8 to UF_6 by gaseous bromine trifluoride proceeded at lower temperatures from 100° to 250°C and at lower pressures of BrF_3 from 10 to 33 mmHg than those for the fluorination by fluorine.

Fluorination of UO_2 pellets

The pellets were fluorinated to UF_6 with almost no formation of solid intermediate. The reaction rate was proportional to the partial pressure of gaseous BrF_3, and the apparent activation energy was 3.9 kcal/mole. The rate constant for the surface reaction of the UO_2 pellet is expressed by

$$k \left[\frac{g}{cm^2 . h} \right] = 0.346 \exp \left(- \frac{3900}{RT} \right) p_{BrF_3}.$$

Fluorination of U_3O_8 pellets

The pellets were fluorinated to UF_6, with the formation of a small amount of solid intermediate in a poor crystalline state and of unknown chemical form. The reaction rate was proportional to the partial pressure of gaseous BrF_3, and the apparent activation energy was 0.9 kcal/mole. The rate constant is expressed by

$$k \left[\frac{g}{cm^2 . h} \right] = 0.024 \exp \left(- \frac{950}{RT} \right) p_{BrF_3} .$$

Mechanism of the reaction

The high reactivity of BrF_3 at low temperatures appear to be related to the adsorption of BrF_3 and the subsequent ionic processes. To the contrary, non-ionic processes seems to predominate during the fluorination reaction with fluorine.

References

1) Labaton, V. Y., J. Inorg. Nucl. Chem., 10, 86 (1959).
2) Davis, W. Jr., Jarry, R. L., K-849 (1953).
3) Nikolaev, N. S., Shishkov, Yu. D., Dokl. Akad. Nauk. SSSR, 143, 130 (1962).
4) Schmets, J. J., Camozzo, G., Francesconi, A., Godrie, P., Heremans, R., Pierini, G., Speeckaert, P., P/771, 3rd United Nations Conference on Peaceful Uses of Atomic Energy, Vol. 10, 520 (1958).

5) Camozzo, G., Heremans, R., Pierini, G., Schmets, J. J., SM-88/20, IAEA Symposium, Use of Plutonium as a Reactor Fuel, Brussels, March (1967).
6) Schmets, J. J., KR-126, p. 425 (1967).
7) Katz, J. J., Rabinowitch, E., The Chemistry of Uranium, N.N.E.S., Division VIII, Vol. 5, p. 400, Dover Publications, Inc., New York (1951).
8) Jarry, R. L., Steindler, M. J., J. Inorg. Nucl. Chem., 29, 1591 (1967).
9) Jarry, R. L., Steindler, M. J., ibid, 30, 127 (1968).
10) Emeleus, H. J., Maddock, A. G., Miles, G. L., Sharpe, A. G., J. Chem. Soc., 1991 (1948).
11) Emeleus, H. J., Woolf, A. A., J. Chem. Soc., 164 (1950).
12) Vogel, R. C., Steunenberg, R. K., Symposium on the Reprocessing of Irradiated Fuels, Held at Brussels, Book 2, Session IV, pp. 498 ~559 (1957).
13) Cathers, G. J., ibid, pp. 560 573 (1957).
14) Oliver, G. D., Grisard, J. W., J. Am. Chem. Soc., 74, 2705 (1952).
15) Tsujimura, S., Fujisawa, G., Takahashi, A., JAERI-1070 (1964).
16) Hoekstra, H. R., Katz, J. J., Anal. Chem., 25, 1608 (1953).
17) Schmeisser, M., Brandle, K., Advances in Inorganic and Radio-chemistry, edited by Emeleus, H. J., Sharpe, A. G., Academic Press Inc., Vol. 5, pp. 41 ~ 89 (1963).
18) Steunenberg, R. K., Vogel, R. C., Fisher, J., J. Am. Chem. Soc., 79, 1320 (1957).
19) Smith, D. F., Tidwell, M., Williams, D., Phys. Rev., 77, 420 (1950).
20) Broderson, P. H., Schumacher, H. J., Z. Naturforsch., 2a, 358 (1947).
21) Stein, L., J. Am. Chem. Soc., 81, 1273 (1959).
22) Katz, J. J., Rabinowitch, E., The Chemistry of Uranium, pp. 523 ~ 526, Dover Publications, Inc. (1951).
23) Iwasaki, M., Sakurai, T., Ishikawa, N., Kobayashi, Y., JAERI-1174 (1969).
24) Cottrell, T. L., The Strength of Chemical Bond, Butterworths Scientific Publications (1954).
25) Wiebenga, E. H., Havinga, E. E., Boswijk, K. H., Advances in Inorganic Chemistry and Radiochemistry, edited by Emeleus, H. J., Sharpe, A. G., Vol. 3, 133, Academic Press, Inc. (1961).
26) Tedder, J. M., Advances in Fluorine Chemistry, edited by Stacey, M., Tatlow, J. C., Sharpe, A. G., Butterworth, Vol. 2, p. 104 (1961).
27) Levy, J. B., Copeland, B. K. W., J. Phys. Chem., 67, 2156 (1963).
28) Magnuson, D. W., J. Chem. Phys., 27, 223 (1957).
29) Rogers, M. T., Pruett, R. D., Thompson, H. B., Speirs, J. L., J. Am. Chem. Soc., 78, 44 (1956).

30) Cartmell, E., Fowles, G. W. A., Valency and Molecular Structure, pp. 185 191, Butterworths, London (1961).
31) Iwasaki, M., Sakurai, T., J. Nucl. Sci. Technol., 6, 225 (1965).
32) Iwasaki, M., J. Inorg. Nucl. Chem., 26, 1853 (1964).
33) Rogers, M. T., Katz, J. J., J. Am. Chem. Soc., 74, 1375 (1952).

Chapter IV

Fluorination of uranium carbides by fluorine*

There are three known uranium carbides, monocarbide UC, dicarbide UC_2, and sesquicarbide U_2C_3; the monocarbide and dicarbide can be synthesized in the form of a single phase, and sesquicarbide is usually obtained, mixed with other component such as uranium monocarbide or carbon. Many phsical and chemical studies have been made on these carbides, but no investigation on their fluorination to UF_6. We chose the uranium monocarbide and dicarbide for the study of the fluorination.

Few reports, only of the qualitative nature, have been made on the fluorination of carbides of metals other than uranium, as described below. Schwartzkoph and kieffer remarked that the reaction between tungsten carbide or molybdenum carbide and fluorine proceeded with inflammation.[1] As both tungsten and molybdenum are similar to uranium in being easily fluorinated to gaseous hexafluoride by fluorine, so the fluorination behavior of uranium carbides appears to be like those of tungsten and molybdenum carbides. Schumb and Aronson[2], on the other hand, reported the formation of several kinds of lower fluorocarbons in the fluorination of tungsten and other metal carbides by fluorine. These results suggest that the fluorination of uranium carbides may proceed more violently and in a more complicated way than the fluorination of uranium oxides.

1. Experimental method

Material

Uranium monocarbide and dicarbide used were commercial products from Spencer Chemical Co. The measured impurities were as follows:

Element	Concentration in ppm (or %)		
	UC		UC_2
free carbon[3]	0.02	0.03 (%)	0.86 (%)
oxygen[4]	0.36	0.44 (%)	0.20 (%)
aluminum	25		25
boron	0.1		0.1
cadmium	20		20
chromium	150		150

* Published in J. Nucl. Sci. Technol., 2, 432 (1965), and 4, 249 (1967).

Element	Concentration in ppm	
	UC	UC_2
manganese	20	20
nickel	20	20
silicon	75	75

The free carbon content was measured by Naito[3], and the oxygen content by Hoshino.[4] The procedures employed in the determination of free carbon and oxygen will be described. The concentration of other elements were measured by flame photometry.[5]

Free carbon

The sample was dissolved in hot 6 N HNO_3. The free carbon was left as undissolved precipitate, which was filtered using an asbestos filter and burned to CO_2 in a stream of oxygen at 1100°C. The CO_2 was adsorbed on an askalite which was set in a glass tube. The amount of free carbon was calculated from the weight change of the askalite.

Oxygen

The sample was dropped into a platinum bath, contained in a graphite crucible which was heated to about 2000°C by induction heating. Oxygen in the sample was liberated as CO, which was carried out of the furnace by the carrier gas of helium, oxydized to CO_2 by CuO heated to 400° ~ 500°C, and absorbed into a solution of barium hydroxide. The amount of CO_2 was measured from the change in electric conductivity of the solution.

Commercial carbides, of large particle sizes, were pulverized in an agate mortar and sieved. Powder from 100 to 150 meshes were used in all the experiments. Since the uranium carbides are readily oxidized in air, their handling and storing were done under argon atmosphere in a glove box.

Experimental method

The experimental procedure was similar to that described in Chapter II Section 1.2. The sample was placed on a nickel pan and the weight change during fluorination was measured thermogravimetrically. The conditions for the typical fluorination experiments were as follows: initial sample weight, 70 to 80 mg; total gas flow rate, 13.7 l/h; total pressure, 1 atm.; fluorine concentration, 11 vol. % (85 mmHg); diluting gas, argon. With the fluorine concentrations near 20 vol. %, which was used in the fluorination of uranium

oxides, the fluorination of uranium carbides proceeded so rapidly that the measurement of the reaction rate was difficult. Therefore, the fluorine concentration in the typical experimental runs was taken as 11 vol. %, about half of that used for the uranium oxides. The reaction rate was measured at temperatures from 200° to 300°C. It was confirmed that the flow velocity of the reacting gas had no effect on the reaction rate, in the range of total gas flow rate from 13.7 l/h to 7.2 l/h. In several experiments, gaseous reaction products of both the carbides were collected in a cold trap cooled with liquid nitrogen. In these cases, helium was used instead of argon as the diluent for fluorine. After fluorine and UF_6, condensed in the same trap above, were removed through reactions with mercury, the rest gases were analyzed by a mass spectrometer of Type 21-103 C of Consolidated Electrodynamics Corporation.

2. Fluorination of uranium monocarbide

At the beginning of the reaction, a sharp rise of the reaction temperature and a slight increase in the weight of the sample were both invariably observed, and were attributed to the formation of uranium tetrafluoride. The peak heights of this temperature rise are shown in Fig. IV-1 for some typical reaction conditions.

At the stage of this temperature rise, the UC powder, black in color, disintegrated into finer grey powder, which changed its grey color to light green in air. X-ray analysis of both grey and light green powders showed only the pattern of uranium tetrafluoride. After the initial temperature rise, the reaction proceeded mildly at a controlled temperature, and the intermediate UF_4 was fluorinated to UF_6.

A white reaction product was always observed to be mixed in the sample powder throughout the reaction and left remaining thereafter. This product was resistant to hot acids, H_2SO_4 and HNO_3, and not disintegrated remarkably at the temperatures below 200°C. Infrared spectrum showed that this product had only one absorption at 1,240 cm^{-1} which is in the range of the characteristic absorption due to stretching vibration between carbon and fluorine. From these results, the white product was presumed to be polymeric fluorocarbon. The relations between the weight % of the white product (1 to 2 %) and the fraction of the weight decrease are shown in Fig. IV-2. The weight of polymeric fluorocarbon was measured after treating the sample in ferric chloride solution which dissolves UF_4.[6] Figure IV-2 indicates that the polymeric fluorocarbon was rapidly produced in the early stage of the

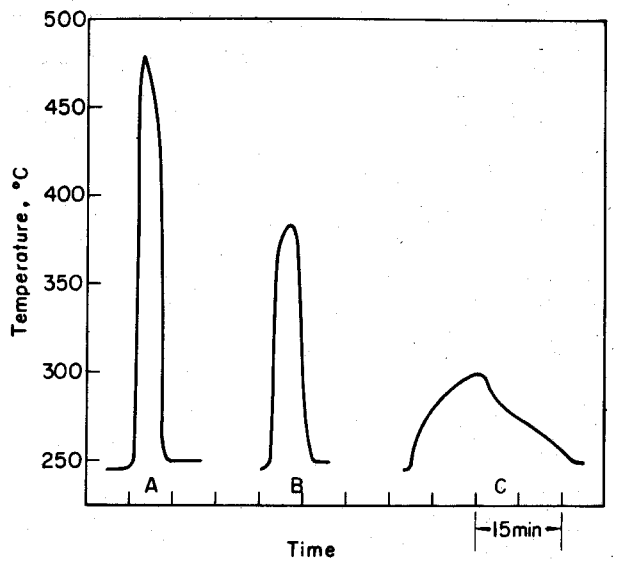

Fig. IV-1. Temperature rise at beginning of reaction.
Sample, uranium monocarbide; reaction temperature, 250°C, total gas flow rate, 13.7 l/h; total pressure, 1 atm.; partial pressure of fluorine, A: 134 mmHg (18 vol. %), B: 84 mmHg (11 vol. %), C: 34 mmHg (4.5 vol. %).

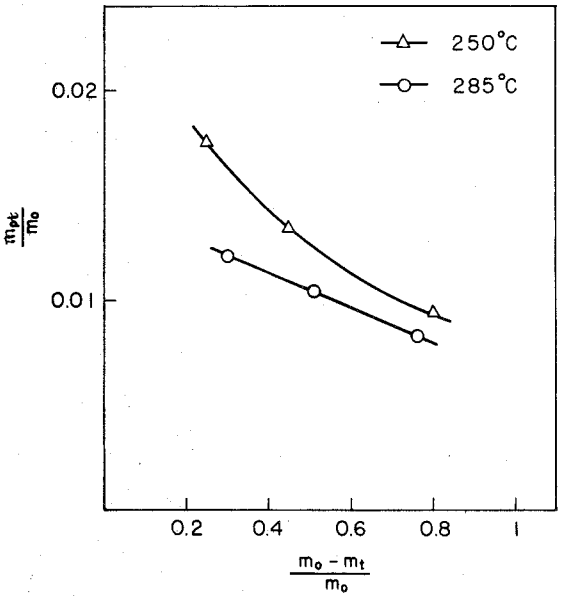

Fig. IV-2. Fraction of weight change of polymeric fluorocarbon.
Sample, uranium monocarbide; m_{pt}, weight of polymeric fluorocarbon at time t; m_t, weight of sample at time t; m_0, initial weight of sample; total gas flow rate, 13.7 l/h; total pressure, 1 atm.; fluorine partial pressure, 84 mmHg (11 vol. %).

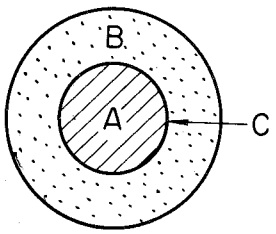

Fig. IV-3. Schematic model of polymer layer and "UF_4 + polymer" core in the second step reaction. A, core, being a mixture of UF_4 and polymer; B, polymer layer; C, surface of core A.

reaction, with simultaneous formation of the intermediate UF_4 and that it then reacted much more slowly with fluorine than UF_4.

It was also observed immediately after the first step reaction that the size and shape of the aggregates composed of the intermediate UF_4 and the polymeric fluorocarbon depended largely on the degree of the initial reaction temperature rise, as described later.

The main overall reaction is assumed to consist of the following two steps:

$$UC + F_2 \longrightarrow UF_4 + \text{polymeric fluorocarbon} + \text{gaseous fluorocarbon} \quad (a)$$

$$UF_4 + F_2 \longrightarrow UF_6 \quad (b\text{-}1)$$

$$\text{polymeric fluorocarbon} + F_2 \longrightarrow \text{gaseous fluorocarbon} \quad (b\text{-}2)$$

The first step (a) proceeds very rapidly and is completed during the initial temperature rise, resulting an intimate mixture of UF_4 and polymeric fluorocarbon. In the second step, the reactions (b-1) and (b-2) simultaneously proceed rather slowly, the reaction rate being measurable by observing the decrease in weight of the sample. Because the reaction (b-2) proceeds even more slowly than (b-1), a polymer layer will be formed on the surface of the particles and the kinetics of the reaction (b-1) will be influenced by the existence of this layer. Figure IV-3 shows a spherical model of the polymer layer and the mixture core. By considering the reaction (b-1) taking place on the surface C of the core A, if in time t the reaction proceeds to point where it has affected the fraction

$$F = \frac{v_o - v_t}{v_o} , \quad (1)$$

where v_o is the initial volume of the core A, and v_t is the volume of the core A at time t, then the linear and parabolic law are expressed by the following equations of which the derivation was already shown in Chap. II, Section 1.1.2.

$$\text{Linear law,} \quad 1 - (1 - F)^{1/3} = k_L\, t. \quad (2)$$

$$\text{Parabolic law,} \quad \left[1 - (1 - F)^{1/3} \right]^2 = k_P\, t . \quad (3)$$

where k_L and k_P are the rate constants. In the linear law, the rate determining step is the reaction between fluorine and unreacted core surface (C in Fig. IV-3), whereas in the parabolic law, the diffusion of fluorine through a layer of reaction products on particle is rate-determining.

Now, by assuming for the reaction (b-1) in question that the composition of the core A does not change during the reaction, from equation (1)

$$F = \frac{(m_o - m_{po}) - (m_t - m_{pt})}{m_o - m_{po}} \qquad (4)$$

where m_o : weight of the sample at the beginning of the steps (b-1) and (b-2),

m_t : weight of the sample at time t,

m_{po}: weight of the polymer at the beginning of the steps (b-1) and (b-2),

m_{pt}: weight of the polymer at time t.

If the total weight of the polymer is only 1 ~ 2% of the sample, and the reaction (b-2) proceeds more slowly than the reaction (b-1),

$$F = \frac{m_o - m_t}{m_o(1 - \alpha)} \left(1 + \frac{\triangle m_{pt} \cdot m_t}{\triangle m_t \cdot m_o}\right) \qquad (5)$$

where $\alpha = \frac{m_{pt}}{m_o}$, $\triangle m_t = m_o - m_t$, $\triangle m_{pt} = m_{po} - m_{pt}$.

Because the second term in the parenthesis of equation (5) is negligibly small,

$$F = \frac{m_o - m_t}{m_o(1 - \alpha)} . \qquad (6)$$

The detail on the derivation of equations (5) and (6) are given in Appendix III.

While, at a temperature of 250°C, the value of α ($= m_{pt}/m_o$) decreases roughly from 0.018 to 0.01 with progress of the reaction as seen in Fig. IV-2, during the initial stage of the reaction where $(m_o - m_t)$ is small, the effect of variation of α on $(1 - F)^{1/3}$ is unimportant (less than the experimental error).

At 285°C, $\alpha = m_{pt}/m_o$ does not appreciably decrease during the reaction, and can be safely taken as roughly constant at around 0.01. Thus, equation (2) or (3) is adequate for expressing the reaction rate, assuming proportionality between the thickness of the polymeric fluorocarbon layer and the fraction of the radius decrease, $(1 - F)^{1/3}$, and adopting for the sake of simplicity in calculation, the value of 0.01 as constant value for α at both temperatures.

The plots of $(1 - F)^{1/3}$ vs. reaction time at different temperatures are shown in Fig. IV-4. At reaction temperatures below 260°C, the plots roughly fit the linear relationship with only a slight tendency to deviate toward the parabolic law. Above 270°C, however, the plots no longer follow the linear law, and those relating $[1 - (1 - F)^{1/3}]^2$ to time, shown in Fig.IV-5, indicate by their linearity that the reaction proceeds according to the parabolic law. This behavior, can be explained as follows: with the conversion of the intermediate UF_4 into the volatile UF_6 a layer of solid residue of

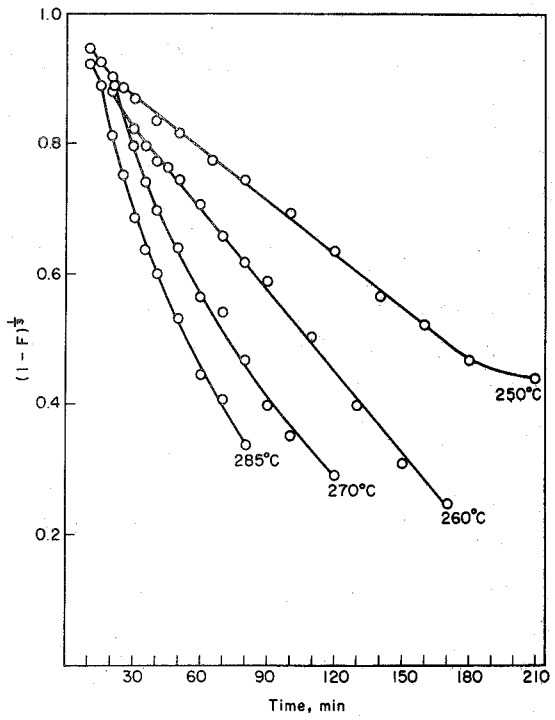

Fig. IV-4. Relationships between $(1-F)^{1/3}$ and time at different temperatures.
Sample, uranium monocarbide; total gas flow rate, 13.7 l/h; total pressure, 1 atm; fluorine partial pressure, 84 mmHg (11 vol. %).

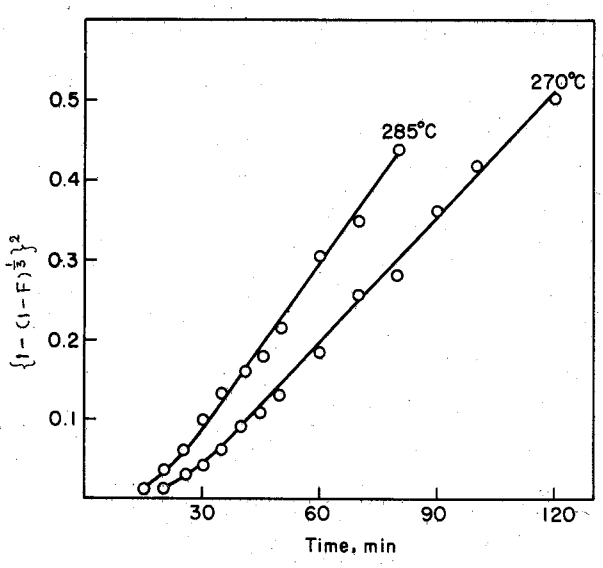

Fig. IV-5. Relationships between $[1-(1-F)^{1/3}]^2$ and time.
Sample, uranium monocarbide; total gas flow rate, 13.7 l/h; total pressure, 1 atm; fluorine partial pressure, 84 mmHg (11 vol. %).

polymeric fluorocarbon is formed on the surface of the particles, so that the reaction velocity becomes primarily dependent on the compactness of the fluorocarbon layer through which the reactive gases diffuse. It is presumed that the compactness of the layer markedly increases above 270°C. In the early stages of the reaction, when these layers are thin, the rate of reaction would be controlled by the surface reaction and would therfore approximately follow the linear law.

The rate of the second step reaction at the interface, above 270°C, was calculated from the asymtotic slope at the initial part of the $(1 - F)^{1/3}$ curve in Fig. IV-4. Using these values, an activation energy of 22.4 kcal/mole is obtained by calculation from the Arrhenius plot shown in Fig. IV-6.

In several experiments, the partial pressure of fluorine was varied, while keeping the total gas flow rate and the reaction temperature constant. The plots of $(1 - F)^{1/3}$ against reaction time with different fluorine concentrations are shown in Fig. IV-7. It is seen that the rate of the second step reaction decreases with increasing fluorine concentration. Microscopic observations of samples taken out soon after the initial temperature rise, indicated that this abnormal phenomenon was caused by difference in particle size of the reaction intermediates. Photomicrographs of these intermediates are shown in Fig. IV-8. As the fluorine concentration increased, the initial temperature rise was accentuated as shown in Fig. IV-1, and the reaction intermediates became sintered, resulting in decreased surface area available for the reaction.

In another series of experiments, the total gas flow rate was varied under constant reaction temperature and constant partial pressure of fluorine; it proved that the gas velocity had no effect on the reaction rate.

Tables IV-1 and IV-2 are the lists of the reaction rate constants.

Table IV-1. Reaction rate constants of uranium monocarbide.
Fluorine concentration, 11 volume % (85 mmHg in partial pressure); total pressure, 1 atm.; diluting gas, argon; total gas flow rate, 13.7 l/h.

Temperature (°C)	Reaction rate constants	
	k (min^{-1}) x 10^3	k (h^{-1})
240	2.30	0.138
250	2.70	0.162
	2.90	0.174

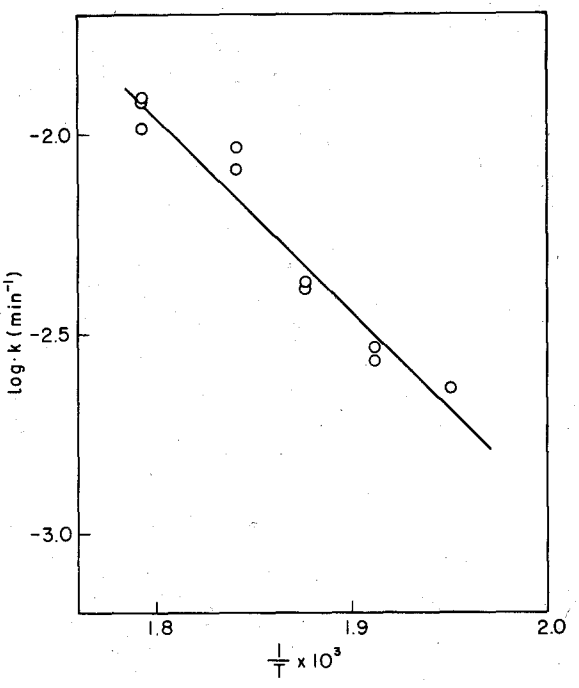

Fig. IV-6. Relationship between log k and 1/T.
Sample, uranium monocarbide.

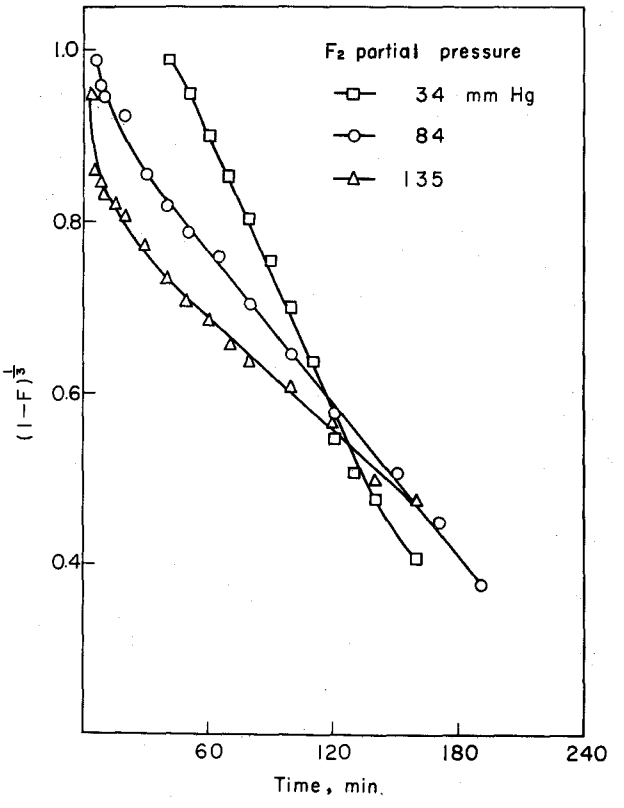

Fig. IV-7. Relationships between $(1 - F)^{1/3}$ and time at different partial pressure of fluorine.
Sample, uranium monocarbide; reaction temperature, 250°C; total gas flow rate, 13.7 l/h; total pressure, 1 atm.

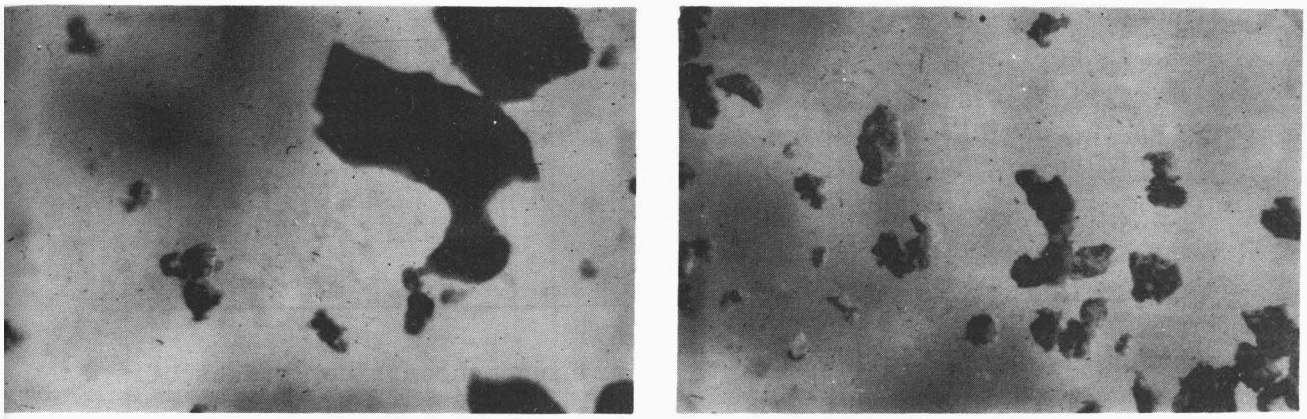

(a)

(b)

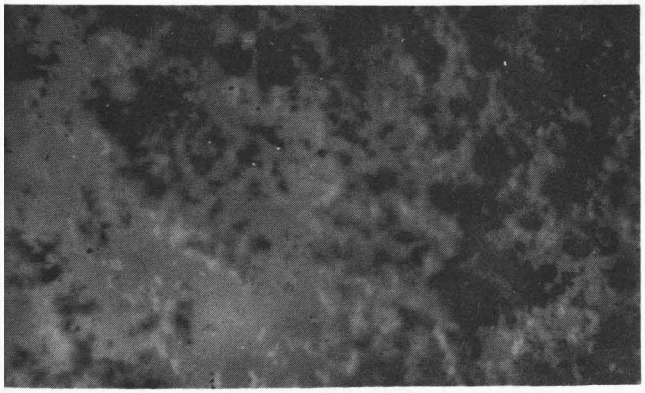

(c)

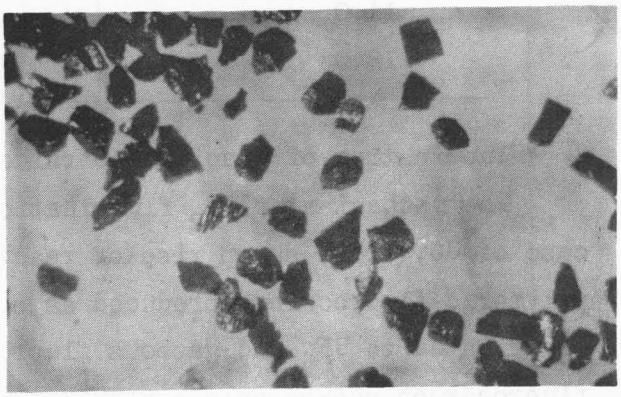

(d)

Fig. IV-8. Photo-micrograph of samples soon after initial peak of temperature rise.
Reaction temperature, 250°C; total gas flow rate, 13.7 l/h; (a), (b), and (c): UC converted at F_2 partial pressure of 135, 84, and 34 mmHg respectively; (d): UC (100 ~ 150 mesh).

Temperature (°C)	Reaction rate constants k (min^{-1}) x 10^3	k (h^{-1})
260	4.10	0.246
	4.20	0.252
270	8.15	0.488
	9.35	0.560
285	10.45	0.627
	12.20	0.732
	12.25	0.735

Table IV-2. Reaction rate constants of uranium monocarbide, effect of fluorine concentration.
Reaction temperature, 250°C; total pressure, 1 atm.; diluting gas, argon; total gas flow rate, 13.7 l/h.

Fluorine conc. vol. %	Reaction rate constants k (min^{-1}) x 10^3	k (h^{-1})
4.5	5.0	0.30
11.0	2.90	0.174
18.0	2.25	0.135

3. Fluorination of uranium dicarbide

The mechanism of UC_2 fluorination was found to be very similar to the case of UC, i.e., sharp rise of reaction temperature at the outset; UF_4 and polymeric fluorocarbon produced as solid intermediates; these being further fluorinated to UF_6 and gaseous fluorocarbon. Infrared spectra of the polymeric fluorocarbon showed only one absorption at 1,220 ~ 1,250 cm^{-1}, corresponding to the stretching vibration between carbon and fluorine. This results is identical to that for UC. The weight of the polymeric fluorocarbon was measured after treating the sample in ferric chloride solution. Figure IV-9 shows the relationship between weight change of the total sample and that of polymer, both in fraction. While there is a wide spread in the plots, the linear relationships were deduced for different temperatures by the least square method. At the points where the lines representing m_{pt}/m_o intersect with that of m_t/m_o, all the UF_4 formed in the sample is fluorinated to UF_6, leaving only polymeric fluorocarbon in the solid phase. The quantity of polymer was always much larger than in the case of UC, being for instance nearly ten times at the early stage of the reaction at 250° ~ 270°C.

Figure IV-10 shows a typical plot of the weight changes in time of total

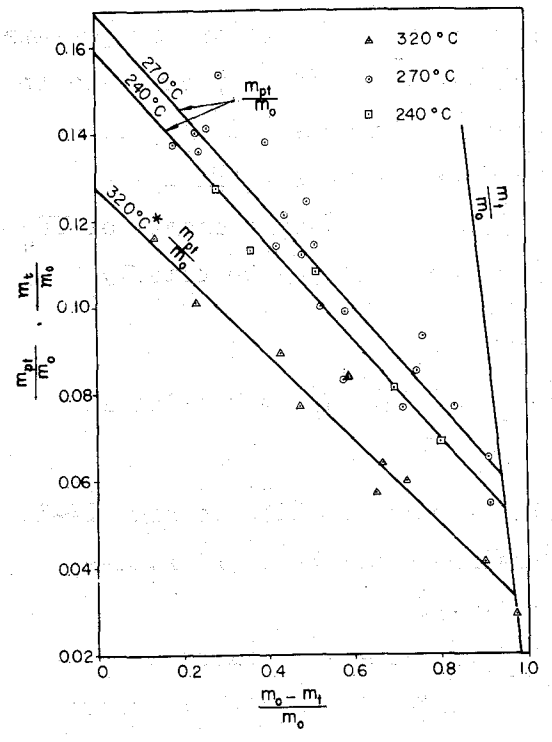

Fig. IV-9. Change in fraction of weight of polymeric fluorocarbon. Sample, uranium dicarbide; total gas flow rate, 13.7 l/h; total pressure, 1 atm.; fluorine partial pressure, 84 mmHg (11 vol. %); m_{pt}, weight of polymeric fluorocarbon at time t; m_t, weight of sample at time t; m_o, initial weight of sample.

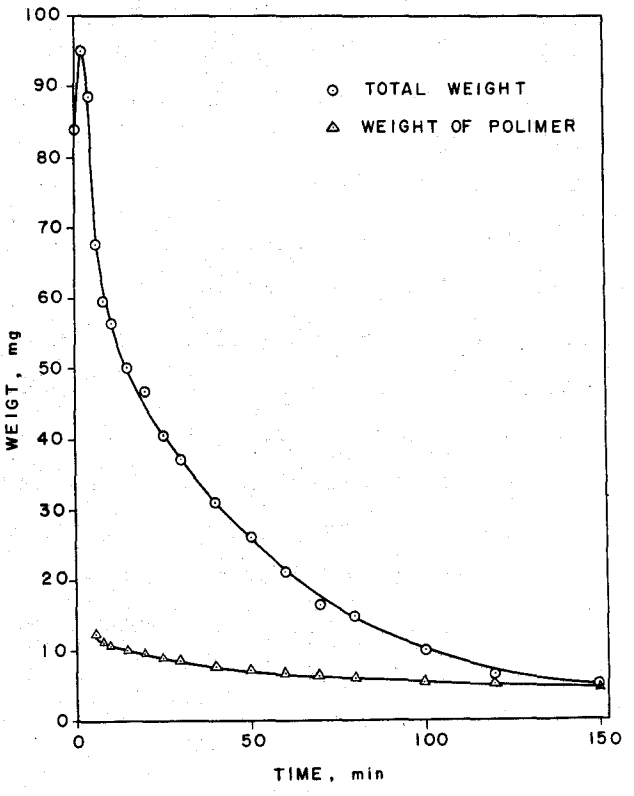

Fig. IV-10. Relationships of the weights of sample and polymer vs. time.
Sample, uranium dicarbide; reaction temperature, 270°C; total gas flow rate, 13.7 l/h; total pressure, 1 atm.; fluorine partial pressure, 84 mmHg (11 vol. %).

sample and of polymer. The weight of polymer was calculated from the linear relationships shown in Fig. IV-9. The initial rapid disintegration of UC_2 into the intermediates makes an intimate mixture of UF_4 and polymer. From Figs. IV-9 and IV-10, it is clear that the reaction rate is slower for polymer than for UF_4 in the second step. This will cause a layer of polymer scale to be left on the core particle surface with progress of the second step reactions. In consideration of the above circumstances, we have defined a modified fraction F which represents the fraction of the weight change of UF_4 and is useful for evaluating the UF_6 production rate. It may be briefly recalled as follows:

$$F = \frac{(m_o - m_{po}) - (m_t - m_{pt})}{(m_o - m_{po})} \quad . \text{ Eq. (4) in Section 2.}$$

The values of m_{pt} were calculated from the linear relationships in Fig. IV-9. The value of m_{po} may be calculated by approximation from the point extrapolated to $t = 0$ in the line of m_{pt}/m_o in Fig. IV-9.

Figure IV-11 shows the plots of $(1 - F)^{1/3}$ vs. time at different temperatures, and Fig. IV-12 the same plots for different partial pressure of fluorine. Generally linear relationships are seen to hold in most of the cases represented. The fluorination rate of intermediate UF_4 was almost the same as in the case of UC. Tables IV-3 to IV-4 are the lists of the reaction rate constants.

From the plot of log k vs. 1/T in Fig. IV-13, where k (h^{-1}) was obtained from the slope of the straight lines in Fig. IV-11, the apparent activation energy of the (b-1) was determined to be 19.5 kcal/mole. Labaton and Johnson[9] investigated the fluorination of UF_4 to UF_6 by fluorine and obtained the activation energies of 19.1 or 19.9 kcal/mole for UF_4 samples, prepared by hydrofluorination of uranium dioxide at 400°C, or by sublimation of a high reactive UF_4, respectively. Thus, all three values are in good agreement. Figure IV-14 shows the plots of fluorine concentration vs. reaction rate k, where k was determined from the slope of the straight parts of curves in Fig. IV-12. No sintering was observed on the powdery intermediates, in contrast to the case of UC when it was seen to occur heavily with increasing fluorine concentration.

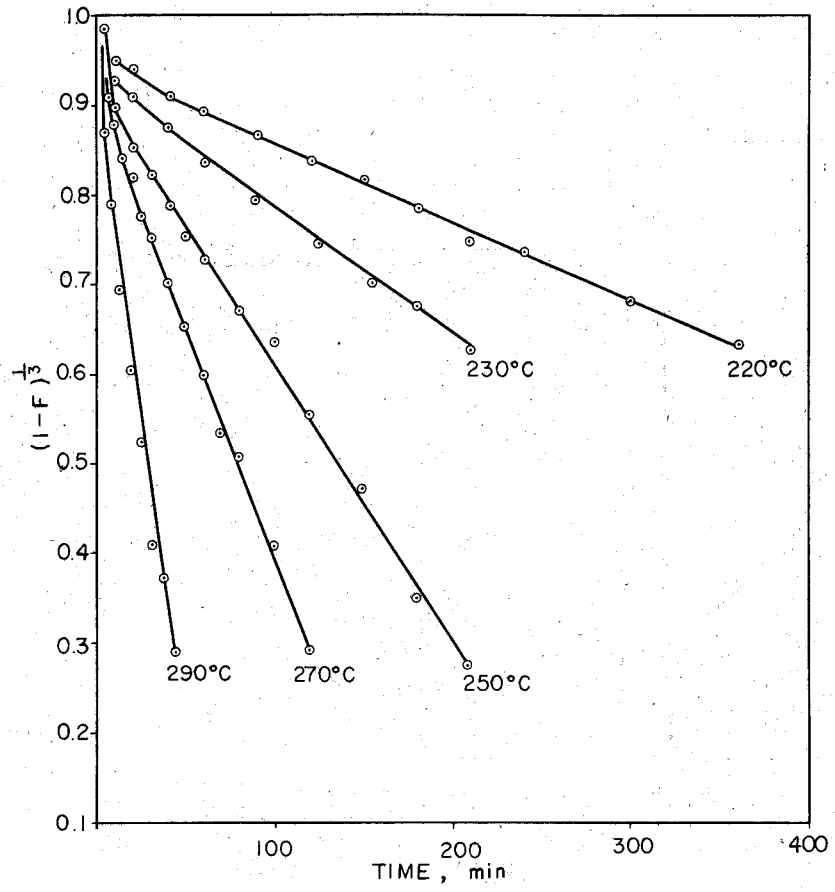

Fig. IV-11. Relationships between $(1 - F)^{1/3}$ and time at different temperatures.
Sample, uranium dicarbide; total gas flow rate, 13.7 l/h; total pressure, 1 atm.; fluorine partial pressure, 84 mmHg (11 vol. %).

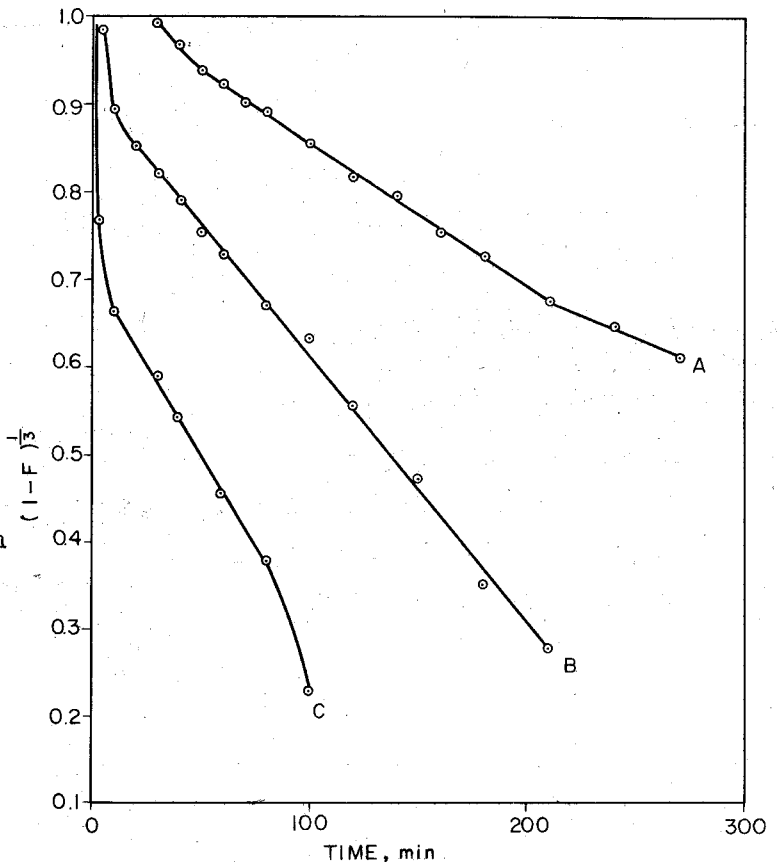

Fig. IV-12. Relationships between $(1 - F)^{1/3}$ and time at different partial pressure of fluorine.
Sample, uranium dicarvide; reaction temperature, 250°C; total gas flow rate, 13.7 l/h; total pressure, 1 atm.; fluorine partial pressure, A; 38 mmHg, B: 76 mmHg, C: 114 mmHg.

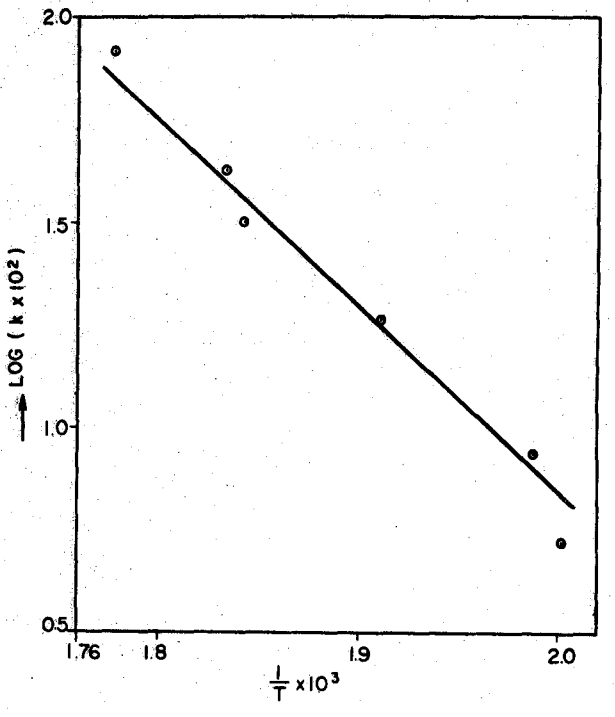

Fig. IV-13. Relationship between log k and 1/T.
Sample, uranium dicarbide.

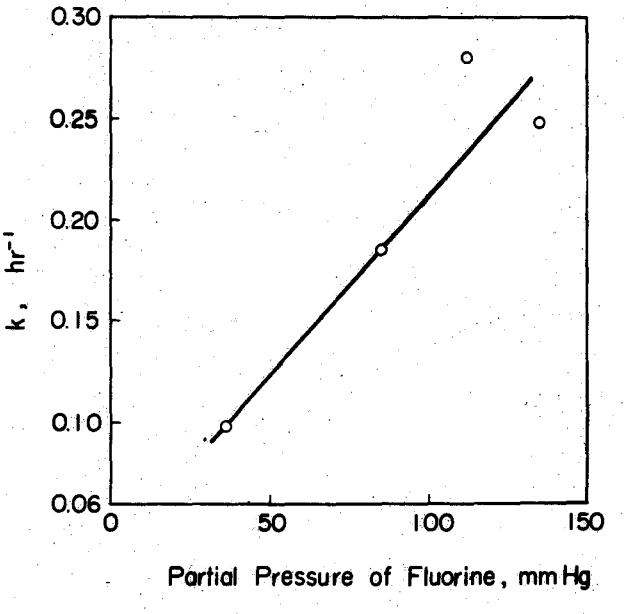

Fig. IV-14. Relationship between k (reaction rate constant) and fluorine partial pressure.
Sample, uranium dicarbide; reaction temperature, 250°C.

Table IV-3. Reaction rate constant of uranium dicarbide, effect of temperature.
Fluorine concentration, 11 volume % (85 mmHg in partial pressure); total pressure, 1 atm.; diluting gas, argon; total gas flow rate, 13.7 l/h.

Temperature (°C)	Reaction rate constant $k(min^{-1}) \times 10^3$	$k\ (h^{-1})$
220	0.884	0.053
230	1.45	0.087
250	3.08	0.185
270	5.24	0.314
275	7.00	0.420
290	13.6	0.816

Table IV-4. Reaction rate constant of uranium dicarbide, effect of fluorine concentration.
Reaction temperature, 250°C; total pressure, 1 atm.; diluting gas, argon; total gas flow rate, 13.7 l/h.

Fluorine conc. vol. %	Reaction rate constant $k(min^{-1}) \times 10^3$	$k\ (h^{-1})$
4.5	1.62	0.098
11.1	3.08	0.185
18.0	4.12	0.248

4. Comparison in fluorination behaviors between the two carbides

The mechanism of the fluorination reaction appears to be nearly the same for the two carbides. At the temperatures between 200° and 300°C, the reaction rate could be measured, while, above 300°C, the rates could not be exactly measured because they were fairly rapid and about 50 weight % of the sample was volatilized during the initial temperature rise.

The mass spectrometric analysis indicated the presence of CF_4, C_2F_4, C_2F_6, and small amounts of other not-identified compounds in the gaseous reaction products for both the carbides. CF_4 seemed to be major product —— over 80 vol. %, for instance, of CF_4 was found. However, the reproducibility of data on the relative yields of these compounds were not good.

The final products and intermediates of the reaction ranged from somewhat

simple molecules such as uranium fluorides and lower fluorocarbons to macromolecules like polymeric fluorocarbon, were formed in complicated ways, so that it was difficult to distinguish the elementary reactions on the reaction steps. With emphasis on the behavior of uranium, however, the main reaction may be considered to proceed as follows:

$$UC \text{ or } UC_2 + F_2 \longrightarrow UF_4 + \text{polymeric and gaseous fluorocarbons} \qquad (a)$$

$$UF_4 + F_2 \longrightarrow UF_6 \qquad (b\text{-}1)$$

$$\text{polymeric fluorocarbon} + F_2 \longrightarrow \text{gaseous fluorocarbons} \qquad (b\text{-}2)$$

In the second step, the two different reactions (b-1) and (b-2) occur simultaneously. The relationships between the magnitudes of the reaction velocities may be expressed as

$$\text{reaction velocity of (a)} \gg \text{(b-1)} > \text{(b-2)}.$$

On the other hand, the difference in the amount of polymer between UC and UC_2 is far larger than expected from the difference in carbon content of the two carbides. Two different schemes may be considered for the formation of polymeric fluorocarbon; one is by the reaction of fluorine with the carbon, which forms the carbide with uranium, and the other by the reaction with free carbon. There is no suitable means to distinguish the fluorination behaviors of these carbon atoms from the two different sources. If the polymeric fluorocarbon is made only from the free carbon, the maximum values of m_{po}/m_o can be calculated to be $0.0009 \sim 0.0017$ for UC and 0.036 for UC_2 by assuming that all the free carbons are used for the formation of the polymer and two fluorine atom combined with each carbon atom. These values all are by far smaller than the observed values, $0.01 \sim 0.02$ for UC and $0.1 \sim 0.16$ for UC_2. The results indicate that the polymeric fluorocarbon may mainly be from the combined carbon. The difference in the amount of polymer between UC and UC_2 may be attributed to the difference in crystal structure —— UC being of the NaCl type, and UC_2 of the CaC_2 type in which two adjacent carbon atoms make a double bond.[10)]

In Table IV-5 are summarized the characteristics of fluorination of the two uranium carbides; i.e., whether the reacting particles sinter or not, and the difference in the mechanism of the rate controlling step. These characteristics would appear to be due to the properties of the polymer. In the fluorination of UC, the parabolic mechanism of the reaction above 270°C indicated that the polymer produced in the first step is thermally deformed to make a compact film. On the other hand, the polymer from UC_2 seemed to be

relatively solid and stable thermally and not to make such a compact film, so the reaction investigated followed the linear law. Further, the larger amount of the polymer produced would act to prevent the particles from sintering by inhibiting the mutual contact of the UF_4 surfaces. These assumptions, however, have not been definitely substantiated by differential thermal analysis of the polymer formed.

Table IV-5. Fluorination behavior of uranium carbides.

	UC	UC_2
Reaction intermediates	UF_4 and polymer	UF_4 and polymer
Rate controlling step of UF_6 production	$250^\circ \sim 270^\circ C$: reaction on the surface of UF_4 Above $270^\circ C$: Diffusion of F_2 through polymer layer	$250^\circ \sim 290^\circ C$ Reaction on the surface of UF_4
Quantity of polymer	Very slight $m_{pt}/m_t = 0.02 \sim 0.01$*	large $m_{pt}/m_t = 0.16 \sim 0.06$*
Effect of F_2 concentration	Sintering of intermediates at higher F_2 concentrations	No sintering; reaction rate is proportional to F_2 concentration

* the values are in the temperature range between $240^\circ \sim 270^\circ C$.

m_{pt}: weight of polymeric fluorocarbon at time t.

m_t: initial weight of sample.

5. Summary

The fluorination reactions of UC and UC_2 by fluorine both proceeded by the following steps:

$$UC \text{ or } UC_2 + F_2 \longrightarrow UF_4 + \text{polymeric and gaseous fluorocarbons} \quad (a)$$

$$UF_4 + F_2 \longrightarrow UF_6 \quad (b\text{-}1)$$

polymeric fluorocarbon + F_2 ⟶ gaseous fluorocarbons (b-2)

The relationship among the reaction rate of each step is

$$(a) \gg (b\text{-}1) > (b\text{-}2) .$$

The amount of polymer produced for UC_2 was much larger than that for UC.

Other characteristics for the reaction behavior are summarized in Table IV-5.

References

1) Schwarzkopf, P., Kieffer, R., Refractory Hard Metals, The Macmillan Company, New York.
2) Schumb, W. C., Aronson, J. R., J. Am. Chem. Soc., 81, 806 (1959).
3) Naito, K., Private Communication.
4) Hoshino, A., Unpublished work.
5) Spencer Chemical Co., Specifications for the uranium carbides.
6) Katz, J. J., Seaborg, G. T., The Chemistry of the Actinide Elements, p. 156, Methuen & Co., Ltd., London (1957).
7) Jander, W., Z. Anorg. Chem., 163, 1 (1927).
8) Farrar, R. L., Smith, H. A., J. Phys. Chem., 59, 763 (1955).
9) Labaton, V. Y., Johnson, K. D. B., J. Inorg. Nucl. Chem., 10, 74 (1959).
10) Atoji, M., Medrud, R. C., J. Chem. Phys., 31, 332 (1958).

Chapter V

Fluorination of bromine by fluorine**

There are three known bromine fluorides, BrF, BrF_3, and BrF_5.[1,2] Of these fluorides, however, BrF is so unstable that it cannot be isolated in pure state.*

Reports were made on the syntheses of BrF_3 and BrF_5 by Lebeau, Ruff and others. The best method to synthesize BrF_3 and BrF_5 is to directly combine bromine and fluorine in gas phase; the behavior of sythesis may be as follows: BrF_3 is formed mainly at a temperature from 20° to 100°C, while BrF_5 is formed above 200°C in good yield.[1,2] The studies presented here were performed to obtain more detailed information on the reaction between fluorine and bromine to produce BrF_3 and BrF_5.

1. Experimental method

Two methods of experiment may be considered for the reaction between fluorine and bromine; one is by a homogeneous reaction in the gas phase and the other by a heterogeneous reaction in which liquid bromine reacts with fluorine gas. Considering the ease of controlling the reaction condition, the former method was adopted: that is, bromine diluted with nitrogen was supplied to a reaction vessel at a constant flow rate under atmospheric pressure.

Apparatus

Figure V-1 shows a schematic diagram of the experimental apparatus. In order to supply bromine vapor at a constant rate to the reaction system, a device shown in Fig. V-2 was used. The liquid bromine, contained in a flexible Daiflon tube, overflowed into an evaporator at a constant rate, by pulling up the end of the tube at a constant rate, and the bromine was evaporated and carried to the reactor with a stream of nitrogen preheated to 40°C. Since the liquid bromine has a strong penetrating nature, any types of

---

* The existence of BrF was first suggested by Ruff and Braida from the physical properties of a component, condensed at temperatures lower than -100°C from the reaction products between bromine and fluorine,[3] and then by Steunenberg et al. from the vapor pressure anomalies observed near room temperatures for a liquid mixture of bromine and BrF_3.[4] Stein confirmed the existence only in gas phase by infrared spectroscopy.[5]

** Published in Nihon Kagaku Zassi, 83, 36 (1962).

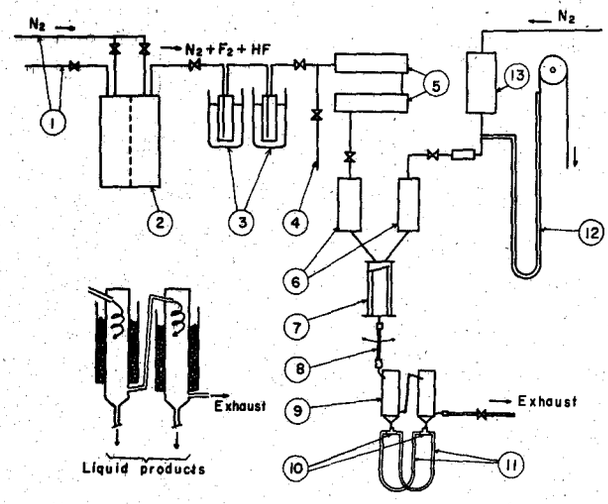

Fig. V-1. Schematic diagram of the system for synthesizing bromine fluorides. (1) inert gas lines for purging fluorine cell; (2) fluorine cell; (3) cold traps for hydrogen fluoride (-80°C); (4) inert gas line for diluting fluorine; (5) sodium fluoride beds for adsorbing hydrogen fluoride (100°C); (6) preheaters; (7) reactor; (8) flexible piping made of Daiflon; (9) cold traps for reaction products; (10) brass tee-joints; (11) vessel for liquid products, made of Daiflon tube; (12) flexible Daiflon pipe for storing bromine; (13) preheater.

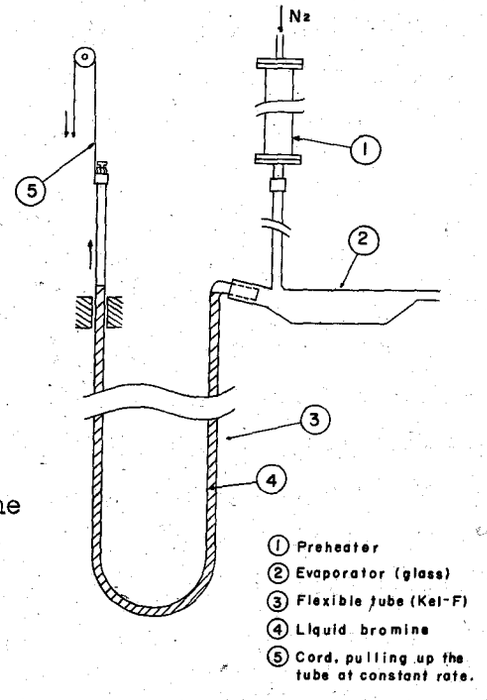

Fig. V-2. Mechanism for supplying bromine at constant flow rate.

stopcocks or mechanical joints could not be used at the possible places of contact with liquid bromine. The flow rate of fluorine was calculated from the cell current as described in the preceding chapters. The preheaters and the reactor were kept at the same temperature. To mix the reacting gases efficiently, a buffle plate was placed at the upper part of the reaction vessel, as shown in Fig. V-3. The products were condensed in a series of cold traps, cooled by dry ice. The cold traps were of a copper cylinders, which were set vertically in order that the liquid products may flow down and be collected in the Daiflon U tubes. Non-condensable gases were exhausted through an outlet tube, connected to the second cold trap at the bottom of the cylinder. After each experimental run, the U tubes were disconnected from the reaction system, and used as the storage vessel of the reaction products by sealing the openings with Teflon plugs. Daiflon (polychlorotrifluoroethylene) and Teflon were resistant to bromine fluorides at room temperatures. The sizes of pipes, valves, and connecting devices like tee and elbow, were standardized to two different inside diameters, 4 and 7 mm. Flare fittings, shown in Fig. V-4, were used to connect the copper tubes, the Teflon tubes, and the copper and the Teflon tubes. The materials used for the apparatus were: monel for preheaters, HF absorption beds, reaction vessel, and valves; copper for cold traps, and pipes; Daiflon for pipes; brass or stainless steel for flare fittings.

Materials

Fluorine gas from the cell was used after being freed from hydrogen fluoride, as described in the preceding chapters. The bromine used was of a reagent grade, commercially available. The purity of nitrogen was more than 99.9 mole %.

2. Fluorination conditions

All the experiments were made at constant flow rates of the reacting gases under atmospheric pressure. The following two reaction conditions —— noted as A and B hereafter —— were used.

Condition A: flow rate of fluorine, 0.88 mole/h (19.7 l/h);
flow rate of bromine, 0.16 mole/h (3.6 l/h);
flow rate of nitrogen (carrier gas of bromine) 10 l/h;
total gas flow rate, 33 l/h;
reaction temperature, 25° to 245°C;

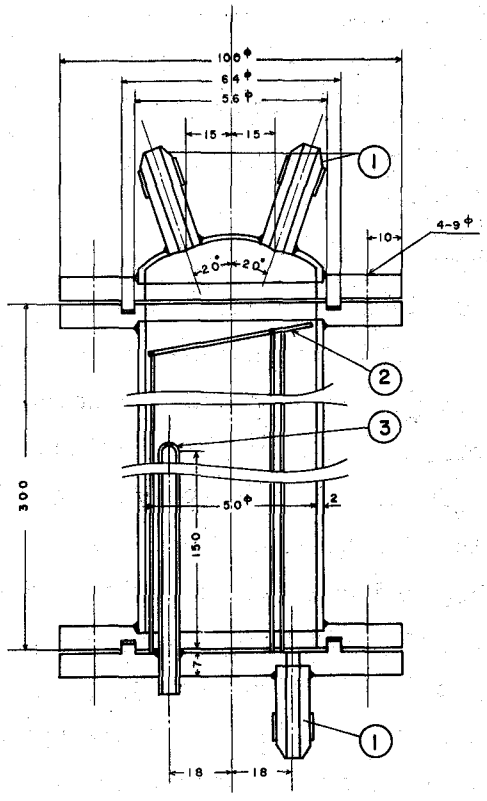

Fig. V-3. Reactor for synthesizing bromine fluorides.
(1) gas inlets and outlet; (2) buffering plate; (3) thermocouple sheath.

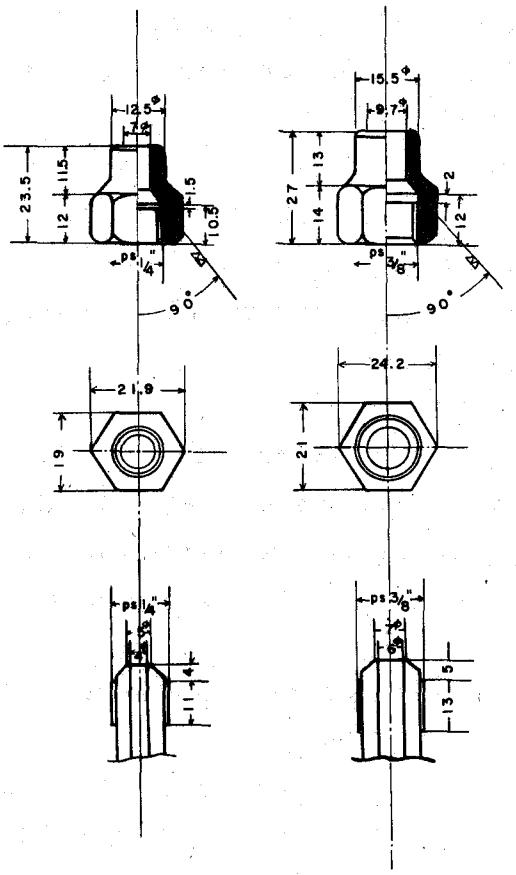

Fig. V-4. Flare fittings.

fluorine was supplied at 10 mole % excess of the stoichiometric amount necessary for synthesizing BrF_5.

Condition B: flow rate of fluorine, 0.78 mole/h (17.5 l/h);
flow rate of bromine, 0.24 mole/h (5.4 l/h);
flow rate of nitrogen, 10 l/h;
reaction temperature, 25° to 145°C;
fluorine was supplied at 10 mole % excess of the stoichiometric amount necessary for synthesizing BrF_3.

First, the temperature of the preheaters and of the reaction vessel filled with atmospheric nitrogen was raised to the desired values, and then the reacting gases were passed through the reaction system at the flow rates in condition A or B for two hours in each run. The reaction products formed during the first one hour and the subsequent one hour, were collected separately; the latter product was used for the chemical analysis, since, in the early stage of the experimental run, the reactions would not be in steady state. To collect the reaction products, two U tubes of the form in Fig. V-1 were connected to the bottom of each cold trap with tees. The collection of above two fractions of product into individual U tubes was accomplished by declining the whole assemblage of cold traps and U tubes in such a direction that the liquid product flow into the particular U tube. This operation was done in bending manually the flexible Daiflon tube, which connected the reaction vessel to the first cold trap.

3. Analysis of the reaction products

Since bromine fluorides are very reactive, special precautions were necessary in sampling, weighing and hydrolyzing prior to the chemical analysis. To avoid such troublesome operations, development of the direct instrumental analysis is desirable. Two different methods of analysis were, therefore, employed: one is the ordinary chemical analysis, and the other is the analysis by N.M.R. spectroscopy.

3.1 Chemical analysis

To apply the conventional analytical technique, it is necessary to convert the sample to its aqueous solution in a stoichiometric way. The reaction products will contain bromine and bromine pentafluoride which have rather high vapor pressures even at room temperature, and so their evaporation loss during the pretreatment must be minimized. The hydrolysis proceeds explosively, so that a special bottle for the hydrolysis was deviced.[6] It was found, however, that the hydrolysis proceeds mildly, when the amount of

sample is small and the sample is in solid state by cooling it to -80°C.

The procedure used in the analysis is as follows. A Daiflon tube, 6 and 4 mm in outside and inside diameter, 50 mm long, thermally sealed at one, end, was used as the sampling vessel for the liquid products. After from 0.3 to 0.7 grams of the product was taken in it, the end was closed with a small teflon plug. Then, it was weighed and cooled with a mixture of dry ice and ethyl alcohol until the liquid sample was completely solidified. The plug was removed and the vessel was dropped into 300 cc of 2 N aqueous ammoniac solution in a 2 litre polyethylene bottle, and then the bottle was quickly closed with a cap; the ammoniac solution had previously been cooled less than 10°C. The hydrolysis of sample progressed slowly with no explosion. Since in addition to Br^-, BrO^-, BrO_3^-, and Br_2 are formed by the hydrolysis of BrF_3 and BrF_5,[2,6,7] they were reduced to Br^- ion with hydrazine. In Fig. V-5, the series of the experimental operations is shown schematically.

All the reaction products were from yellow to reddish yellow in color; while it is reported that the colors of pure BrF_3 and BrF_5 are pale yellow and colorless, correspondingly.[8,9] Therefore, it was certain that free bromine was present in the products. The amount of free bromine, however, appeared to be small, because the reddish color, characteristic of bromine, was not deep. Unfortunately, there is no method for measuring the amounts of bromine and fluorine. However, it will bring no significant error if it is assumed that only two components, BrF_3 and BrF_5, were present in the liquid product by neglecting the presence of the small amount of free bromine. Under this assumption, the mole percent of BrF_3 or BrF_5 in the liquid product was calculated from the quantities of bromine, determined by chemical analysis.

3.2 Analysis by N.M.R.

The strong nuclear magnetic property of the fluorine atom was applied for measuring directly the amount of BrF_3 and BrF_5 in their mixture. The sample was taken in a Daiflon tube, shown in Fig. V-6, and its spectrum of nuclear magnetic resonance was measured by a N.M.R. spectrometer —— Varian V-4300-C. There is essentially no difference in strength of the resonance of the fluorine atoms in BrF_3 and BrF_5, irrespective of the position of fluorine atoms in the molecules and of their molecular structure, so that the amount of BrF_3 and BrF_5 in the reaction product will be determined by measuring the area of each resonance peak. Figure V-7 shows a typical resonance spectrum of the reaction product. The spectrum of BrF_5 consists of two separate peaks; the stronger one corresponds to the absorption by four fluorine atoms at the base of the symmetrical tetragonal pyramid

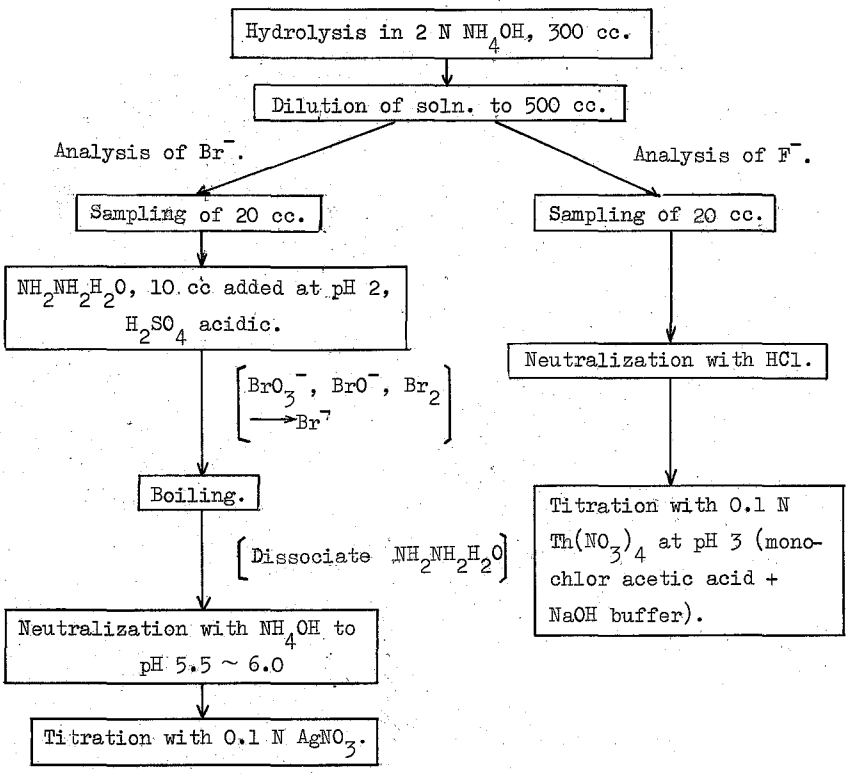

Fig. V-5. Procedure in the chemical analysis of bromine fluorides.

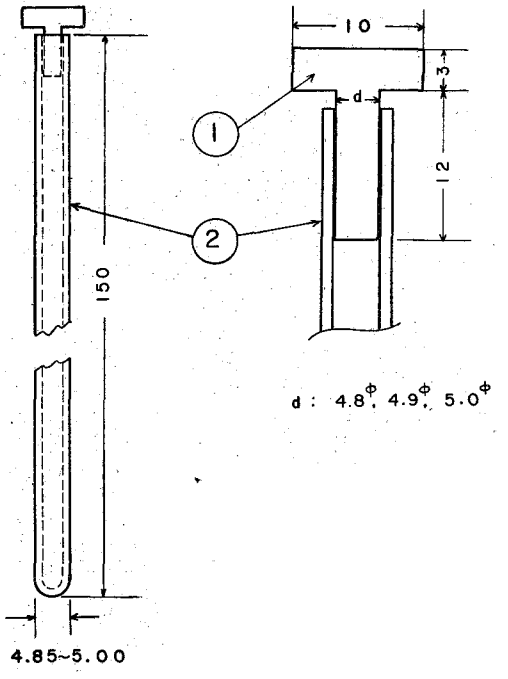

Fig. V-6. N.M.R. sample tube.

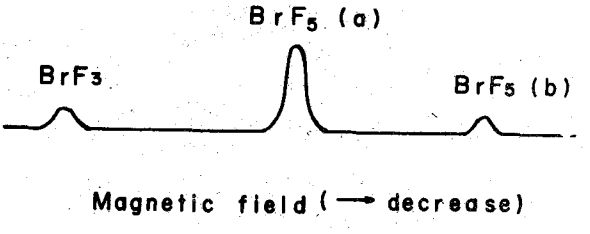

Fig. V-7. N.M.R. spectra of BrF_3 and BrF_5.

structure of BrF_5 molecule and the other to one fluorine atom at the apex of pyramid.[10] The spectrum of BrF_3 has only one resonance peak. No other peaks were observed besides the three peaks described. The mole fraction of each component was determined by measuring the area of BrF_3 peak or the stronger peak of BrF_5. The amount of free bromine cannot be measured by this method, as in the chemical analysis.

4. Experimental results

In condition A, all the products were faint yellow in color and had an irritative fume. The quantity of unreacted bromine in the products seemed to be negligibly small from its color; In condition B, all the products were reddish yellow in color; this indicated the presence of small amounts of free bromine in the products.

In Figs V-8 and V-9, the concentration of BrF_5 is plotted against the reaction temperature. The reliability of the analytical data obtained by the chemical analysis, seems to be larger than for the N.M.R., because of the poor reproducibility and the difficulty in measuring the area of resonance peaks in the latter. The plots both in Figs. V-8 and V-9, however, show in general the same tendency. It has been previously been reported that BrF_3 is mainly formed when fluorine and bromine react in gas phase at the temperatures below 100°C.[1,2] Contrary to this reported result, the concentration of BrF_5 in the products was unexpectedly large below 100°C, at condition A. Even in the case of condition B, in which fluorine was supplied to form BrF_3 and therefore insufficiently to form BrF_5, 20 to 30 mole % of BrF_5 was formed. Since BrF_5 will be formed through the following two steps;

$$\frac{1}{2}Br_2 + \frac{3}{2}F_2 \longrightarrow BrF_3, \text{ and} \qquad \text{(a)}$$

$$BrF_3 + F_2 \longrightarrow BrF_5, \qquad \text{(b)}$$

the above results indicate that the rate of step (b) is high compared with the rate of step (a).

5. Summary

The reaction between bromine and fluorine in gas phase was studied in the temperature range between 25° and 250°C. The amounts of BrF_3 and BrF_5 in the products were determined by chemical analysis and by N.M.R. Spectroscopy; the results obtained by the two methods were nearly the same.

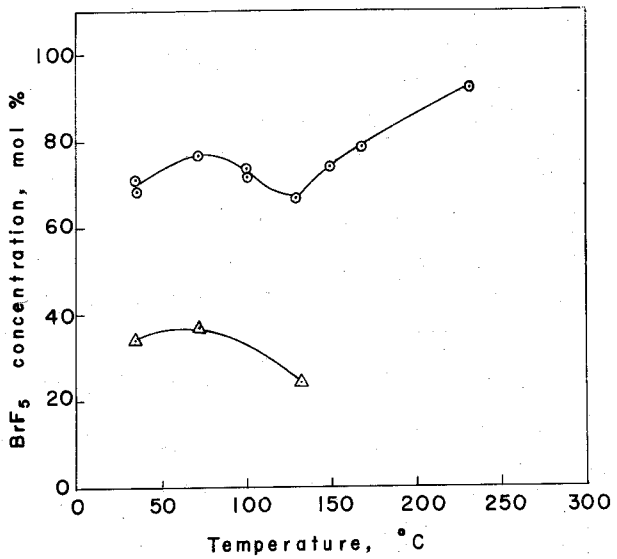

Fig. V-8. Composition of the products at various reaction temperatures, determined by chemical analysis.
⊙, condition A; △, condition B

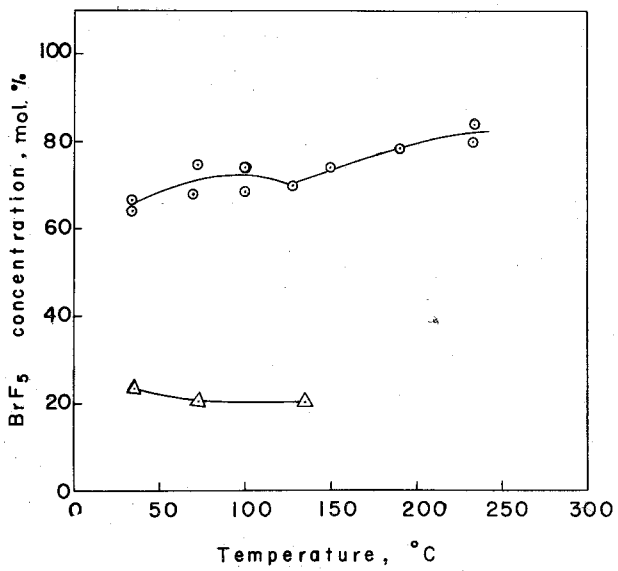

Fig. V-9. Composition of the products at various reaction temperatures, determined by N.M.R.
⊙, condition A; △, condition B.

A relatively large amount of BrF_5 was always contained in the products; when fluorine was supplied in an amount 10 mole % in excess of the stoichiometric amount necessary for the formation of BrF_5, the amounts of BrF_5 in the products were above 65 mole %, and when fluorine was supplied 10 mole % in excess for BrF_3, the amounts of BrF_5 were 20 ~ 40 mole %.

References

1) Musgrave, W. K. R., Advances in Fluorine Chemistry, Edited by Stacey, M., Tatlow, J. G., Sharpe, A. G., vol. 1, pp. 10~12, Butterworths Scientific Publications London (1960).
2) Booth, H. S., Fluorine Chemistry, Edited by Simons, J. H., vol. 1, p. 189, Academic Press (1950).
3) Ruff, O., Braida, A., Z. Anorg. Chem., 214, 81 (1933).
4) Steunenberg, R. K., Vogel, R. C., Fisher, J., J. Am. Chem. Soc., 79, 1320 (1957).
5) Stein, L., J, Am. Chem. Soc., 81, 1273 (1959).
6) Liimatainen, R. C., ANL-6003 (1959).
7) Ivins, R. C., ANL-6362, p. 58 (1962).
8) Ruff, O., Braida, A., Z. Anorg. Chem., 206, 63 (1932).
9) Ruff. O., Menzel, W., Z. Anorg. Chem., 202, 49 (1931).
10) Gutowsky, H. S., Hoffman, C. J., J. Chem. Phys., 19, 1259 (1951).

General conclusion

This study is concerned with the behaviors of the fluorination reactions to produce volatile fluorides such as UF_6, WF_6, and bromine fluorides. Solid materials fluorinated were tungsten metal, uranium metal, uranium oxides (UO_2, U_3O_8, and UO_3), and uranium carbides (UC and UC_2). Uranium oxides are important compounds related with nuclear fuel and so their reaction behaviors studied in details.

In most of the experiments, the fluorinating gas diluted by argon was allowed to flow at a constant flow rate under atmospheric pressure. The weight change was measured by using a thermobalance and the reaction rate was determined.

i) W-F_2 reaction (temp., 200° ~ 500°C; p_{F_2}, ~100 mmHg)

Tungsten metal powder was fluorinated to WF_6 without formation of solid intermediate, that is,

$$W + F_2 \longrightarrow WF_6.$$

The reaction rate was nearly proportional to the surface area of sample.

ii) U-F_2 reaction (temp., 200° ~ 400°C; p_{F_2}, ~90 mmHg)

Uranium metal was fluorinated to UF_6 after an induction period during which the intermediates, UF_3, UF_4, and UO_2F_2 (oxygen probably supplied as an impurity) were formed. The main reaction steps are considered to be the following two:

$$U + F_2 + (O_2) \longrightarrow UF_3,\ UF_4,\ (UO_2F_2) \qquad (a)$$

$$UF_3,\ UF_4,\ (UO_2F_2) + F_2 \longrightarrow UF_6 \qquad (b)$$

The rate of the first-step reaction increased with fluorine concentration, but the rate of the second-step was not influenced by the fluorine concentration.

iii) UO_2, U_3O_8, UO_3 powders - F_2 reactions (temp., 350° ~ 430°C; p_{F_2}, 80 ~ 160 mmHg; particle size, 100 ~ 150 meshes)

All the reactions consisted of the following two steps:

$$UO_2 + F_2 \xrightarrow{k_1} UO_2F_2$$

$$1/3\ U_3O_8 + F_2 \xrightarrow{k_1} UO_2F_2 + 1/3\ O_2 \qquad \text{(a)}$$

$$UO_3 + F_2 \xrightarrow{k_1} UO_2F_2 + 1/2\ O_2$$

$$UO_2F_2 + F_2 \xrightarrow{k_2} UF_6 + O_2 \qquad \text{(b)}$$

The characteristics of the reaction behaviors are as follows.

UO_2: $k_1 \gg k_2$.

U_3O_8: the overall reaction rate was nearly proportional to the surface area of sample.

$k_1 \gtrsim k_2$ for powders having a relatively large surface area.

$k_1 < k_2$ for powders having a small surface area.

UO_3: $k_1 \gg k_2$ (p_{F_2}, 170 mmHg).

Using the diminishing sphere model, the kinetics of the second step reactions may be expressed by equations having the following general form:

$$(1 - F)^{1/3} = (1 + k_2/k_1) - k_2 t\ , \qquad F = \frac{M_o - M_t}{M_o}$$

$$k_2 = A \exp\left(-\frac{E}{RT}\right) p^n\ .$$

For active UO_2

$$(1 - F)^{1/3} = 1 - k_2 t$$

$$k_2 = 2.7 \times 10^3 \exp\left(-\frac{23000}{RT}\right) p_{F_2}.$$

For inactive UO_2,

$$(1 - F)^{1/3} = 1 - k_2 t$$

$$k_2 = 3.3 \times 10^2 \exp\left(-\frac{20700}{RT}\right) p_{F_2}\ .$$

For U_3O_8 (A-2)

$$(1 - F)^{1/3} = 1.2 - k_2 t$$

$$k_2 = 5.5 \times 10^2 \exp\left(-\frac{21300}{RT}\right) p_{F_2}^{0.9}$$

These equations are all for the second step reaction, so there is not so much differences among the values of apparent activation energy "E".

iv) UO_2, U_3O_8 pellets - F_2 reactions (temp., $300^\circ \sim 540^\circ C$; p_{F_2}, 80 ~ 300 mmHg; pellet size, 6 ϕ, x 2 mm).

UO_2 pellets - F_2 reaction

Two types of reactions, classified as Types I and II, occurred below 430°C and above 430°C respectively. To explain this results, the following consecutive processes were considered:

$$UO_2 \text{ pellet} \xrightarrow{k_1} UO_2 \text{ powder (partly fluorinated)} \xrightarrow{k_2}$$

$$UO_2F_2 \text{ powder} \xrightarrow{k_3} UF_6$$

where at $300^\circ \sim 430^\circ C$, $k_1 > k_2 \gg k_3$ (Type I), and
at $430^\circ \sim 540^\circ C$, $k_1 \ll k_2 < k_3$ (Type II).

In the region of Type I, the fluorine gas was considered to be chemically adsorbed in the first step, whereas, in Type II, simple collision mechanism was assumed. The reaction behavior is so complicated that it cannot be expressed in simple form of mathematical equations.

U_3O_8 pellets - F_2 reaction

The reaction proceeded in the following two steps:

$$U_3O_8 \text{ pellet} \xrightarrow{k_1} UO_2F_2 \xrightarrow{k_2} UF_6,$$

where $k_1 < k_2$ above 500°C, and $k_1 > k_2$ below 430°C. The kinetic equations derived are:

$$\frac{dM_t}{dt} = k\, S_t, \text{ or } \rho\,(l_o - l_t) = \rho\,(r_o - r_t) = k\, t,$$

$$k\left[\frac{g}{cm^2.h}\right] = 2.4 \times 10^3 \exp\left(-\frac{23000}{RT}\right) p_{F_2},$$

(temp., $430^\circ \sim 540^\circ C$; p_{F_2}, 80 ~ 300 mmHg; ρ, 7.25 g/cm^3)

v) UO_2, U_3O_8 pellets - gaseous BrF_3 reactions (temp., $100^\circ \sim 150^\circ C$; p_{BrF_3}, 10 ~ 33 mmHg)

Both pellets were fluorinated to UF_6 with hardly any formation of solid intermediate. The kinetics are expressed by the following equations:

$$\frac{dM_t}{dt} = k\, S_t, \text{ or } \rho\,(l_o - l_t) = \rho\,(r_o - r_t) = k\, t,$$

$$k\left[\frac{g}{cm^2.h}\right] = 0.346 \exp\left(-\frac{3900}{RT}\right) p_{BrF_3} \text{ for } UO_2 \text{ pellets, and}$$

$$k\left[\frac{g}{cm^2.h}\right] = 0.024 \exp\left(-\frac{950}{RT}\right) p_{BrF_3} \quad \text{for } U_3O_8 \text{ pellets}$$

(ρ , 10.5 and 7.25 g/cm^3 for UO_2 and U_3O_8 pellets, respectively).

Adsorption of gaseous BrF_3 on the oxide surface and subsequent ionic processes appear to be the cause for the high reactivity of BrF_3 at low temperatures, compared with the reaction temperatures of fluorine. The lone pairs of electrons in BrF_3 and BrF_5 also appear to be related to the reaction processes.

vi) UC, UC_2 - F_2 reactions (temp., $220^\circ \sim 290^\circ C$; p_{F_2}, 34 ~ 135 mmHg)

Both the reactions proceeded in the following two steps:

UC, UC_2 + F_2 ⟶ UF_4 + polymeric and gaseous fluorocarbons (a)

$UF_4 + F_2 \longrightarrow UF_6$ (b-1)

polymeric fluorocarbons + F_2 ⟶ gaseous fluorocarbons; (b-2)

reaction velocity of (a) $\gg$ (b-1) $>$ (b-2).

The amount of polymer formed in the fluorination of UC_2 was much larger than that for UC. The reaction velocities in the rate determining step for UF_6 production, (b-1), in UC and UC_2, were nearly the same.

vii) Br_2 - F_2 reaction (temp., $25^\circ \sim 250^\circ C$)

The reaction between bromine vapor and fluorine was studied. The reaction product contained a relatively large amount of BrF_5, a little smaller amount of BrF_3, and a slight amount of Br_2, when fluorine was supplied in an amount sufficient to give BrF_5.

Notation

E: activation energy

l_o: half of the initial length of pellet

M_o: initial weight of sample

p_{BrF_3}: partial pressure of BrF_3

r_o: initial radius of solid particle or pellet at time t

R: gas constant

T: absolute temperature

k: reaction rate constant

l_t: half of the length of the pellet at time t

M_t: weight of sample at time t

p_{F_2}: partial pressure of F_2

r_t: radius of solid particle or pellet at time t

S_t: surface area of solid particle or pellet at time t

List of the papers in this connection published by the author:

Operation of fluorine cell	JAERI-1046 (1963).
Reaction between bromine and fluorine	Nihon Kagaku Zassi, 83, 36 (1962).
Fluorination of tungsten by fluorine	Kogyo Kagaku Zassi, 65, 1165 (1962).
Kinetic studies of the fluorination of uranium oxides by fluorine I, the fluorination of U_3O_8 and UO_3	J. Inorg. Nucl. Chem., 26, 1853 (1964).
Kinetic studies of the fluorination of uranium oxides by fluorine II, the fluorination of UO_2	J. Inorg. Nucl. Chem., 26, 1863 (1964).
Fluorination of uranium compounds by bromine trifluoride vapor I, fluorination of U_3O_8	J. Nucl. Sci. Technol., 2, 225 (1965).
Kinetics studies of fluorination of uranium carbides by fluorine I, fluorination of uranium mono-carbide	J. Nucl. Sci. Technol., 2, 432 (1965).
Kinetic studies of fluorination of uranium carbides by fluorine II, fluorination of uranium di-carbide	J. Nucl. Sci. Technol., 4, 249 (1967).
Kinetics of the fluorination of uranium dioxide pellet by fluorine	J. Nucl. Mat., 25, 216 (1968).

Appendix I

Handling of the fluorine cell*

The preparation of pure fluorine gas is important for obtaining correct experimental data on the fluorination reactions. Fluorine gas was supplied from an electrolytic cell in this work. Here, technical experimences obtained in the work are described of the operation of the cell.

1. Fluorine cell

Fluorine gas was produced with an electrolytic cell, made by Harshaw Chemical Co. Its main operating characteristics[1] are the following:

maximum load current,	50 A;
composition of electrolyte,	KF 2HF with 1.5 w/o LiF;
HF concentration in electrolyte,	38 to 41 w/o;
temperature of electrolyte,	95 to 100°C.

Figure 1 shows its construction.[2] The cathode and anode probes shown in Fig. 1 were used to control the electrolyte level of each chamber; and device connected to the probes provides a means of automatically breaking the electric circuit to the cell if the level of electrolyte become displaced from obstructions in the gas outlet system. The concentration of HF in the bath was controlled by keeping the electrolyte level in its specified range. The electrolyte level was measured with a movable pin in the cathods probe. The anode and cathode materials are a carbon and monel respectively.

Modifications of the cell

The cell was modified for the production of high purity fluorine gas; that is, (1) a fluorocarbon elastomer, instead of copper gasket, was used as the gasket on the flange of the cell body in order to improve the tightness of the cell, (2) an inlet for the inert gas was added to make it easy to purge the inner atmosphere of the anode chamber.

Reagents used in the fluorine cell

Hydrogen fluorides were commercial products from Daikin Kogyo Co., of which the typical compositions are as follows:[3]

---

* Published in JAERI-1046 (1963).

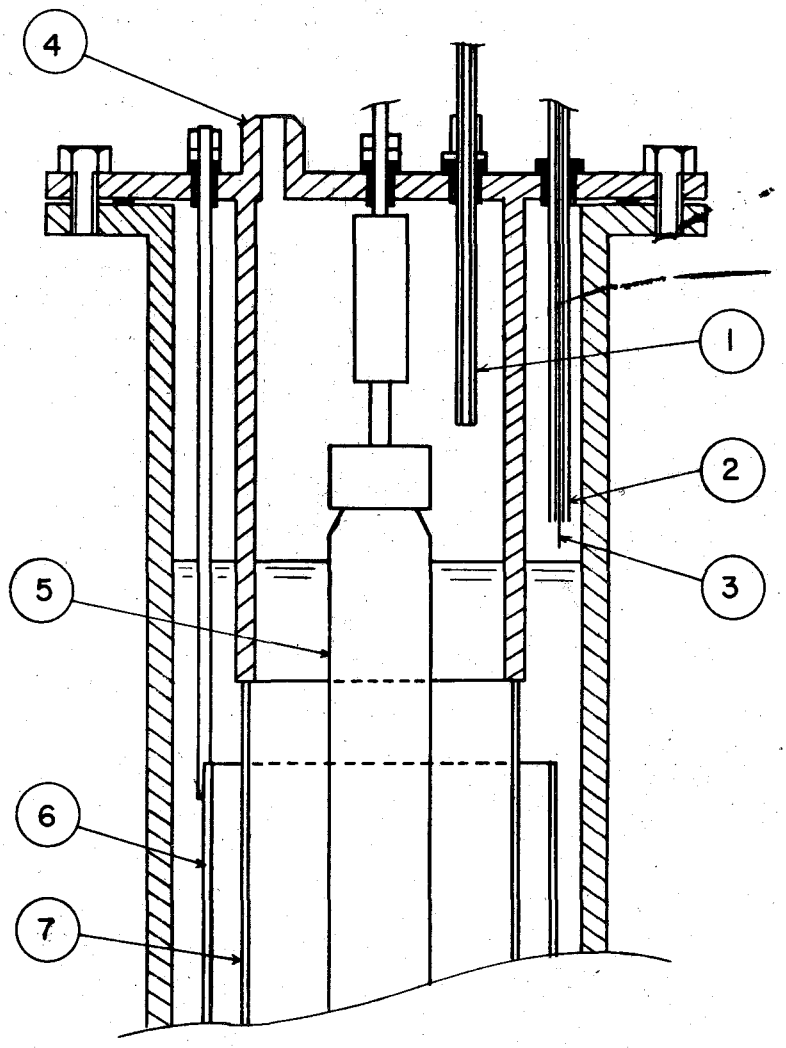

Fig. 1. Harshaw fluorine cell. (1) probe in anode chamber, serving as the liquid level indicator and the inert gas inlet; (2) probe in cathode chamber; (3) movable pin measuring hydrogen fluoride concentration; (4) fluorine outlet; (5) anode electrode; (6) cylindrical cathode; (7) diaphragm.

Component	Weight %		
HF	99.7	99.38	99.95
H_2SiF_6		0.14	0.01
SO_2	0.23	0.13	0.2
H_2SO_4	0.23	trace	0.02
H_2O		0.3	0.1

The electrolyte KF·2HF was prepared by blowing KF·HF powder with hydrogen fluoride. KF·HF used was a commercial product of Morita Kagaku Kogyo Co., of which the composition was:

Component	Weight %
KF·HF	99.0
K_2SiF_6	0.3
SO_4	0.01
Cl_2	0.01

NaF pellets, also from Morita Kagaku Kogyo Co., were used for absorbing HF contained in the produced fluorine. The pellets were in sphere of about 6 mm in diameter.

2. Difficulties in operation of the cell

A number of difficulties interrupted the operation of the cell. These troubles, occurred in the nine years of the operation, are the following:

Explosion in the cell

The splashing of electrolyte in explosions caused plugging of the gas outlet tube, with solidified electrolyte.

Deterioration of the anode

The life of anodes all terminated with occurrence of the anode effect, except one case in which the anode broke into two separate pieces. The duration of each anode was not the same; it ranged from 3 months to about one year.

Corrosion

Teflon packing, used for insulation of anode and cathode probes, was corroded at constant rate, so that it was exchanged periodically. The HF inlet tube and the flange of the cell body were each repaired once in the nine years. Other parts were strong enough for long-period uses.

In the early stages, the explosion in the cell was the most serious, so that its cause was investigated.

3. Explosion in the cell

When the cell voltage was raised gradually to 4.5 ~ 5.0 volts, at which fluorine began to produce, the explosions occurred frequently. For this explosion, the following causes were considered to be possible: (a) the formation of an explosive gas-mixture in the cathode chamber, from the produced hydrogen and remaining air; (b) direct contact between fluorine in the anode chamber and hydrogen in the cathode chamber, due to breakage of the balance of the electrolyte level; and, (c) the reaction between moisture in the electrolyte and fluorine in the electrolyte soon after the production at the anode. The causes, (a), and (b), can be removed by purging the two chambers with an inert gas and operating the cell cautiously without breaking the balance of the electrolyte level. But most explosions were not eliminated by this means, so that cause (c) appeared to be the most probable.

In order to clarify the cause of explosions and examine the above assumptions, an electronic device, which helps to detect the occurring place of explosions in the cell, was made. The principle of this device is as follows. When an explosion occurs in the space above the liquid level in one chamber, the level in this chamber will rapidly be lowered; while, in the other chamber, the level will be raised and the electrolyte here will be short-circuited by contact with a probe in that chamber. Simultaneously, the function of another probe is locked, and therefore, we may know the probe first contacted with the electrolyte. Figs. 2 and 3 show the diagram of this locking circuit and also the diagram of the connection of the device and the probes of the cell. Through a high ohmic resistance, 20 k ohm, a voltage of -2 to -10 volts is applied between the respective probes in the chambers and the electrolyte. In the normal state, the grid of both thyratrons, 2 D 21 (I) is kept at a negative potential, and both the circuits are cut there. When the electrolyte touches probe 1, the grid potential of 2 D 21 (I) becomes zero and the circuits through relay R (I) and PL (I) are closed, whereas HgSW (I) and C_5 of D.C. source circuit are cut. With this state, even if 2D 21 (II) and R (II) were operated, R' (II) would not be switched on, since C_3 had been cut off.

The results obtained by this descriminating circuit indicated that there were three types of explosion: explosion in gaseous phase in the upper space of the anode or cathode chamber, and an explosion in the electrolyte near the anode. The existence of these three types of explosion were also suggested from the differences in sound of explosions. Table 1 lists the characteristics of different types of the explosions. The one occurring

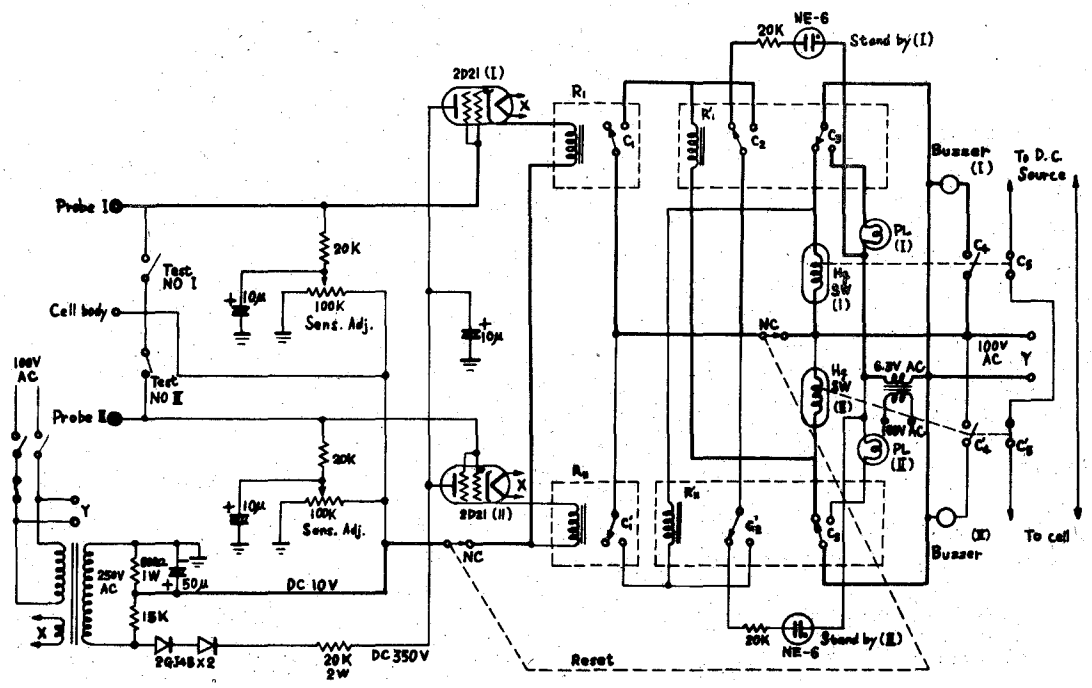

Fig. 2. Wiring diagram of lock circuit.

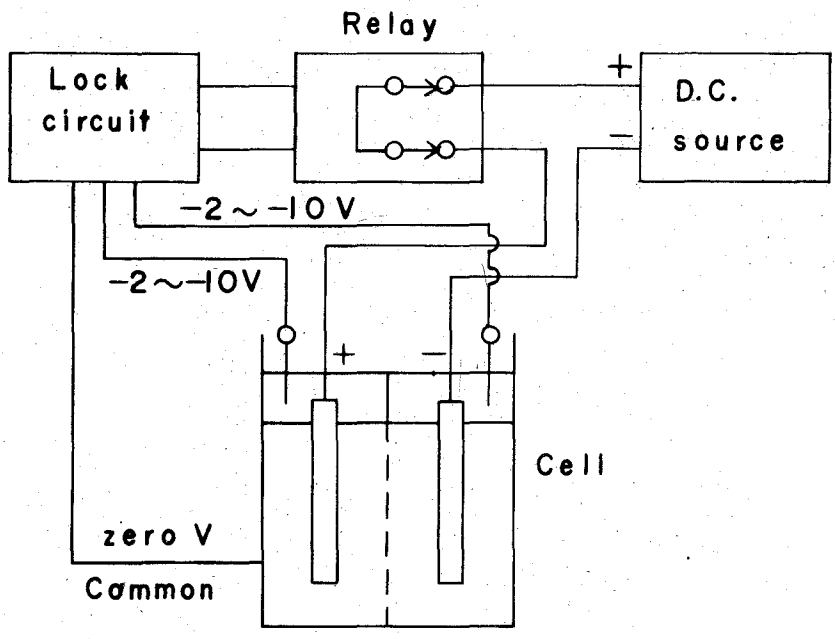

Fig. 3. Schematic diagram of the electric circuit of cell.

most frequently was that in the electrolyte. Its low tone sound may be explained by the sound of explosion being absorbed much into the electrolyte. When the explosion took place in the electrolyte, the electrolyte was splashed strongly, so that the function of the probes stopped by the contamination with splashed electrolyte, and the gas outlet tubes were plugged by solidification of the splashed electrolyte.

Table 1. Characteristics of the different types of explosion.

Location of explosion		Sound of explosion	Dispersion of electrolyte	Discrimination by lock circuit
Anode chamber	In electrolyte	Low pitched tone	Severe	Cathode PL on, cathods and anode PLs on simultaneously, or anode PL on rarely
	In gas phase	Intermediate tone	No	Cathode PL on
	In electrolyte	———	———	———
Cathode chamber	In gas phase	High pitched tone	No	Anode PL on

4. Cause of the explosions in the electrolyte

The explosion in the electrolyte appears to be caused by the reaction of a small amount of water in the electrolyte with the fluorine produced on the anode. This supposition agrees fairly well with the results of previous studies for the reaction between fluorine and moisture, as described below.

Lebeau and Damiens[5] found the formation of gaseous compound, OF_2, when the elementary fluorine was absorbed in water. Burg[6] remarked that OF_2 was also found among the products of electrolysis in a slightly moist-fluorine cell at 100°C or lower. Although OF_2 has a fluorinating property similar to elementary fluorine, it usually requires far more energy of activation than is needed for fluorine. In accordance with this high energy of activation,

the hydrolysis reaction

$$OF_2 + H_2O \longrightarrow O_2 + 2\,HF\,, \qquad H = -75 \text{ kcal/mole},$$

is very slow at ordinary temperatures; but a steam-OF_2 mixture can easily explode. This chemical behavior of OF_2, described by Burg[6], seems to explain the explosion processes in the electrolyte; the produced fluorine reacts with moisture in the electrolyte to form OF_2, which is accumulated to a certain concentration and then reacts explosively with moisture in the electrolyte. The temperature of the electrolyte is 90° to 100°C, so that the moisture in the electrolyte reacts explosively with OF_2 like the steam-OF_2 mixture, as indicated by Burg.

Other oxygen fluorides, O_2F_2 and O_3F_2, decompose to oxygen and fluorine at temperatures above -80°C,[7,8] so they would not be involved into the explosion processes, which would occur at about 100°C.

5. Elimination of water in the electrolyte

From the considerations in the preceding section, the elimination of water from the electrolyte is required before operating the fluorine cell. The water content in the electrolyte tends to increase, because HF contained in the electrolyte is highly hygroscopic. This water content can be reduced by the preliminary electrolysis, at the lower voltages than the minimum voltage for production of fluorine, less than 4 volts for this cell. The maximum current available for the preliminary electrolysis was 0.4A, being considerably low for rapid reducing of the water content. Therefore, any causes, which increase the water content in the electrolyte, must be cautiously removed. The route of water contamination into the cell will be through supplying hydrogen fluoride in which a small quantity of water is always contained. The tightness of the cell was improved by replacing a copper O-ring gasket used between the cell body and the cell cover by a gasket made of fluorocarbon elastomer, which has sufficient elasticity and is resistant against corrosion by the atmosphere of hydrogen fluoride and hydrogen in the cathode chamber. When hydrogen fluoride was supplied to the cell, the supplying pipe had throughly been dried previously. The preliminary electrolysis was always continued except when the cell was operated. By the preliminary electrolysis and purging both the chambers with argon before cell operation, the occurrence of explosions in the cell could almost be eliminated.

6. Anode effect

The cause for the anode effect is generally considered to the formation of a non-conductive fluorocarbon film on the anode surface.[9,10] Recently, Watanabe et al.have studied in detail the mechanism of formation of this film and the relationship with the anode effect.[11,12,13]

Most of the anodes used were deteriorated due to the anode effect. The life of the anodes was from 3 months to over a year, nearly independent of the cumulative amount of electricity during its life. No distinct change was observed in the appearance of the deteriorated electrodes, except in the few cases where the formation of a white product was found on the surface of electrode. The differential thermal analysis or the absorption infrared spectrometry of this anode surface, showed no definite evidence for formation of fluorocarbon compounds.

7. Refining of the produced fluorine gas

The fluorine gas produced contained 5 to 10 vol. % of hydrogen fluoride. The majority of it was removed by two series of cold traps, which were kept at $-80^{\circ}C$ with a mixture of dry ice and trichloroethylene, and then, the trace amount left was removed by adsorbing it on the pellets of sodium fluoride.

8. Analysis of fluorine

Figure 4 shows the apparatus employed for analysis of fluorine gas. After the apparatus was evacuated to below 10^{-4} mmHg, the fluorine gas, diluted with argon, was introduced into the fluorine absorption flask, in which the fluorine was allowed to react with mercury, and finally the residual gases were analyzed by mass spectrometry. Typical examples of the results obtained are the following:

components	concentration, vol. %		
F_2	99.8	99.6	99.4
O_2	0.04	0.06	0.5
N_2	0.07	0.34	—

9. Results of the cell operation

Figures 5, 6, and 7 show the relationships among cell voltage, current, and current efficiency. It is shown in Fig. 7 that the current efficiency is reduced markedly at the high voltages due to the anode effect —— when the anode effect occurs, the cell voltage must be raised to such high values

to hold the current to the initial value. In this case, the cell voltage becomes very unstable; the plot in the range of 14 to 17 volts in Fig. 7 is a typical instance. The cause for the reduction in current efficiency is possibly that a large part of the current is consumed to form solid or gaseous fluorocarbons. A similar loss in current has been observed in the electrolysis of alumina in fused cryolite when the anode effect occurred; generation of CF_4 was then observed.[10,14] The apparatus shown in Fig. 8 was used for determining the amount of fluorine produced for a given time at a constant current. By passing through a NaCl bed, kept at 300°C, fluorine gas, after refining, was converted into the equivalent moles of chlorine gas by the reaction with NaCl; the chlorine gas was then absorbed into 5 % NaOH solution which flowed down through a absorption column filled with glass beads. After the solution was collected in a bottle, an amount of hydrogen peroxide was added to this solution in order to reduce the partly formed NaOCl to NaCl, and finally the amount of Cl^- ion was measured by titrating with $AgNO_3$ standard solution. The current efficiency was calculated by

$$\text{current efficiency } (\%) = \frac{\text{the amount of fluorine measured by the chemical analysis}}{\text{the amount of fluorine calculated from the amount of electricity}} \times 100 .$$

References

1) Pikston, J. T., Ind. Eng. Chem., 39, 258 (1947).
2) Harshaw Chemical Co., Instruction Manual on the Harshaw Fluorine Cell.
3) Daikin Kogyo Co., Private Communications.
4) Morita Kagaku Kogyo Co., Private Communications.
5) Lebeau, P., Damiens, A., Compt. rend., 185, 652 (1927).
6) Burg, A. B., "Fluorine Chemistry" edited by Simons, J. H., vol. 1, p. 82 Academic Press Inc., Publishers, New York (1950).
7) Kirshenbaum, A. D., Grosse, A. V., J. Am. Chem. Soc., 81, 1277 (1959).
8) Kirshenbaum, A. D., Grosse, A. V., Aston, J. G., ibid, 81, 6398 (1959).
9) Ruddorf, W., Emeleus, H. J., Sharpe, A. G., Advances in Inorganic Chemistry and Radiochemistry, vol. 1, p. 231, Academic Press, New York(1959).
10) Watanabe, N., Ishii, M., Denki Kagaku, 29, 364 (1961).
11) Watanabe, N., Ishii, M., Yoshizawa, S., ibid, 29, 492 (1961).
12) Watanabe, N., Ishii, M., Yoshizawa, S., ibid, 29, 497 (1961).
13) Watanabe, N., Hujii, Y., Yoshizawa, S., ibid, 31, 611 (1963).
14) Kameyama, N., Denki Kagaku no Riron Oyo, vol. 2-1, p. 126 (1955).

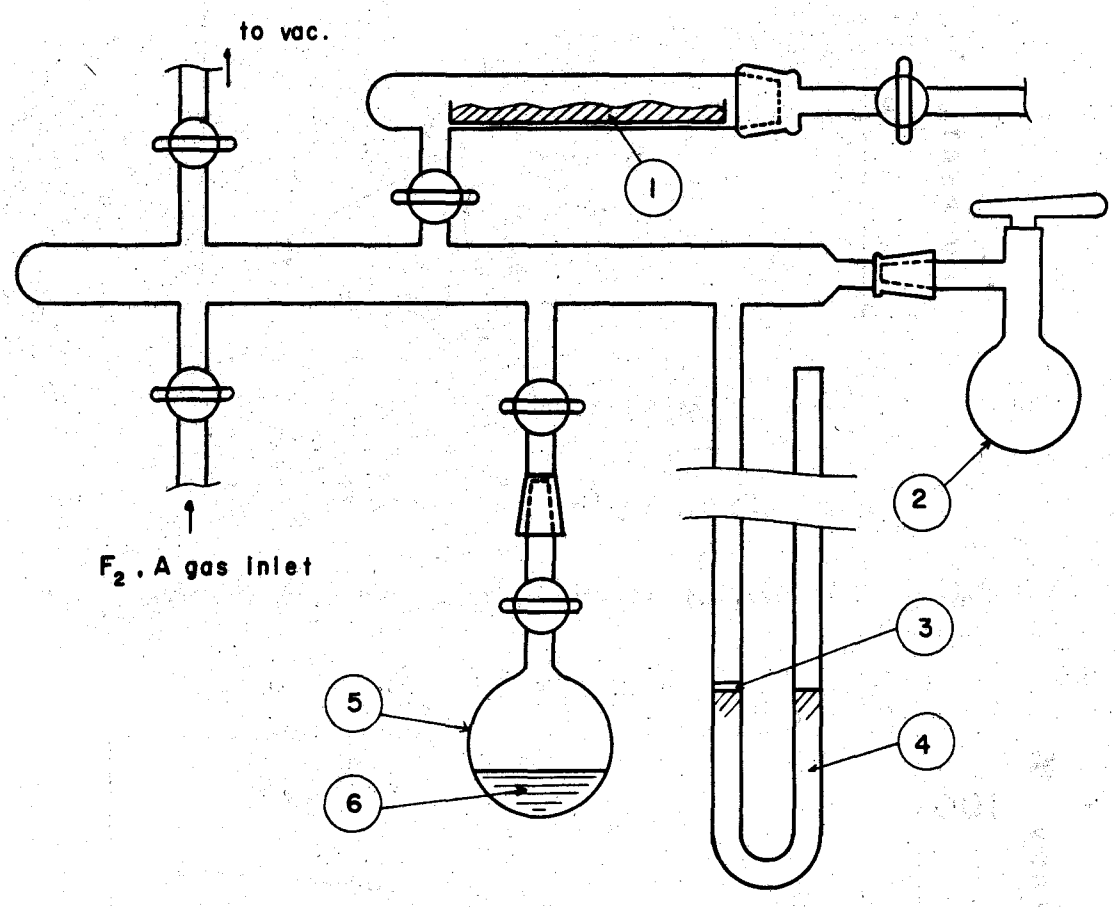

Fig. 4. Apparatus for the analysis of fluorine gas.
(1) sodalime bed; (2) sampling vessel for mass spectrometry; (3) fluorocarbon oil; (4) mercury; (5) vessel for removing fluorine; (6) mercury reacting with fluorine.

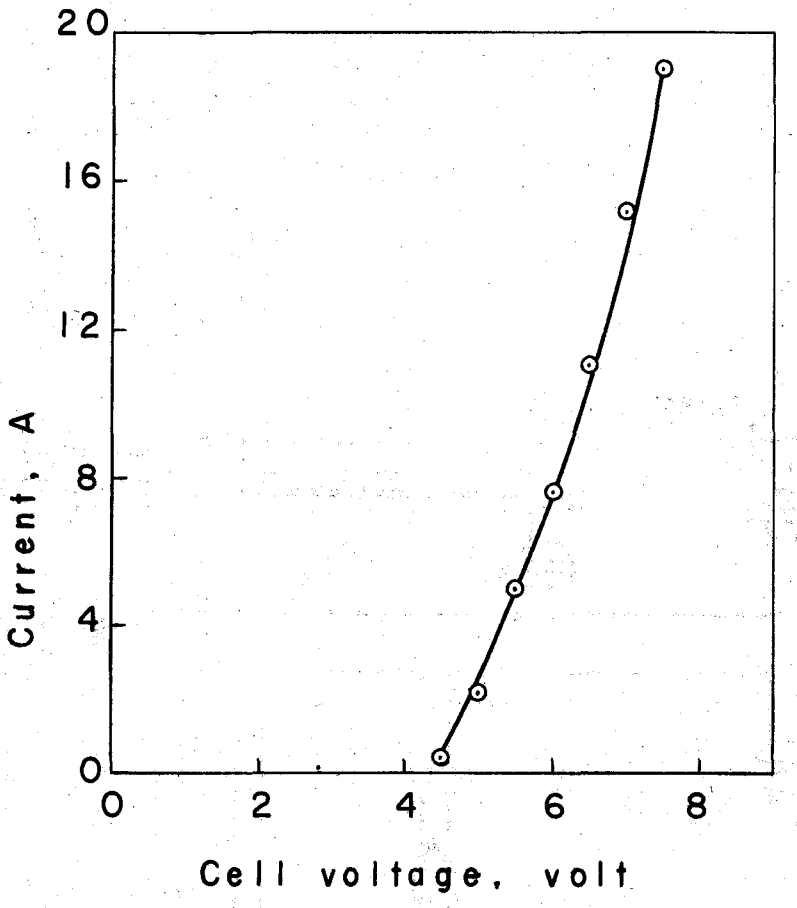

Fig. 5. Relationship between current and cell voltage.

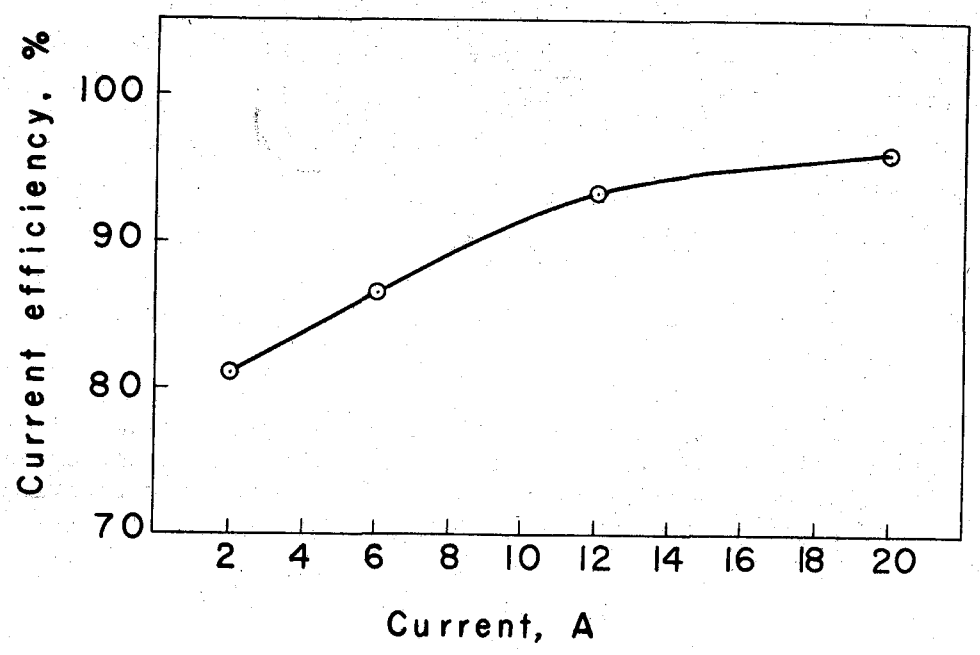

Fig. 6. Relationship between current and current efficiency.

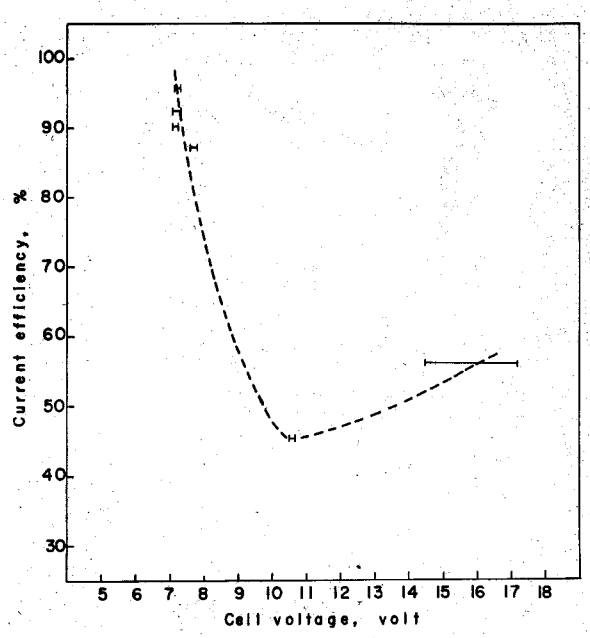

Fig. 7. Relationship between cell voltage and current efficiency. current, 20 ± 0.1 A.

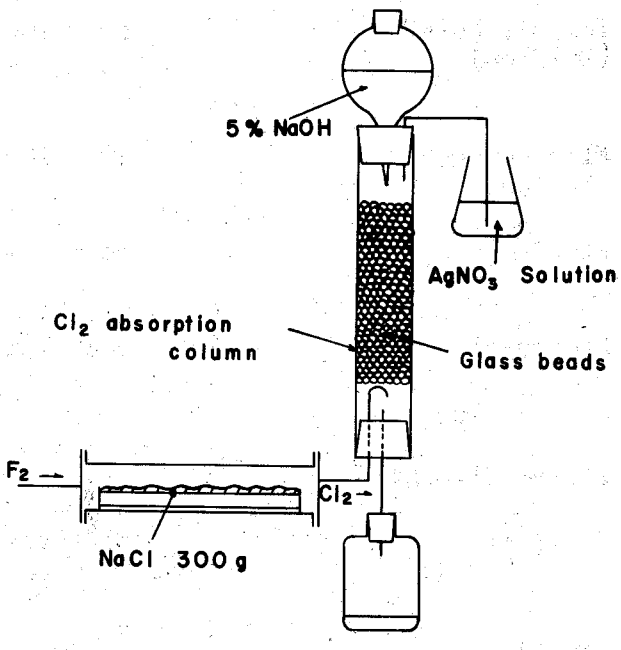

Fig. 8. Apparatus for measuring the amount of fluorine produced.

Appendix II

Structural materials for the apparatus

For fluorine, (diluted to 0 ~ 40 vol. % with inert gas)

Material	Temperature (°C)	Supplement
Monel	< 600	
Nickel	< 600	
Copper	< 100	
Brass	< 100	
Stainless steel	< 100	
Alumina	< 600	
Pyrex glass	< 300	Without HF
Silica	< 300	Without HF
Teflon, Kel-F (Daiflon)	50 ~ 100	Daiflon was ignited in 100% fluorine at room temps.
Fluorocarbon elastomer	50 ~ 100	
Fluoro-grease	room temps.	Ignited in 100% fluorine.
Fluoro-oil	room temps.	Gradually disintegrated to gaseous fluorocarbon.

For bromine fluorides

Material	Temperature (°C)	Supplement
Monel	< 300	
Nickel	< 300	
Teflon, Kel-F (Daiflon)	50 ~ 100	
Fluorocarbon elastomer	room temps.	Gradually swells.

Appendix III

Derivation of equation (5) and (6) in Chapter IV

From equation (4) in chap. IV

$$F = \frac{(m_o - m_{po}) - (m_t - m_{pt})}{m_o - m_{po}} = \frac{(m_o - m_t) - \triangle m_{pt}}{(m_o - m_{pt}) - \triangle m_{pt}}$$

where $\triangle m_{pt} = m_{po} - m_{pt}$.

Since $\frac{\triangle m_{pt}}{m_o - m_{pt}} \ll 1$,

$$F \cong \frac{m_o - m_t}{m_o(1 - \alpha)} \left(1 - \frac{\triangle m_{pt}}{m_o - m_t}\right)\left(1 + \frac{\triangle m_{pt}}{m_o - m_{pt}}\right)$$

where $\alpha = \frac{m_{pt}}{m_o}$.

$m_o \gg m_{pt}, \triangle m_{pt}$, therefore

$$F \cong \frac{m_o - m_t}{m_o(1 - \alpha)} \left[1 + \triangle m_{pt} \frac{m_t - m_{pt}}{(m_o - m_{pt})(m_o - m_t)}\right]$$

$$\cong \frac{m_o - m_t}{m_o(1 - \alpha)} \left[1 + \frac{\triangle m_{pt} \cdot m_t}{\triangle m_t \cdot m_o}\right] \quad \text{(ap. 1): eq. (5) in chap. IV}$$

where $\triangle m_t = m_o - m_t$.

From eq. (5) above,

$$F = \frac{m_o - m_t}{m_o(1 - \alpha)} - \frac{\triangle m_{pt} \cdot m_t(m_o - m_t)}{\triangle m_t \cdot m_o^2(1 - \alpha)} \qquad \text{(ap. 2)}$$

The reaction (b-1) proceeds more slowly than (b-1), and the amount of polymeric fluorocarbon is in the order 1 to 2 weight % for that of UF_4 formed, so that

$$\frac{\triangle m_{pt}}{\triangle m_t} \cong 0.01.$$

On the other hand,

$$\frac{m_t(m_o - m_t)}{m_o^2(1 - \alpha)} = \frac{m_t(m_o - m_t)}{m_o^2} \leqq 0.25 ,$$

therefore,

$$\frac{\triangle m_{pt} \cdot m_t(m_o - m_t)}{\triangle m_t \cdot m_o^2(1 - \alpha)} \leqq 0.0025,$$

and further, towards the end of the reaction, the value of the second term in equation (ap. 2) decreases to much smaller value of 0.0025, whereas the influence of factor α to the value of the first term in equation (ap. 2) increases with the progress of the reaction. Consequently, the second term in equation (ap. 2) may be neglected to simplify the equation; i.e.,

$$F = \frac{m_o - m_t}{m_o(1 - \alpha)} . \qquad \text{(ap. 3) ; eq. (6) in chap. IV}$$

Appendix IV

Physical properties of uranium compounds, halogen fluorides, fluorine, and bromine[1-7)]

Compound	M.P. (°C)	Symmetry	Lattice parameter a_o	b_o	c_o	Density (g/cc)	$-\triangle H_f^o$ ($\frac{kcal}{mole}$)	$-\triangle F_f^o$ ($\frac{kcal}{mole}$)
UO_2	2800	F.C. cubic	5.470			10.95	259.2	246.6
U_3O_8	1450 dec.	ortho-rhombic	6.717	11.97	4.15	8.39	853.5	804
UO_3		amor-phous					289.6	
UC	2500	cubic	4.961			13.6	21.7 ±1.0	22.0
UC_2	2400	tetra-gonal	3.517	5.987		11.68	23.0 ±2.0	27.8
UF_3	1140	hexa-gonal	4.146		7.348	8.95	357	339
UF_4	960	mono-clinic	12.82	10.74	8.41 $\alpha_2=126°10'$	6.70	443	421
UF_5	400 dec.	tetra-gonal	6.525		4.472	5.81	483.7	458.2
UF_5		tetra-gonal	11.473		5.209	6.45	485.2	458.7
UF_6 solid	64.02	ortho-rhombic	9.900	8.966	5.207	5.06	517	486
UF_6	1137 mmHg						505	485
UF_6 gas								485
UO_2F_2		rhombo-hedral	5.767	$\alpha=42°47'$		6.37	399	

Compound	m.p. (°C)	b.p. (°C)	density at 25 °C (g/cc)	$-\triangle H^{\circ}$	$-\triangle F^{\circ}$ (kcal/mole)
ClF	-100.1	- 14		14	13.8
ClF_3	- 76.34	11.75	1.798	37.9	29.5
BrF	~ - 33	~20		17.7	18.0
BrF_3	8.77	125.75	2.798	64.8	55.2
BrF_5	- 60.5	40.76	2.466	106.2	84.1
F_2	- 219.62	- 187.99			
Br_2	- 7.3	58.78	3.12 at 20°C		

1) Katz, J. J., Seaborg, G. T., The Chemistry of the Actinide Elements, Methuen & Co., LTD (1957).
2) Cordfunke, E. H. P., J. Phys. Chem., 68, 3353 (1964).
3) Rand, M. H., Kubaschewski, O., The Thermochemical Properties of Uranium Compounds, Oliver and Boyd LTD. (1963).
4) Tagawa, H., JAERI-4042 (1968).
5) Wiebenga, E. H., Havinga, E. E., Boswijk, K. H., Advances in Inorganic Chemistry and Radiochemistry, edited by Emeleus, H. J., Sharpe, A. G., vol. 3, pp. 133~169 (1961).
6) Kemitt, R. D. W., Sharpe, D. W. A., Advances in Fluorine Chemistry, edited by Stacey, M., Tatlow, J. C., Sharpe, A. G., vol. 4, pp. 142~252 (1965).
7) Kagaku Binran, Maruzen, Tokyo (1958).